Mathematical Modeling of Electronic Systems: From Oscillators to Multipliers

Thesis by

Brian Daffern Hong

In Partial Fulfillment of the Requirements for the
degree of
Electrical Engineer

CALIFORNIA INSTITUTE OF TECHNOLOGY
Pasadena, California

2017
Defended April 28th, 2017

Brian Daffern Hong
ORCID: 0000-0001-8099-0312

For my mom and dad.

ACKNOWLEDGEMENTS

It is pertinent and appropriate that I begin my acknowledgments by expressing my most profound gratitude for my advisor, Professor Ali Hajimiri. Having attended college and graduate school at a younger age, my experiences thus far have been somewhat unconventional. My time here at Caltech, although often turbulent, has been incredibly formative. It goes without saying that Ali is a brilliant, intellectually inspiring academic advisor. Beyond that, however, Ali has served not only as a life mentor whose unparalleled wisdom is driven by his indefatigable sense of right and wrong, but also as a close friend who cares deeply for the people around him. He is an incredible human being who has done so much for my future (even though I did not always deserve it) and who has taught me to never take my opportunities for granted. I am saddened by the prospect that I may never encounter someone like Professor Ali Hajimiri again.

I am also forever indebted to my parents for supporting me in every way possible and allowing me to wholeheartedly focus on my studies throughout my life.

Next, I would like to thank my committee members Professor Azita Emami and Professor Babak Hassibi for their support in my pursuit of this degree.

Of course, I would not be where I am today if it were not for my network of loyal friends. Dr. Alex (Hao-Yu) Pai: you have been the older brother I never had (and I the younger brother he never wanted). Thank you for always telling me what I needed to hear as opposed to what I wanted to hear; your advice has kept me humble over the years. Aroutin Khachaturian's incredible work ethic and boundless compassion is an inspiration to us all. Dr. Constantine (Costis) Sideris has shown me that relentless perseverance will not go unrewarded. The kind-hearted Parham Porsandeh Khial exudes an idealism that has rekindled the optimism that I seem to have lost over the years. Through the wisdom that Seyed Mohammadreza (Reza) Fatemi exhibits, I have learned how to "change my mind about how I look at things, and see that there might be another way to look at it that I have not been shown." I am grateful to Matan Gal-Katziri for instilling within me doses of maturity and common sense from time to time. I am privileged to have met Behrooz Abiri, whose vast knowledge and impeccable intellectual capabilities never fail to impress me. I reminisce about the times I spent with Dr. Kaushik Dasgupta, whose benevolence and shared love of good food lightened my earlier years of graduate school. Seeing

Dr. Amirreza (Amir) Safaripour Tabbalvandani smile as I pass him down the halls of Moore has never failed to brighten my days. Dr. Florian Bohn has been an invaluable, no-nonsense teacher from whom I've learned many of the technical skills that I've needed. David (Elliott) Williams, you have assured me that there is always light at the end of the tunnel. Austin Fikes, you have demonstrated the importance of keeping my head down in persisting through life's many challenges. To my dear friend Abhinav Agarwal—you have consistently served as a reliable source of support, information, and guidance since the beginning of our time here at Caltech. Corina Bianca Panda, through your patience and love, you have shown me that being rational and intelligent does not come at the cost of happiness. Surabhi Sachdev, from you I have experienced the undying power of combining empathy with morality. Ramya Korlakai Vinayak[1], our many conversations have made me realize that our ability to struggle is what defines our strength. Armeen Taeb, you have connected with me in some of my darkest moments. Maxim (Max) Budninskiy, your calmness has kept me level-headed and shown me that life is sometimes much simpler than the world we live in. Utkan Onur Candoğan, your sense of humor has kept me sane and melted away the ice that sometimes plagued my outlook on life. Last but not least, Stefan William Turkowski, from you I have learned that life is too short to take too seriously, and with you I have explored Taiwan (Taipei), Vietnam (Ho Chi Minh City, Mũi Né), Cambodia (Phnom Penh, Siem Reap, Angkor ruins), Thailand (Bangkok, Chiang Mai, Pai, Phuket, Ko Phi Phi, Ko Lanta), and Malaysia (Kuala Lumpur, Melaka).

Finally, to my travel and temple buddy Joy Dou—without you, I would not have experienced the greatest adventures of my life so far: from gazing at the natural wonders of Utah, to summiting the tallest mountain in the contiguous United States, to backpacking the surreal scenery and gorgeous turquoise waters of Havasupai.

[1] Ramya deserves a special acknowledgment here, because she is the one who originally suggested that I pursue the Engineer's (Eng.) degree before leaving for law school.

ABSTRACT

The ubiquity of electronics in modern technology is undeniable. Although it is not feasible to design or analyze circuits in an exhaustively detailed fashion, it is still imperative that circuit design engineers understand the pertinent physical tradeoffs and are able to think at the appropriate level of mathematical abstraction. This thesis presents several mathematical modeling techniques of common electronic systems.

First, we derive, ab initio, a general analytical model for the behavior of electrical oscillators under injection without making any assumptions about the type of oscillator or the size or shape of the injection. This model provides novel insights into the phenomena of injection locking and pulling while subsuming existing theories found in the literature. Next, we focus on the familiar scenario of an inductor-capacitor (LC) oscillator locked to a sinusoidal signal. An exact analysis of this circuit is carried out for an arbitrary injection strength and frequency, a task which has not been executed to fruition in the existing literature. This analysis intuitively illuminates the fundamental physics underlying the synchronization of electrical harmonic oscillators, and it generalizes the notion of the lock range for such oscillators into separate necessary and sufficient conditions. We then turn to the classical estimate of the bandwidth of a linear time-invariant (LTI) system via the sum of its zero-value time constants (ZVTs), and we show that this sum can actually be used to tightly bound the bandwidth—both from above and from below—in addition to simply estimating it. Finally, we look at a natural generalization of the Gilbert cell topology: an analog multiplier for an arbitrary number of inputs; we then analyze its large- and small-signal characteristics as well as its frequency response.

Throughout, we will demonstrate how infusing physical intuition with mathematical rigor whilst seeking a balance between detailed analysis and abstract modularity results in models that are conceptually insightful, sufficiently accurate, and computationally feasible.

PUBLISHED CONTENT AND CONTRIBUTIONS

[1] B. Hong and A. Hajimiri, "A general theory of electrical oscillators under injection, with applications to locking and pulling," under preparation for *IEEE Transactions on Circuits and Systems I: Regular Papers*,
B. Hong conceived of the project, conducted all of the research, and authored the manuscript.

[2] ——, "An exact analysis of LC oscillators under sinusoidal injection," under preparation for *IEEE Transactions on Circuits and Systems I: Regular Papers*,
B. Hong conceived of the project, conducted all of the research, and authored the manuscript.

[3] ——, "Analysis of a balanced analog multiplier for an arbitrary number of signed inputs," *International Journal of Circuit Theory and Applications*, vol. 45, no. 4, pp. 483–501, Apr. 2017. DOI: 10.1002/cta.2243,
B. Hong conceived of the project, conducted all of the research, and authored the manuscript.

[4] ——, "Upper and lower bounds on a system's bandwidth based on its zero-value time constants," *Electronics Letters*, vol. 52, no. 16, pp. 1383–1385, Aug. 2016. DOI: 10.1049/el.2016.1724,
B. Hong conceived of the project, conducted all of the research, and authored the manuscript.

TABLE OF CONTENTS

LIST OF ILLUSTRATIONS

LIST OF TABLES

Chapter 1

INTRODUCTION

It goes without saying that electrical engineering has revolutionized the world we live in. From the wireless communication of information in our quest to enable global connectivity, to the efficient storage of energy and distribution of power for millions of people, to the design of sensors for low-cost lab-on-a-chips and actuators for novel biomedical treatment techniques, electronics is ubiquitous in modern technology. However, the design of electronic systems continues to be a uniquely challenging task for engineers. Numerous design variables need to be simultaneously optimized yet form an intricate high-dimensional network of internal tradeoffs. Coupling this dichotomy with the complexity of the physics of the devices used, circuit design cannot be feasibly executed in an exact fashion—no engineering or scientific endeavor can be; as the old saying goes, "All models are wrong, but some are useful." Still, the approach to good circuit design is far from being ad hoc or heuristic oriented: it must be systematic, based on a fundamental understanding of the pertinent physical issues, and contemplated at the right level of mathematical abstraction. In this thesis, we will focus on several widely used electronic systems. Throughout, we will see how seeking the right balance between rigor and intuition, between looking at physical details and thinking in terms of conceptual abstractions, and between exact derivations and approximate analysis will allow us to glean hitherto unknown insights that are both significant and cogent.

We will first direct our attention toward the *oscillator*, which generates the "heartbeat" of virtually all modern electronic systems. This is because 1) electronics is typically clocked—they must have a time reference by which they operate, and 2) transceivers for wireless and wireline communication systems must convert data between baseband and the frequency of transmission. However, oscillators suffer from two major issues, both of which boil down to how an oscillator's "cycling" or *phase* is influenced by external perturbations. Since an oscillator has no absolute time reference, phase disturbances are never eliminated and persist indefinitely. First, oscillators have a propensity to synchronize to one another, leading to injection *locking* (when this tendency consummates) or *pulling* otherwise. This phenomenon can be desirable, when different oscillators need to produce correlated time references; or undesirable, when distinct yet proximate oscillators need to operate

independently. The second problem is how random fluctuations, typically generated by the oscillator's constituent components, create jitter and degrade the oscillator's spectral purity. Known as *phase noise*, this issue has been successfully modeled by Hajimiri [1]–[4] using the impulse sensitivity function (ISF). Chapter 2 generalizes Hajimiri's theory and presents a methodology for computing how the phase and amplitude of any type of electrical oscillator responds to injections of arbitrary size and shape. This general framework allows us to gain novel insights into injection locking and pulling. Chapter 3 hones in on *harmonic* electrical (i.e., LC) oscillators and performs an exact physical analysis of their steady-state behavior under sinusoidal injection. In doing so, we "generalize" the lock range by deriving *separate* necessary and sufficient conditions for locking to occur. We also analyze the overlooked issue of how the oscillator's core nonlinearity processes phase modulation.

Next, Chapter 4 concerns itself with analyzing the *bandwidth* of an LTI electronic circuit. A well-known approximation for a low-pass circuit is the reciprocal of the sum of the zero-value time constants (ZVTs); here, we make a more precise statement and prove tight lower and upper bounds based on the ZVT sum assuming real poles. Specifically, we show that for a given system order, the bandwidth is infimized by making one of the poles increasingly dominant and maximized by making all the poles identical. The impact of zeros and complex poles is also discussed.

We then turn to analog electronic *multipliers* in Chapter 5, which have found tremendous utility as frequency mixers in communication transceivers. We generalize the Gilbert cell topology into a circuit capable of multiplying an arbitrary number of signed inputs, analyze the large- and small-signal behavior of the circuit for an arbitrary device nonlinearity, and present a relatively intuitive way of looking at the frequency response of the multiplier.

Finally, Chapter 6 briefly discusses two other works done during my time here. The first is the design of an on-chip thermometer based on a proportional-to-absolute-temperature (PTAT) current for use in space-based solar power applications. The temperature sensor is operable from -25°C to 150°C, features a linear output characteristic with a gain of 7.6 ± 0.15 mV/°C over the operation range, and exhibits output variations bounded by ±1°C over process corners, ±2.5°C over anticipated worst-case supply variations, and ±6°C over device mismatch (3σ). The second is the design of a DC-DC converter which uses a novel "co-prime" cascading technique to achieve several performance improvements over the state-of-the-art: nearly triple the number of conversion ratios while occupying less than 40% chip area.

Chapter 2

TOWARD A GENERAL THEORY OF ELECTRICAL OSCILLATORS UNDER INJECTION, WITH APPLICATIONS TO LOCKING AND PULLING

2.1 Introduction

Injection locking refers to the fascinating natural phenomenon whereby an oscillator which is perturbed, or injected, by a sufficiently strong periodic signal at a nearby frequency will tend to oscillate at the injection frequency. In doing so, the oscillator also exhibits a fixed phase difference with the injection signal, and we say that the oscillator is *injection locked*. If the injection and free-running oscillation frequencies coincide, this phase difference is zero, implying that the oscillator is synchronized to the injection. In the event that the injection is too weak or has a frequency that is too far away from the oscillator's free-running one, the oscillator will instead be *pulled* by the injection, in which case the oscillator's spectrum displays a countably infinite number of tones [5], [6]. Due to the prevalence of oscillators and clocks in electronic systems, the need to synchronize them to external references on the one hand, and their propensity to be disturbed by (unwanted) external signals on the other, injection locking and pulling has been studied and utilized extensively, particularly within the context of electrical engineering [5], [7]–[23].

To formulate a general theory of injection locking and pulling in electrical oscillators, we attack the more general problem of describing how an oscillator responds when perturbed by an external signal of any type, periodic or not. Although such a theory of oscillators has been developed considerably from a mathematical standpoint (see [24]–[28], for e.g.), particularly in the dynamical systems community using Floquet theory, such analyses are often too abstract or too complicated for engineers to use them effectively and efficiently. On the other hand, the existing models of injection locking and pulling within the electrical engineering community may not be rigorous or general enough to produce sufficiently accurate results for a variety of scenarios. Therefore, there is a gap between these two approaches for studying the perturbation of electrical oscillators. We seek to bridge that gap.

This chapter is broadly organized into two parts. First, we begin by looking at the "simplest" case: a harmonic oscillator subjected to a small, sinusoidal injec-

tion. Our analysis of this situation sets the stage for our general framework, which aims to model the response of an oscillator of any type injected by a signal of arbitrary strength and shape, and which may or may not be periodic. Specifically, Section 2.2 uses a thought experiment involving an impulse train to introduce an alternative perspective into the injection locking of harmonic oscillators. Based on a mathematical analysis of the oscillator and injection waveforms, the lock range of an LC oscillator under a small sinusoidal injection, originally derived by Adler, is also obtained. Section 2.3 generalizes the thought experiment to obtain both the steady-state solution to Adler's equation as well as quantify how the *amplitude* of oscillation is affected. Section 2.4 briefly "stretches" the thought experiment even further to account for phase dynamics (Adler's equation) and amplitude modulation while serving to transition into this chapter's main material. Section 2.5 describes a generalized model of electrical oscillators that captures how the amplitude and phase respond to an injection of arbitrary size, shape, and periodicity. Section 2.6 explores some special cases of the proposed model and formulates the computation of the lock range as an optimization problem. Finally, Section 2.7 introduces another thought experiment, namely the "step response" of an oscillator, which gives us a new way of thinking about how an oscillator's amplitude and phase are affected by a finite, continuous injection, and asks whether or not the amplitude and phase responses can actually be conceptually decoupled.

2.2 A Thought Experiment: Injecting a Sinusoid with an Impulse Train

We start with the following thought experiment. Consider the sinusoidal output waveform of a harmonic electrical oscillator (i.e., an LC oscillator); specifically, we will use the charge swing $q(t)$ (across the capacitor) as our output variable (Fig. 2.1). Now, a small impulse of current is injected periodically onto this sinusoidal charge waveform in such a way that each injection does not alter the system's amplitude $q_{\max}$ (or energy)—it merely switches the polarity of the instantaneous charge (Fig. 2.2). We will adopt the convention where a positive injection of charge advances the phase (Fig. 2.3a), whereas injecting negative charge retards the phase (Fig. 2.3b). It should be apparent that for a given normalized injection strength $q_{\text{inj}}/q_{\max}$, there is only a single time instant during each period that the injection can occur. That is, there exists a relationship between the injection strength $q_{\text{inj}}/q_{\max}$ and the deviation between the injection period and the sinusoid's natural period $\Delta T := T_{\text{inj}} - T_0$. Also, the *injection phase*, defined as the phase difference between the *fundamental component* (in a Fourier series sense) of the impulse-train injection input and the

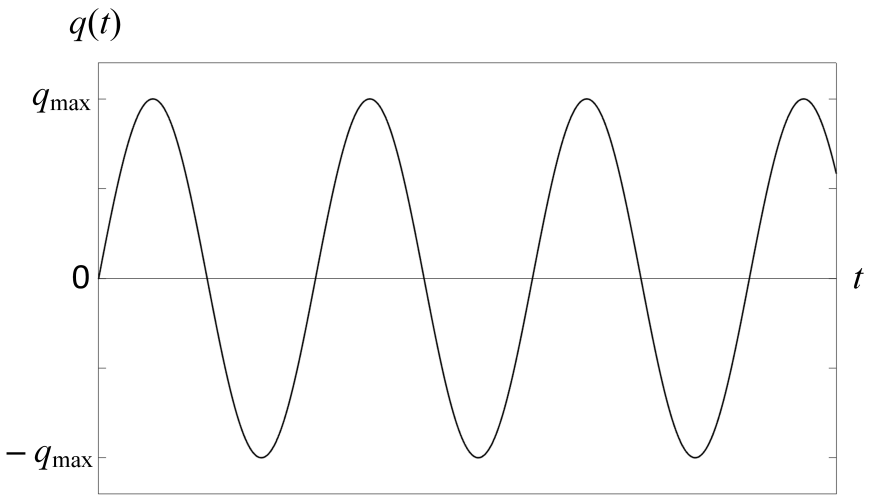

Figure 2.1: Unperturbed harmonic oscillator output.

oscillator output, must be $\theta = -\operatorname{sign}(q_{\text{inj}}) \cdot 90°$.

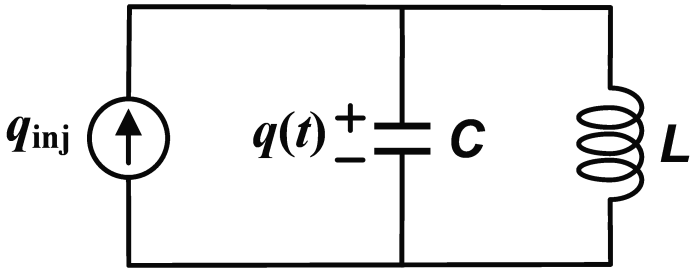

Figure 2.2: Idealized conceptual setup for the thought experiment of Section 2.2. Can we instantaneously deposit charge onto the capacitor without changing the energy stored in the LC tank? For a given amount of stored energy, how much charge q_{inj} should be *periodically* deposited to shift the frequency of the resultant output waveform $q(t)$ by a certain amount?

Let us compute the phase shift caused by each injection (per cycle) so we can specify the relationship between the frequency difference $\Delta\omega$ and the injection strength. By construction, each injection merely switches the polarity of the instantaneous charge, which, if we adopt a sine reference, changes the instantaneous phase from $-\phi$ to ϕ (where ϕ has the same sign as q_{inj}). The amount of charge needed to advance the phase by $\Delta\varphi = 2\phi$ is the negative of twice the charge at the instant when it is

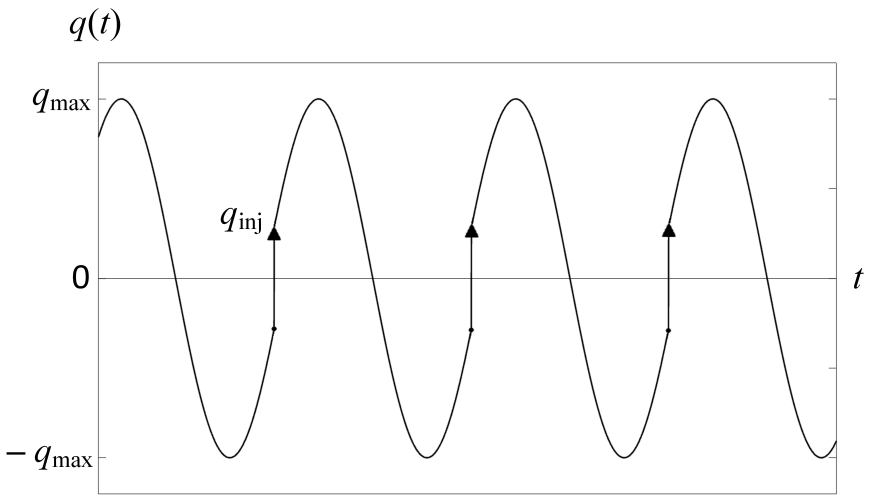

(a) $q_{\text{inj}} > 0$, $\omega_{\text{inj}} > \omega_0$

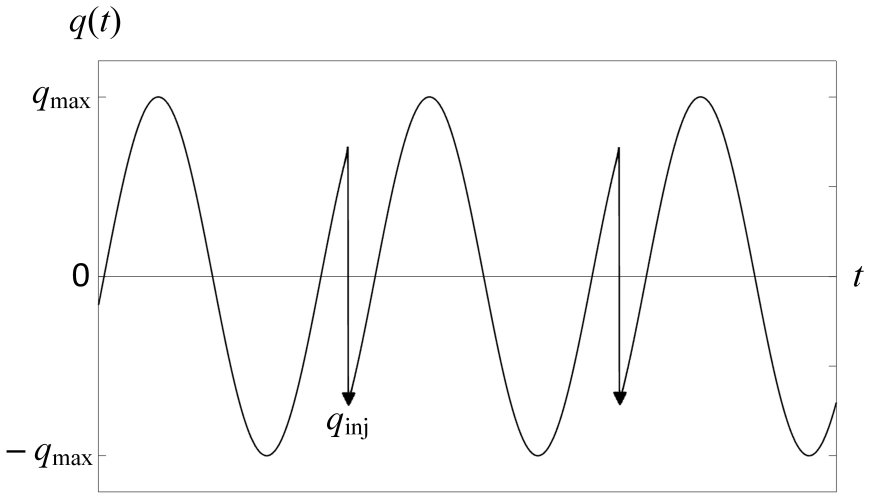

(b) $q_{\text{inj}} < 0$, $\omega_{\text{inj}} < \omega_0$

Figure 2.3: Illustration of the thought experiment: an impulse train of injected charge that (a) speeds up or (b) slows down the oscillation without altering the amplitude.

injected:

$$q_{\text{inj}} = -2q_{\text{max}} \sin(-\phi) = 2q_{\text{max}} \sin\left(\frac{\Delta\varphi}{2}\right). \tag{2.1}$$

This phase shift $\Delta\varphi$ corresponds to a period difference of

$$\Delta T \equiv T_{\text{inj}} - T_0 = -\frac{\Delta\varphi}{2\pi} \cdot T_0. \tag{2.2}$$

Noting that $\Delta T/T_0 = -\Delta\omega/\omega_{\text{inj}}$, the phase shift caused by each injection per cycle can thus be written as

$$\Delta\varphi = 2\pi\left(\frac{\Delta\omega}{\omega_{\text{inj}}}\right) = 2\sin^{-1}\left(\frac{q_{\text{inj}}}{2q_{\max}}\right). \tag{2.3}$$

Assuming the injection strength is much smaller than unity, we approximate

$$2\pi\left(\frac{\Delta\omega}{\omega_{\text{inj}}}\right) \approx \frac{q_{\text{inj}}}{q_{\max}}. \tag{2.4}$$

One might have noticed that our mathematical analysis thus far has really only dealt with an ideal LC tank or *resonator*—to extend our reasoning to LC *oscillators*, which feature nonlinear amplitude restoration, we augment the setup of Fig. 2.2 to the more complete circuit of Fig. 2.4.

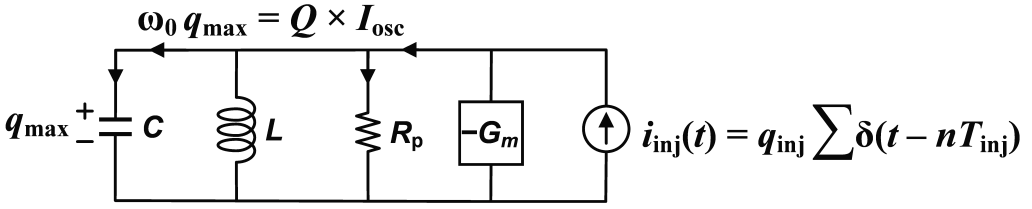

Figure 2.4: Schematic for the thought experiments discussed in Sections 2.2–2.4. The injection source $i_{\text{inj}}(t)$ is a current impulse train, periodically injecting a discrete amount of charge q_{inj} every T_{inj} time units. It should be apparent that all of this injected current flows onto the capacitor. The current exchanged between the inductor (L) and the capacitor (C) has a peak value of $\omega_0 q_{\max}$, whereas a peak current of I_{osc} is exchanged between the loss resistance R_P and the transconductor $-G_m$-cell. We are primarily interested in the steady-state behavior of this circuit.

Arguendo, let us look at the *fundamental component* of this current impulse train $i_{\text{inj}}(t)$; its amplitude, which we shall denote by I_{inj}, is

$$\begin{aligned} I_{\text{inj}} &= \frac{2}{T_{\text{inj}}}\left|\int_{T_{\text{inj}}} q_{\text{inj}} \sum_{n=-\infty}^{\infty} \delta(t - nT_{\text{inj}})\, e^{-j\omega_{\text{inj}}t}\, dt\right| \\ &= \frac{2\left|q_{\text{inj}}\right|}{T_{\text{inj}}} = \frac{\left|q_{\text{inj}}\right|\omega_{\text{inj}}}{\pi} \end{aligned} \tag{2.5}$$

Also, recall that the amplitude of the current sloshing within the LC tank is Q (the quality factor) times the oscillator current (see Fig. 2.4), which both comes from the active devices and is consumed by the parallel loss R_P:

$$\omega_0 q_{\max} = Q I_{\text{osc}}. \tag{2.6}$$

Taking the absolute value of Eq. (2.4) and using Eqs. (2.5) and (2.6) to substitute for q_{inj} and q_{max}, we get

$$|\Delta\omega| = \frac{\omega_0}{2Q}\frac{I_{\text{inj}}}{I_{\text{osc}}}, \tag{2.7}$$

which is Adler's lock range!

Notice that this signifies that the current setup is poised at the edge of the lock range, or more insightfully, that *all* of the injection current is "reactive" and is being used to change the oscillation frequency. Mathematically, this follows from the fact that the impulse train's fundamental component is in quadrature with the oscillation. The concept of the injection's "reactive" and "in-phase" components will be discussed in great detail in Chapter 3.

Also, carefully observe that this system is clearly nonlinear—changing the amplitude of the input changes the *frequency* of the output. As such, traditional techniques for dealing with linear systems (i.e., convolution or superposition integrals) cannot be used here.

2.3 Locked Oscillators: Adler's Equation's Steady-State Solution

What if the impulses do not occur at $\theta = \pm 90^\circ$ and instead are capable of instantaneously altering the system's energy? Over the course of a single injection period, we assume that the oscillation amplitude (or the system's energy) is completely restored by the oscillator's inherent nonlinearities, but the phase perturbation remains. Also, suppose the injections are set up such that the system returns to the same phase at each injection, resulting in a periodic waveform. Here, we need to specify the injection strength $q_{\text{inj}}/q_{\text{max}}$ *and* the injection phase θ to set ΔT. Let us calculate this relationship below.

Phase Perturbation

When charge is injected into the waveform, how does the oscillator respond afterwards? In a physical oscillator, this charge is dumped onto the capacitor within the tank—the inductor is not disturbed. Since the inductor current is proportional to the time derivative of the tank's voltage, we have the following invariant: the injection instantaneously alters $q(t)$ by q_{inj}, but it does not change $q'(t)$. Let us assume the injection occurs at some time t_0, which corresponds to an initial phase $\phi_i = \omega_0 t_0$. Without loss of generality, we adopt a sine reference: $q(t_0^-) = q_{\text{max}} \sin(\phi_i)$ and

$q'(t_0) = \omega_0 q_{\max} \cos(\phi_i)$. Then the oscillator's phase immediately post-injection is[1]

$$\begin{aligned}\phi_f &= \tan^{-1}\left(\frac{\omega_0 \cdot q(t_0^+)}{q'(t_0)}\right) \\ &= \tan^{-1}\left(\frac{\omega_0\left[q(t_0^-) + q_{\text{inj}}\right]}{q'(t_0)}\right) \\ &= \tan^{-1}\left(\tan\phi_i + \frac{q_{\text{inj}}}{q_{\max}}\sec\phi_i\right).\end{aligned} \tag{2.8}$$

Again assuming the injection strength is small, we linearize Eq. (2.8) about $q_{\text{inj}} = 0$ to get

$$\phi_f \approx \phi_i + \frac{q_{\text{inj}}}{q_{\max}}\cos\phi_i \tag{2.9}$$

and so the phase perturbation due to q_{inj} is

$$\Delta\varphi \coloneqq \phi_f - \phi_i = \frac{q_{\text{inj}}}{q_{\max}}\cos\phi_i. \tag{2.10}$$

To express this result in terms of θ, note that the phase of (the fundamental component of) the impulse train at any one of the injection instants is $\text{sign}(q_{\text{inj}}) \cdot \pi/2$ (since we adopted a sine reference), and so $\theta = \phi_i - \text{sign}(q_{\text{inj}}) \cdot \pi/2$. This gives

$$\Delta\varphi = -\,\text{sign}(q_{\text{inj}}) \cdot \frac{q_{\text{inj}}}{q_{\max}}\sin\theta = -\frac{\left|q_{\text{inj}}\right|}{q_{\max}}\sin\theta. \tag{2.11}$$

Notice that we have essentially computed Hajimiri's impulse sensitivity function (ISF) $\Gamma(\theta)$ [1], defined as the steady-state phase perturbation incurred due to an injection at a relative phase θ, normalized to the injection strength $q_{\text{inj}}/q_{\max}$. For an ideal harmonic LC oscillator, $\Gamma(\theta) = -\sin\theta$. We therefore postulate the following generalization for non-harmonic oscillators:

$$\Delta\varphi = \frac{\left|q_{\text{inj}}\right|}{q_{\max}}\Gamma(\theta), \tag{2.12}$$

We will return to this idea later in Section 2.5.

Amplitude Perturbation

For the sake of posterity (and because we will need this analysis later), we can also compute the instantaneous change in the oscillator's amplitude $q_{\max}$ using an energy

[1] Technically, Eq. (2.8) is only valid when $q'(t_0) > 0$. When $q'(t_0) < 0$, we need to add π so ϕ can take on angles outside of $[-\pi/2, \pi/2]$. However, this technicality is inconsequential to our analysis since $q'(t)$, and hence its sign, remain unaltered by the injection, and so π is merely an additive constant that vanishes when we consider by how much the phase *changes*: $\phi_f - \phi_i$.

conservation argument:

$$E_{\text{total}} = \frac{q(t)^2}{2C} + \frac{1}{2}Lq'(t)^2 = \frac{{q_{\max}}^2}{2C}. \tag{2.13}$$

Substituting in the time instant immediately after the injection ($t = t_0^+$) and noting that $LC = 1/{\omega_0}^2$, we get

$$q_{\max,f} = \sqrt{{q_{\max,i}}^2 + {q_{\text{inj}}}^2 + 2q_{\max,i}q_{\text{inj}} \sin\phi_i}. \tag{2.14}$$

Using $\phi_i = \theta + \text{sign}(q_{\text{inj}}) \cdot \pi/2$ once again, we arrive at

$$q_{\max,f} = \sqrt{{q_{\max,i}}^2 + {q_{\text{inj}}}^2 + 2\left|q_{\text{inj}}\right| q_{\max,i} \cos\theta}, \tag{2.15}$$

which we can also linearize about $q_{\text{inj}} = 0$ to get

$$\Delta q_{\max} \approx \left|q_{\text{inj}}\right| \cos\theta. \tag{2.16}$$

Thus, $\cos\theta$ is essentially the "amplitude ISF" for harmonic oscillators.

Adler's Steady-State Solution

Returning to our result Eq. (2.11), since Eqs. (2.2), (2.5), and (2.6) still hold, we arrive at the following:

$$\Delta\omega = -\frac{\omega_0}{2Q}\frac{I_{\text{inj}}}{I_{\text{osc}}} \sin\theta. \tag{2.17}$$

This is the steady-state solution to Adler's equation!

2.4 Stretching the Thought Experiment

Here, we will explore two conceptually intuitive (but not necessarily analytically rigorous) generalizations of the presented thought experiment. We will describe the generalizations as "hand-wavy" below to emphasize their ephemeral logical basis. These generalizations serve to demonstrate the potential insight which can be gleaned from the thought experiment, underline the significance of thinking about an oscillator's "impulse response", and set the stage of the main topic of this chapter: modeling oscillators under injection in the most general setting. Finally, note that these two generalizations are not mutually exclusive.

"Hand-Wavy" Generalization 1: Adler's Equation

Let us briefly consider what happens if the system has not yet reached steady state. That is, the system does not return to the same phase at each injection. Then the oscillator's response does not have a well-defined period. Still, we can imagine an

instantaneous oscillation frequency ω_{osc} whose deviation from the natural resonant frequency ω_0 is governed by Eq. (2.17). Noting that the instantaneous phase of the oscillator is $\omega_{\text{inj}}t + \theta$ and that ω_{osc} is its time-derivative, we get

$$\frac{d\theta}{dt} = \omega_0 - \omega_{\text{inj}} - \frac{\omega_0}{2Q}\frac{I_{\text{inj}}}{I_{\text{osc}}}\sin\theta \tag{2.18}$$

which is Adler's equation.

If we were to use the impulse sensitivity function to generalize this result, i.e., replace $-\sin(\theta) \rightarrow \Gamma(\theta)$, and use the total charge swing q_{max} instead of the oscillator current I_{osc}, we would get

$$\frac{d\theta}{dt} = \omega_0 - \omega_{\text{inj}} + \frac{I_{\text{inj}}}{2q_{\text{max}}}\Gamma(\theta). \tag{2.19}$$

Given the fact that the ISF and the perturbation projection vector (PPV) from [24] are the same [29], this equation is essentially an alternate way of expressing the so-called "Gen-Adler's equation" derived in [11].

"Hand-Wavy" Generalization 2: Steady-State Amplitude Modulation

It should not be surprising that for injections which *do* instantaneously alter the maximum charge swing (i.e., $\theta \neq \pm 90°$), the steady-state amount of energy in the system, and therefore the steady-state oscillation amplitude, are also affected by the impulse train. Let us quantify this. The free-running maximum charge swing $q_{\text{max,0}}$, which satisfies $\omega_0 q_{\text{max,0}} = QI_{\text{osc}}$ (see Fig. 2.4), is sustained by an energetic balance between the transconductor (which supplies I_{osc}) and the tank loss (which sets Q). Any deviation of the amplitude from $q_{\text{max,0}}$ decays exponentially with a time constant equal to the relaxation time of the parallel RLC circuit: $\tau_0 = 2R_P C = 2Q/\omega_0$. Each injection instantaneously changes the amount of energy stored in the LC tank, but the oscillator also continuously attempts to restore its amplitude to the free-running amount in accordance with the aforementioned exponential decay time dynamic. Eventually, this process reaches an equilibrium. Let δq_{max} denote the maximum charge swing *in excess* (positive or negative) of $q_{\text{max,0}}$ immediately after an injection. From Eq. (2.16), we know that each injection instantaneously changes the maximum charge swing by $\Delta q_{\text{max}} = \left|q_{\text{inj}}\right|\cos\theta$. In steady state, the oscillator must return to the same amplitude over each period, and so we require

$$\delta q_{\text{max}} e^{-T_{\text{inj}}/\tau_0} = \delta q_{\text{max}} - \Delta q_{\text{max}}. \tag{2.20}$$

Solving for δq_{max}, we get

$$\delta q_{\text{max}} = \frac{\Delta q_{\text{max}}}{1 - e^{-T_{\text{inj}}/\tau_0}}. \tag{2.21}$$

We know that between successive injections, the maximum charge swing as a function of time is given by

$$q_{\max}(t) = q_{\max,0} + \delta q_{\max} e^{-t/\tau_0}. \tag{2.22}$$

Arguendo, within the realm of our thought experiment, let us consider the *time-average* of the maximum charge swing:

$$\langle q_{\max} \rangle \coloneqq \frac{1}{T_{\text{inj}}} \int_0^{T_{\text{inj}}} q_{\max}(t)\, dt = q_{\max,0} + \frac{\tau_0}{T_{\text{inj}}} \delta q_{\max} \left(1 - e^{-T_{\text{inj}}/\tau_0}\right). \tag{2.23}$$

Substituting for $\delta q_{\max}$ from Eq. (2.21), we get

$$\langle q_{\max} \rangle = q_{\max,0} + \frac{\tau_0}{T_{\text{inj}}} \Delta q_{\max}. \tag{2.24}$$

This equation makes sense: the longer it takes to dissipate energy (a larger τ_0), or the more frequent the injections (a smaller T_{inj}), the more influence the injections will have on the average amplitude in steady state. Replacing $q_{\max}$ with $\langle q_{\max} \rangle$ in Eq. (2.11), one can show that the frequency shift is now

$$\Delta\omega = -\frac{\omega_0}{2Q} \frac{I_{\text{inj}} \sin\theta}{I_{\text{osc}} + I_{\text{inj}} \cos\theta}. \tag{2.25}$$

Further applying "Hand-Wavy" Generalization 1, namely that the instantaneous frequency shift before the onset of steady state is

$$\Delta\omega \equiv \frac{d\theta}{dt} + \omega_{\text{inj}} - \omega_0, \tag{2.26}$$

we get

$$\frac{d\theta}{dt} = \omega_0 - \omega_{\text{inj}} - \frac{\omega_0}{2Q} \frac{I_{\text{inj}} \sin\theta}{I_{\text{osc}} + I_{\text{inj}} \cos\theta}, \tag{2.27}$$

which is Mirzaei's Generalized Adler's equation [9]. We will return to Mirzaei's work numerous times from various perspectives in our subsequent discussions.

2.5 An ISF-based General Model of Oscillators under Injection

Following the spirit of the analysis in the previous section, we postulate the following generalized model for the response of an oscillator's amplitude and phase to *any* perturbation, of arbitrary size/shape and not necessarily periodic. In the most general setting, an oscillator can be represented by a phase variable ϕ and $n > 0$ amplitude variables $A_1, \ldots, A_n$. Note that for an oscillator under perturbation, the amplitude may be disturbed as well, and so the oscillator may not be traversing

along its free-running limit cycle. In this case, the concept of "phase" is not well-defined. Instead, ϕ more generally represents the *isochron* that the system resides on, where all points on the same isochron will eventually converge to the same point on the free-running limit cycle in the unperturbed case [27]. That is, an isochron is essentially an "equi-phase" manifold in the state space [21]. We assume that for most practical electronic oscillators, we can capture the essential behavior of all the A_i's via a single unit-less amplitude perturbation variable ξ. We define ξ such that if the nominal free-running oscillation voltage waveform is $f(\omega_0 t)$, then under injection the oscillation waveform is given by

$$\begin{aligned} v_{\text{osc}}(t) &\equiv [1 + \xi(t)] \cdot f[\phi(t)] \\ &\equiv [1 + \xi(t)] \cdot f(\omega_0 t + \varphi) \\ &\equiv [1 + \xi(t)] \cdot f\left(\omega_{\text{inj}} t + \theta\right), \end{aligned} \tag{2.28}$$

where we have defined three different phase variables: ϕ is the oscillator's "absolute" phase, φ is the oscillator's phase referred to free-running, and θ is the oscillator's phase referred to the injection (assuming it's periodic).

We now define two generalized impulse sensitivity functions (ISFs). Note that in our model, our ISFs will be normalized to the injection amplitude q_{inj}, not the injection strength $q_{\text{inj}}/q_{\text{max}}$ as Hajimiri has done so. Specifically, the *phase* ISF Γ can be defined as the rate of change of ϕ with respect to the amount of charge that is injected into the oscillator q_{inj}:

$$\Gamma(\phi, \xi) \coloneqq \frac{\partial \phi}{\partial q_{\text{inj}}}, \tag{2.29}$$

whereas the *amplitude* ISF Λ can be defined as the gradient of ξ with respect to the injected charge:

$$\Lambda(\phi, \xi) \coloneqq \frac{\partial \xi}{\partial q_{\text{inj}}}. \tag{2.30}$$

A key insight at this point is that both ISFs are functions of the oscillator's state (ϕ, ξ); that is, we write $\Gamma(\phi, \xi)$ and $\Lambda(\phi, \xi)$. Note that both ISFs are periodic in their first arguments ϕ with period 2π. The simulation and computation of Γ in the absence of ξ has been discussed extensively in numerous references [1]–[4], [30].

If the injection current $i_{\text{inj}}(t)$ is finite, then the amount of charge injected into the time interval $[t, t + dt]$ is always infinitesimally small, and hence within the *linear response region* [1], [21]. That is, the relationship between the amount by which the phase is perturbed $d\phi$ during this time interval features a linear relationship with the

amount of injected charge $i_{\text{inj}}(t)\,dt$. Therefore, we can write any of the following three equivalent relations:

$$\frac{d\phi}{dt} = \omega_0 + \Gamma(\phi, \xi) \cdot i_{\text{inj}}(t) \tag{2.31a}$$

$$\frac{d\varphi}{dt} = \Gamma(\omega_0 t + \varphi, \xi) \cdot i_{\text{inj}}(t) \tag{2.31b}$$

$$\frac{d\theta}{dt} = \omega_0 - \omega_{\text{inj}} + \Gamma\big(\omega_{\text{inj}} t + \theta, \xi\big) \cdot i_{\text{inj}}(t). \tag{2.31c}$$

For the amplitude, we know that ξ must return to 0 in steady state in the absence of perturbation ($i_{\text{inj}} = 0$). However, the dynamics under which this decay occurs may be of arbitrary order. We therefore postulate:

$$\sum_{k=1}^{n} a_k \frac{d^k \xi}{dt^k} = -\frac{\xi}{\tau_0} + \Lambda(\phi, \xi) \cdot i_{\text{inj}}(t) \tag{2.32}$$

where τ_0 is a first-order energy restoration time constant[2].

2.6 Special Cases

Periodic Injections and Time-Averaging

Note that in the locked case, we expect θ to be a constant (i.e., $d\theta/dt = 0$), since the oscillator's phase should track the injection phase, up to a constant delay. However, looking at Eq. (2.31c), and assuming a small injection so $\xi \ll 1$, we see that the product $\Gamma(\omega_{\text{inj}} t + \theta) \cdot i_{\text{inj}}(t)$ cannot be equal to a constant (specifically, $\omega_{\text{inj}} - \omega_0$) due to the presence of higher order harmonics that result from multiplying two periodic functions. Therefore, θ being a constant is *not* a solution to Eq. (2.31c). To alleviate this apparent paradox, we postulate that θ features small variations which vanish on *average* over a single injection period if the oscillator is locked. Mathematically, we appeal to the theory of averaging [31] to formulate the following time-averaged differential equations for the phase and amplitude:

$$\frac{d\theta}{dt} \approx \omega_0 - \omega_{\text{inj}} + \frac{1}{T_{\text{inj}}} \int_{T_{\text{inj}}} \Gamma\big(\omega_{\text{inj}} \tau + \theta, \xi\big)\, i_{\text{inj}}(\tau)\, d\tau \tag{2.33a}$$

$$\sum_{k=1}^{n} a_k \frac{d^k \xi}{dt^k} \approx -\frac{\xi}{\tau_0} + \frac{1}{T_{\text{inj}}} \int_{T_{\text{inj}}} \Lambda\big(\omega_{\text{inj}} \tau + \theta, \xi\big)\, i_{\text{inj}}(\tau)\, d\tau. \tag{2.33b}$$

[2]We conjecture that τ_0 is proportional to the ratio of the energy stored in the free-running oscillator to the power dissipated by the oscillator; therefore, $\tau_0 \propto Q/\omega_0$ where Q is the oscillator's quality factor, assuming it is well-defined.

Since both the injection and the ISFs are periodic with period T_{inj} and 2π respectively, we can expand them via a Fourier series:

$$\begin{aligned} i_{\text{inj}}(t) &= I_{\text{inj},0} + \sum_{m=1}^{\infty} I_{\text{inj},m} \sin\left(m\omega_{\text{inj}} t + \alpha_m\right) \\ \Gamma(\phi,\xi) &= \frac{\Gamma_0(\xi)}{2} + \sum_{m=1}^{\infty} \Gamma_m(\xi) \sin\left(m\phi + \beta_m\right) \\ \Lambda(\phi,\xi) &= \frac{\Lambda_0(\xi)}{2} + \sum_{m=1}^{\infty} \Lambda_m(\xi) \sin\left(m\phi + \gamma_m\right). \end{aligned} \tag{2.34}$$

Note that the DC components are defined in such a way to make the next set of equations easier to express. If we assume the dependence of the ISFs upon ξ is weak, then their Fourier coefficients become time-independent. This allows us to carry out the integrals of Eqs. (2.33) to obtain

$$\frac{d\theta}{dt} \approx \omega_0 - \omega_{\text{inj}} + \frac{1}{2} \sum_{m=0}^{\infty} I_{\text{inj},m} \Gamma_m \cos\left(m\theta + \beta_m - \alpha_m\right) \tag{2.35a}$$

$$\sum_{k=1}^{n} a_k \frac{d^k \xi}{dt^k} \approx -\frac{\xi}{\tau_0} + \frac{1}{2} \sum_{m=0}^{\infty} I_{\text{inj},m} \Lambda_m \cos\left(m\theta + \gamma_m - \alpha_m\right), \tag{2.35b}$$

where $\alpha_0 = \beta_0 = \gamma_0 = 0$. From Eqs. (2.35), we can see that the ability for an injection at the m^{th} harmonic to influence the oscillator depends directly upon the ISFs' m^{th} order harmonic. Furthermore, the formulation of Eqs. (2.35) can also serve as a foundation for the effective analysis of locking onto higher order harmonics (e.g., injection locked frequency dividers [32], [33]). For example, in [16], Maffezzoni derives the lock range for an oscillator injected by a small sinusoidal signal with amplitude I_{inj} and frequency near the free-running oscillator's m^{th} harmonic $m\omega_0$ to be

$$\omega_L = \frac{I_{\text{inj}}}{2q_{\max}} \Gamma_m, \tag{2.36}$$

where Γ_m is the amplitude of the m^{th} Fourier coefficient of Hajimiri's impulse sensitivity function (ISF), which can be computed using

$$\Gamma_m = \frac{1}{\pi} \left| \int_0^{2\pi} \Gamma(\theta) e^{-jm\theta} \, d\theta \right|. \tag{2.37}$$

Correcting for the normalization factor $q_{\max}$ which is absorbed into our ISF but not Hajimiri's, we can easily see from Eq. (2.35a) that Maffezzoni's lock range is

indeed the maximum achievable frequency difference $|\omega_{\text{inj}}/m - \omega_0|$ under the locked condition ($d\theta/dt = 0$) for an injection of the form $I_{\text{inj}} \sin(\omega_{\text{inj}} t)$.

As a simple example, consider the phase of an LC oscillator under small sinusoidal injection (so $\xi \ll 1$). The only nonzero terms in the Fourier series expansions of both the injection and the phase ISF are the first harmonic ($k = 1$), where $\Gamma_1 = 1/q_{\max}$ and $\beta_1 - \alpha_1 = 90°$, which yields Adler's equation.

The Lock Range

Using the time-averaged equations of Eqs. (2.33), we can obtain the one-sided upper/lower lock ranges by setting $d\theta/dt$ and $d\xi/dt$ to zero and respectively maximizing/minimizing the frequency difference $\omega_{\text{inj}} - \omega_0$ subject to the constraint that the amplitude remain constant on average over a single period. This constraint is an alternative way of stating that if the oscillator is injection locked, the injection should not introduce any energy into the oscillator on average. This leads us to the following optimization problem:

$$\omega_L^{\pm} = \max_{\theta,\xi} / \min_{\theta,\xi} \frac{1}{T_{\text{inj}}} \int_{\text{T}_{\text{inj}}} \Gamma\big(\omega_{\text{inj}}\tau + \theta, \xi\big)\, i_{\text{inj}}(\tau)\, d\tau \tag{2.38}$$

subject to

$$\frac{\xi}{\tau_0} = \frac{1}{T_{\text{inj}}} \int_{\text{T}_{\text{inj}}} \Lambda\big(\omega_{\text{inj}}\tau + \theta, \xi\big)\, i_{\text{inj}}(\tau)\, d\tau. \tag{2.39}$$

LC Oscillators under Large Sinusoidal Injection

Here, we seek to reduce the time-averaged model derived above to Mirzaei's "Generalized Adler's equation" [9], [10]. For an LC oscillator under the following sinusoidal injection: $i_{\text{inj}}(t) = I_{\text{inj}} \cos(\omega_{\text{inj}} t)$, we note from Eqs. (2.11) and (2.16) that the phase and amplitude ISFs are

$$\Gamma(\phi, \xi) = -\frac{1}{q_{\max}(1+\xi)} \sin\phi \tag{2.40}$$

and

$$\Lambda(\phi, \xi) = \frac{1}{q_{\max}} \cos\phi. \tag{2.41}$$

Note that the amplitude ISF does not depend on the amplitude perturbation ξ since an injection of charge will alter the amplitude by the same amount regardless of the current amplitude.[3] On the other hand, the same charge injection induces

[3] If this point is confusing, consider the following analogy. Let's say you are collecting apples, and I give you 3 apples. Then, the number of apples you have increases by 3 regardless of how many apples you already have.

less phase shift in oscillators with larger swings. Matching the injection current and the ISFs with the Fourier expansions of Eqs. (2.34), we have the following nonzero coefficients: $I_{\text{inj},1} = I_{\text{inj}}$, $\alpha_1 = \pi/2$, $\Gamma_1(\xi) = 1/[q_{\max}(1+\xi)]$, $\beta_1 = \pi$, $\Lambda_1(\xi) = 1/q_{\max}$, and $\gamma_1 = \pi/2$. Next, the energy restoration time constant for an RLC circuit can be computed to be $\tau_0 = 2R_PC = 2Q/\omega_0$. We will also approximate the dynamics of the amplitude restoration as being first order: so $a_1 = 1$ and $a_k = 0$ for $k > 1$. Finally, recall the identity $\omega_0 q_{\max} = QI_{\text{osc}}$.

Let us first turn our attention to the amplitude dynamics ξ. Either carrying out the integral of Eq. (2.33b) or using the harmonic decomposition of Eq. (2.35b), we get

$$2R_PC\frac{d\xi}{dt} = -\xi + \frac{I_{\text{inj}}}{I_{\text{osc}}}\cos\theta. \tag{2.42}$$

Since the oscillation amplitude under injection A is related to the free-running oscillation amplitude A_0 by $A = (1+\xi)A_0$, we have that

$$\frac{dA}{dt} = A_0\frac{d\xi}{dt}. \tag{2.43}$$

Therefore, the differential equation in the amplitude perturbation ξ can be rewritten as

$$2R_PC\frac{dA}{dt} + A = A_0\left(1 + \frac{I_{\text{inj}}}{I_{\text{osc}}}\cos\theta\right). \tag{2.44}$$

Recalling that the free-running oscillation amplitude is given by $A_0 = I_{\text{osc}}R_P$, we finally get

$$2R_PC\frac{dA}{dt} + A = R_P\left(I_{\text{osc}} + I_{\text{inj}}\cos\theta\right), \tag{2.45}$$

which matches Mirzaei's Generalized Adler's equation for the amplitude up to a typo[4] (c.f. Eq. (7) in [10]) , if we note that $I_{\text{osc}} = 4I/\pi$ and that our θ is equivalent to their $\theta - \theta_{\text{inj}}$. Next, we turn to the phase. Approximating ξ with its zeroth order steady-state value $\xi \approx I_{\text{inj}}\cos\theta/I_{\text{osc}}$, Eqs. (2.33a) or (2.35a) can be written as

$$\frac{d\theta}{dt} = \omega_0 - \omega_{\text{inj}} - \frac{\omega_0}{2Q}\frac{I_{\text{inj}}\sin\theta}{I_{\text{osc}} + I_{\text{inj}}\cos\theta}, \tag{2.46}$$

which is equivalent to Mirzaei's Generalized Adler's equation for the phase (c.f. Eq. (8) in [10]).

Finally, we can solve the optimization problem posed in Section 2.6 to obtain the large-signal lock range for an LC oscillator under sinusoidal injection. Denote the

[4]Eq. (7) in [10] is missing the factor of 2 in front of $R_PC(dA/dt)$.

optimal values for the decision variables as θ^* and ξ^*. The constraint Eq. (2.39) immediately yields

$$\xi^* = \frac{I_{\text{inj}}}{I_{\text{osc}}} \cos\theta^*. \tag{2.47}$$

Substituting this into the objective Eq. (2.38) and optimizing over θ yields[5]

$$\cos\theta^* = \begin{cases} -\dfrac{I_{\text{inj}}}{I_{\text{osc}}}, & I_{\text{inj}} \leq I_{\text{osc}} \\ -\dfrac{I_{\text{osc}}}{I_{\text{inj}}}, & I_{\text{inj}} \geq I_{\text{osc}} \end{cases} \tag{2.48}$$

The second case actually indicates that the objective is unbounded. This yields the following lock range:

$$\omega_L = \begin{cases} \dfrac{\omega_0}{2Q}\dfrac{I_{\text{inj}}}{I_{\text{osc}}}\dfrac{1}{\sqrt{1-\dfrac{{I_{\text{inj}}}^2}{{I_{\text{osc}}}^2}}}, & I_{\text{inj}} < I_{\text{osc}} \\ +\infty \qquad\qquad , & I_{\text{inj}} \geq I_{\text{osc}} \end{cases} \tag{2.49}$$

which is the lock range derived by Razavi [5]. Note that the lock range is not actually infinite when the injection current exceeds the oscillator current. In that (unlikely) scenario, the stability of the system from an energetics standpoint becomes prominent and the phase and amplitude models proposed above begin to break down. This is explored more in Chapter 3.

2.7 An Aside: The "Step Response" of an Oscillator

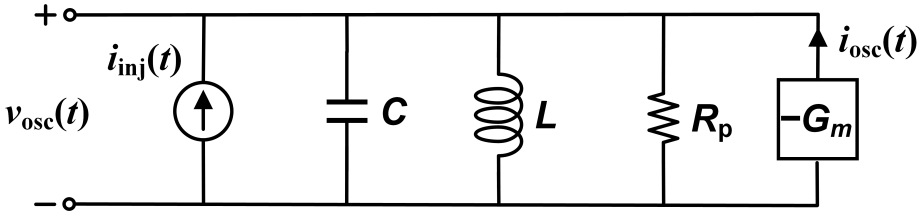

Figure 2.5: Schematic of the ideal LC oscillator used as the simulation test bench. The component values are $L = 5\ \mu$H, $C = 5.066059182117$ nF, $R_P = 1$ kΩ, and $I_{\text{bias}} = 1$ mA. This leads to a free-running oscillation frequency of $f_0 = 1/(2\pi\sqrt{LC}) \approx 1$ MHz and oscillation amplitude of $V_0 = (4/\pi)I_{\text{bias}}R_P \approx 1.27$V.

Again, we start with a thought experiment. Consider an oscillator whose phase ISF, $\Gamma(\cdot)$, has zero DC component, such as an ideal LC oscillator. We then inject into

[5]Note that the lock range is *symmetric* for this scenario. In other words, $\omega_L^+ = \omega_L^-$ and so maximizing and minimizing the objective yield the same result.

this oscillator a constant pulse of current whose duration is equal to a single period. If the injection is sufficiently small, then the instantaneous phase perturbation from free-running is also small: $\varphi \ll \omega_0 t$, and so we can approximate the the integral form of Eq. (2.31b) as

$$\varphi(t) \approx \int_{t_0}^{t} \Gamma(\omega_0 \tau)\, i_{\text{inj}}(\tau)\, d\tau. \tag{2.50}$$

Integrating over the injection's duration, where $i_{\text{inj}}(t) = I_{\text{inj}}$, to compute the induced phase perturbation, we get

$$\varphi(T) \approx I_{\text{inj}} \int_{T} \Gamma(\omega_0 \tau)\, d\tau \tag{2.51}$$

which evaluates to 0 if the phase ISF has no DC component. To explore this idea, we used SpectreRF to simulate an ideal LC oscillator (see Fig. 2.5), which is constructed as a parallel RLC tank connected to an ideal transconductor (i.e., one whose output current is equal to $i_{\text{osc}} = \text{sign}(v_{\text{osc}}) \cdot I_{\text{bias}}$).

However, what we notice from simulation is that the situation is not actually as simple as the previous argument seems to suggest. First and foremost, as depicted in Fig. 2.6, the phenomenon of incurring zero phase shift still holds true for large injections. Of course, if the pulse's duration is not an integer multiple of a single period, the injection does perturb the oscillator's phase by a nonzero amount in steady state. In the simulations of Fig. 2.7, our injection persists for only a half period, for example. Exploring this concept of injecting a *constant* current into an oscillator a little bit more generally, let us look at the oscillator's "step response," namely what happens when an indefinite pulse of constant current is suddenly injected into the oscillator. This scenario is depicted in Fig. 2.8. Notice that in steady state, the oscillation *amplitude* remains unchanged by the step injection. This makes sense, since in steady state, the DC injection current is simply consumed in its entirety by the inductor and so does not affect the energetics of the oscillator.

One crucial way of thinking about what happens when there is a sudden change in the injection current is that there is an immediate disturbance in the tank's harmonic balance. More specifically, recall that an inductor cannot withstand an instantaneous change in its current, while a capacitor cannot withstand an instantaneous change in its voltage. The latter further implies that the resistor, which is in parallel with the capacitor, cannot sustain an instantaneous change in either its voltage or its current. Therefore, the sudden change in the injection current must initially flow in its entirety onto the capacitor. This statement can be extended to non-LC oscillators.

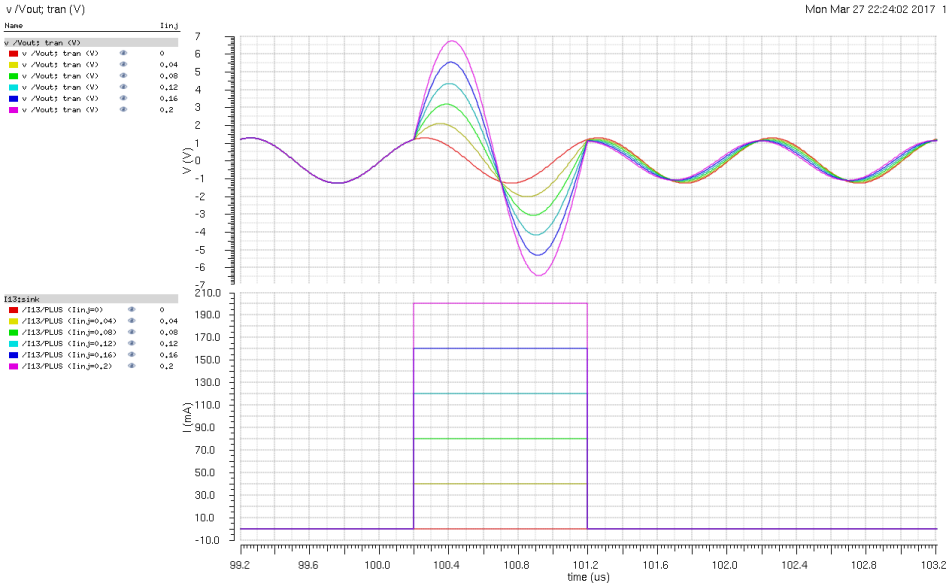

(a) Transient

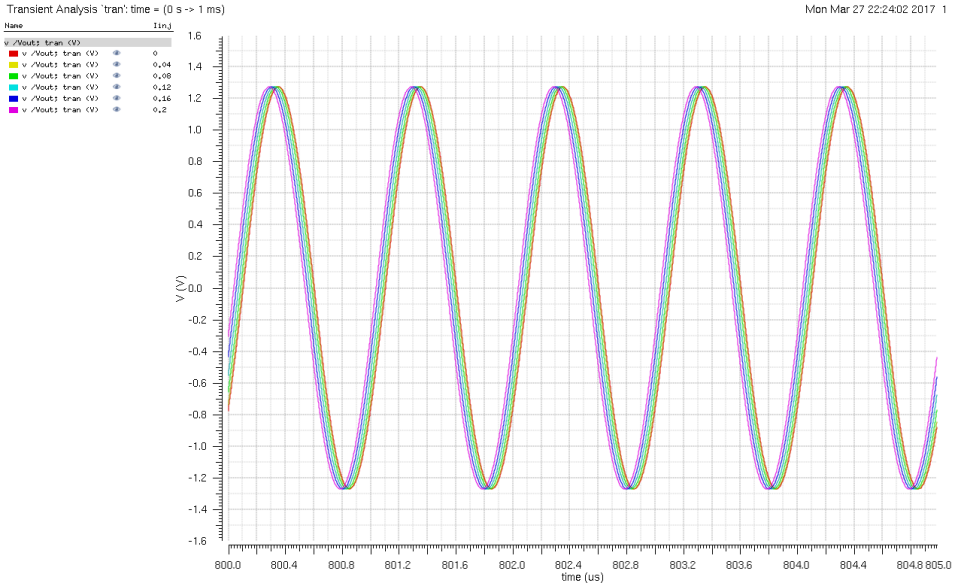

(b) Steady-State

Figure 2.6: Constant injections of varying amplitudes into an ideal LC oscillator over a single period (1 μs). Notice that the oscillator returns to the same phase in every instance. The red waveform corresponds to no injection: $i_{\text{inj}} = 0$.

Any immediate change in the injection current of an oscillator must flow onto the capacitance of the injection node, since the capacitor is the only circuit element that can withstand an instantaneous change in its current without resulting in a corresponding abrupt change in its voltage.

To conclude, one might wonder of what use was the thought experiment conducted

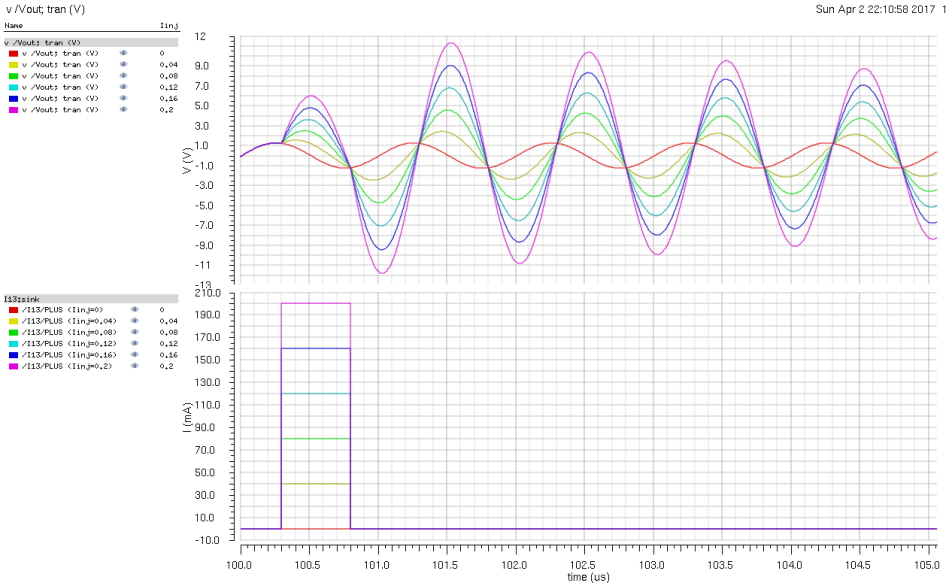

(a) Transient

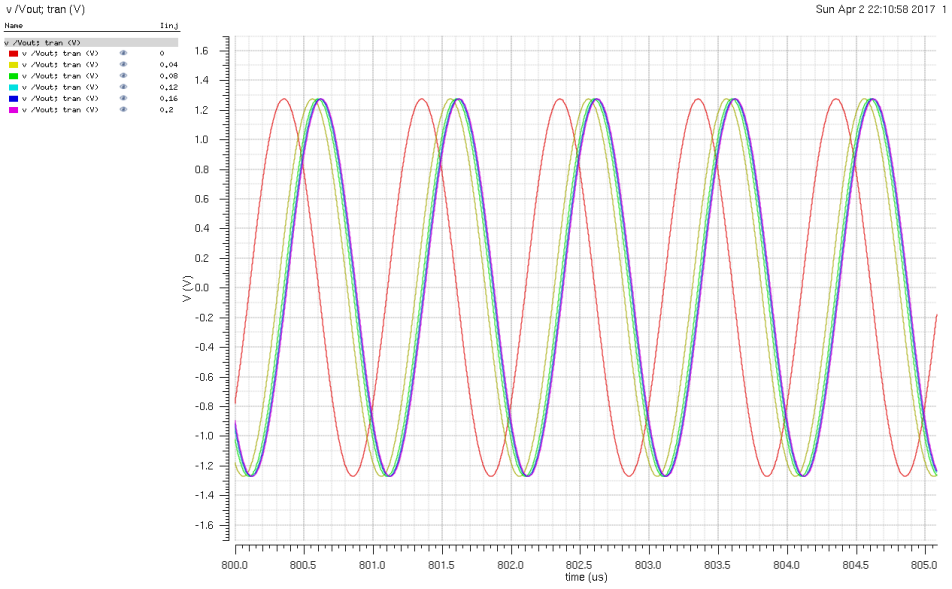

(b) Steady-State

Figure 2.7: Constant injections of varying amplitudes into an ideal LC oscillator over a half period (0.5 μs), resulting in a net perturbation to the oscillator's phase. The red waveform corresponds to no injection: $i_{\text{inj}} = 0$.

in this section. The utility of this thinking about the step response of an oscillator lies in the fact that any signal can be modeled to an arbitrary degree of accuracy by a superposition of step functions. Therefore, if the response to a sudden but finite change in the injection is understood, a powerful road-map toward a generalized perturbation theory of oscillators could easily be paved.

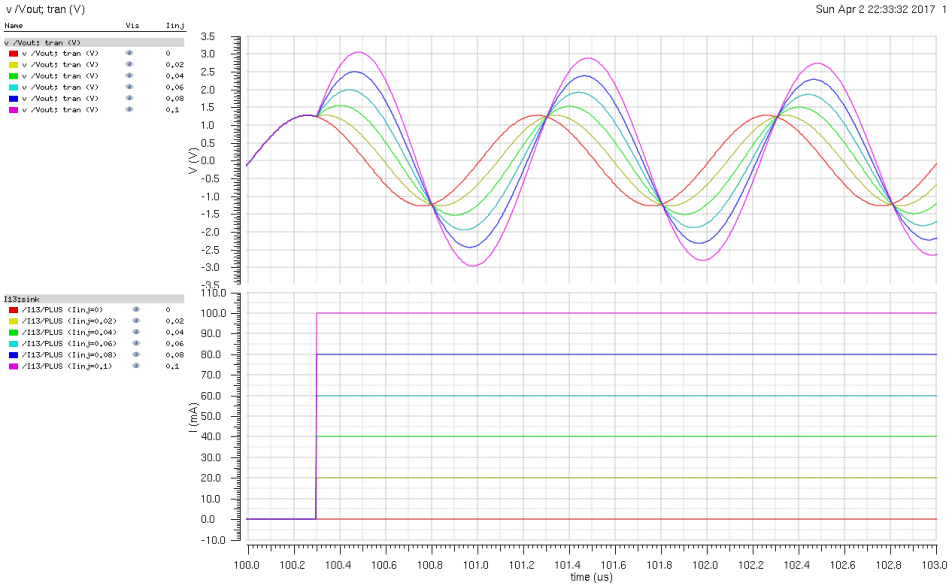

(a) Transient

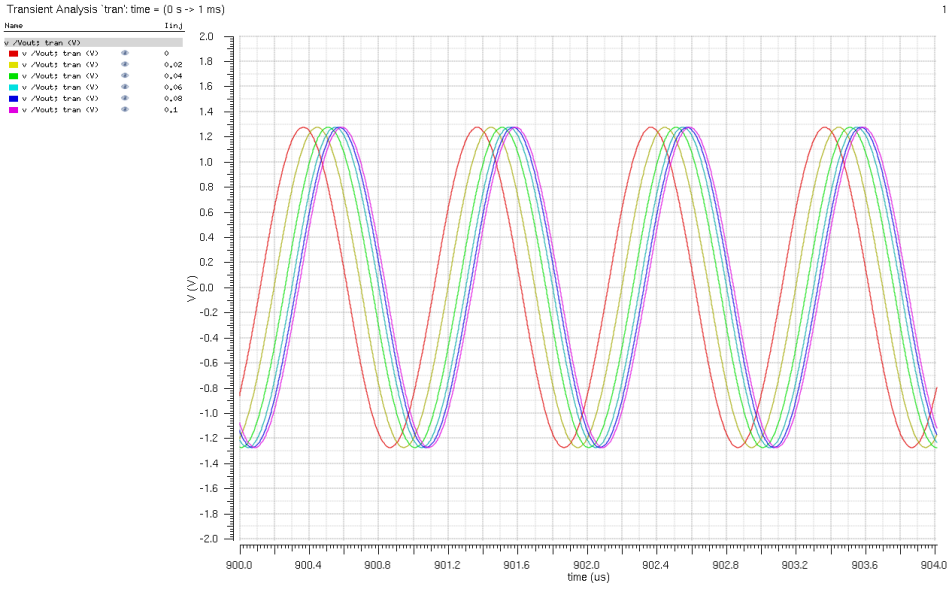

(b) Steady-State

Figure 2.8: The "step response" of an oscillator: constant, indefinite injections of varying amplitudes into an ideal LC oscillator. The red waveform corresponds to no injection: $i_{\text{inj}} = 0$.

2.8 Summary and Future Directions

In this chapter, we formulated a general analytical framework for modeling electrical oscillators under injection. We did so by extending Hajimiri's impulse sensitivity function (ISF) [1] for modeling how the oscillator's phase responds to small injections of current, which has found great success in analyzing oscillator phase noise.

We started off by considering a "contrived" periodic waveform—the steady-state response of a harmonic oscillator injected with a periodic train of impulses subject to certain constraints. This thought experiment gave us new physical insight into how injection locking works, yielded an alternative, simpler derivation of Adler's equation, and laid the groundwork for using the ISF to compute how the oscillator's amplitude and phase responds to injections of arbitrary size and shape.

Potential Application: Phase Noise in Locked Oscillators

It would be interesting and potentially fruitful to use this framework to analyze the phase noise characteristics of injection locked oscillators. Intuitively, injections "take time" to influence the phase of an oscillator, quantified in some sense by the phase difference θ. Thus, injection locking high-pass filters the free-running phase noise $\mathcal{L}_0\{\Delta\omega\}$ and low-pass filters the injection's phase noise $\mathcal{L}_{\text{inj}}\{\Delta\omega\}$, yielding a total phase noise of [34]

$$\mathcal{L}\{\Delta\omega\} = \frac{\Delta\omega^2}{\Delta\omega^2 + {\omega_c}^2}\mathcal{L}_0\{\Delta\omega\} + \frac{{\omega_c}^2}{\Delta\omega^2 + {\omega_c}^2}\mathcal{L}_{\text{inj}}\{\Delta\omega\}, \tag{2.52}$$

where the filter's 3-dB cutoff frequency is

$$\omega_c = \sqrt{{\omega_L}^2 - \Delta\omega^2} = \omega_L \cos\theta. \tag{2.53}$$

Given that a free-running oscillator's phase noise "diffuses" according to a Wiener process (i.e., Brownian motion) [35], how would a periodic injection of charge into the oscillator change the statistics of the phase and the output voltage?

Conclusion

This chapter demonstrated how reasoning at the right level of abstraction allows us to reduce the complicated behavior of a rather complicated system—an oscillator under injection—down to an intuitive and computationally feasible framework which possesses a powerful level of generality. In the next chapter, we take a different approach and apply a mathematically rigorous, fully detailed analysis of a specific type of oscillator under a specific type of injection. We will then see how the results thus obtained connect with those derived in this chapter.

Chapter 3

AN EXACT ANALYSIS OF LC OSCILLATORS UNDER SINUSOIDAL INJECTION

3.1 Introduction

The behavior of LC oscillators under a sinusoidal injection of current has been studied pretty extensively over the years, first by Adler [7] and then by Razavi [5] and Mirzaei [9], [10], among others. Still, the analyses thus far have made various assumptions that yield a non-exact solution which is inaccurate in various scenarios. For example, [5] predicts an infinite lock range when the injection current exceeds the oscillator current, which can be verified via simulation to be untrue. All of these analyses have also glossed over the important question of how the oscillator's core nonlinearity (typically known as the transconductor) reacts to phase modulation in the oscillation voltage, an issue of critical concern for pulled oscillators. This chapter derives an exact, large-signal model of injection locked LC oscillators from a physical analysis of the currents flowing through the circuit in sinusoidal steady state.

The material is organized as follows. Section 3.2 sets up the problem statement and introduces notation. Section 3.3 shows how the lock range derived by Razavi [5] can be rigorously obtained using a purely geometric argument, even though such an analysis fails to provide any physical insight into the lock edge. Section 3.4 presents a physically based analysis which calculates the various currents flowing within the oscillator, as well as derives separate necessary and sufficient conditions for injection locking to occur. Section 3.5 discusses the physics of the edge of lock in detail and explores why an injection locking condition that is both sufficient and necessary does not exist, and Section 3.6 organizes the results of the analysis. Section 3.7 draws some connections between the presented analysis and the current literature. Section 3.7 corrects a small analytical error we found in the prominent reference [5]. We conclude the chapter in Section 3.8.

3.2 Statement of the Problem

Our problem setup is depicted in Fig. 3.1. The oscillator is modeled as an ideal LC tank in parallel with a loss resistance R_P, compensated for by an active transconductor (i.e., the $-G_m$-cell). The transconductor's instantaneous current $i_{G_m}(t)$ is a

memoryless, time-invariant, nonlinear function $f(\cdot)$ of the instantaneous voltage $v_{\text{osc}}(t)$ across it. We adopt the usual assumption [2], [9], [10] that the LC tank filters out all but the fundamental component of the transconductor current $i_{G_m}(t)$ near the tank's resonant frequency $\omega_0 = 1/\sqrt{LC}$, resulting in a sinusoidal oscillation voltage $v_{\text{osc}}(t)$ with amplitude V_{osc} and frequency ω_{osc}. We will refer to this component of $i_{G_m}(t)$ as the *oscillator current*; its phasor $\overrightarrow{I}_{\text{osc}}$ is shown in Fig. 3.1. This set of abstractions allows us to henceforth work exclusively with phasors in sinusoidal steady state.

Since the $-G_m$-cell is memoryless, time-invariant, and active, the oscillation voltage and the oscillator current must be in phase. To see this, assume without loss of generality that $v_{\text{osc}}(t) = V_{\text{osc}} \cos(\omega_{\text{osc}} t)$, which is an even, periodic function of time with frequency ω_{osc}. Since $f(\cdot)$ is memoryless and time-invariant, we can see that $i_{G_m}(t) = f[v_{\text{osc}}(t)]$ is also an even, periodic function of time with the same fundamental period. Since the Fourier series representation of an even, periodic function contains no "sine" components, we can expand the transconductor current as

$$i_{G_m}(t) = \sum_{n=0}^{\infty} G_n \cos\left(n\omega_{\text{osc}} t\right). \tag{3.1}$$

Therefore, the fundamental component of $i_{G_m}(t)$ is $G_1 \cos\left(\omega_{\text{osc}} t\right)$, which is in phase with $v_{\text{osc}}(t)$. Time invariance of f then completes our argument for a sinusoidal $v_{\text{osc}}(t)$ with an arbitrary phase reference. The amplitude of the oscillator current $I_{\text{osc}} = G_1$ can thus be computed to be

$$I_{\text{osc}} = \frac{2}{T} \int_{-T/2}^{T/2} f[V_{\text{osc}} \cos(\omega_{\text{osc}} t)] \cdot \cos(\omega_{\text{osc}} t)\, dt. \tag{3.2}$$

For example, if the transconductor is a hard-limited current commutator $f(x) = \text{sign}(x) \cdot I_{\text{bias}}$, then $I_{\text{osc}} = (4/\pi) I_{\text{bias}}$. This serves as a reasonable model of a cross-coupled differential pair wherein $I_{\text{bias}} = I_{\text{tail}}/2$ (or for complementary pairs $I_{\text{bias}} = I_{\text{tail}}$). Finally, observe the very important fact that because the oscillator current $\overrightarrow{I}_{\text{osc}}$ is in phase with the oscillation voltage $\overrightarrow{V}_{\text{osc}}$, it can only flow into the parallel loss resistance R_P.

In the absence of injection ($\overrightarrow{I}_{\text{inj}} = 0$), the oscillation frequency is[1] $\omega_{\text{osc}} = \omega_0$, and the oscillation amplitude is $V_{\text{osc}} = I_{\text{osc}} R_P$ [2]. Now, suppose the oscillator is perturbed by some periodic injection current $i_{\text{inj}}(t)$ at a frequency ω_{inj} near ω_0. We

[1] In actuality, higher order harmonics in $i_{G_m}(t)$ slightly disrupt the tank's harmonic balance and *decrease* the free-running oscillation frequency away from resonance [36], [37].

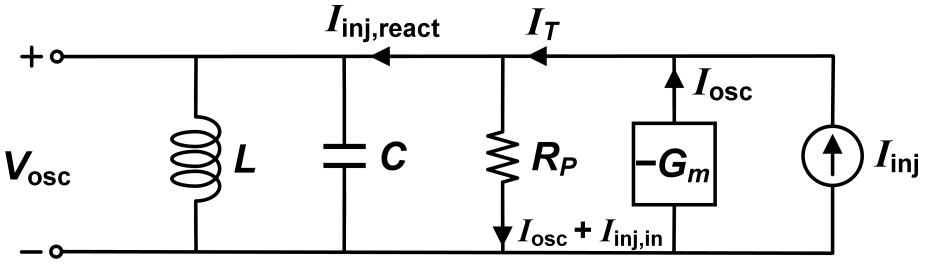

Figure 3.1: Conceptual circuit model of an injection locked LC oscillator. All depicted signals are sinusoidal steady-state phasors at ω_{inj}, the injection frequency.

can once again assume that the filtering action of the LC tank leaves us with only its fundamental component at ω_{inj}, whose phasor we shall denote by $\overrightarrow{I}_{\text{inj}}$. In order for the circuit to oscillate at the injection frequency (i.e., for the oscillator to be injection locked) if $\omega_{\text{inj}} \neq \omega_0$, current must be supplied to the LC tank, since it no longer appears as an open circuit at ω_{inj} as it would at resonance. Based on our reasoning above, this current, which is $\pm 90^\circ$ out of phase with $\overrightarrow{V}_{\text{osc}}$, cannot be provided by the transconductor. Instead, this *reactive* current must be supplied in its entirety by the injection—we thus label it as $\overrightarrow{I}_{\text{inj,react}}$. This key observation forms the basis of all the analysis that follows. The remaining injection current, denoted as $\overrightarrow{I}_{\text{inj,in}}$, is obviously in parallel with $\overrightarrow{V}_{\text{osc}}$ and $\overrightarrow{I}_{\text{osc}}$. Therefore, we have the following phasor decomposition of the injection current:

$$\overrightarrow{I}_{\text{inj}} = \overrightarrow{I}_{\text{inj,in}} + \overrightarrow{I}_{\text{inj,react}}, \tag{3.3}$$

which, by the Pythagorean theorem implies

$$I_{\text{inj}}{}^2 = I_{\text{inj,in}}{}^2 + I_{\text{inj,react}}{}^2. \tag{3.4}$$

Finally, by KCL, it is obvious that the total current $\overrightarrow{I}_T$ flowing into the lossy tank (LC tank + parallel resistance R_P) comes from the oscillator and injection currents:

$$\overrightarrow{I}_T = \overrightarrow{I}_{\text{osc}} + \overrightarrow{I}_{\text{inj}}. \tag{3.5}$$

These decompositions are depicted conceptually in Fig. 3.1 and graphically in Fig. 3.2.

Now, we will introduce a new parameter, χ_{tank}, defined as the ratio of the tank's parallel resistance R_P to the LC tank's reactance (or the ratio of the real and imaginary

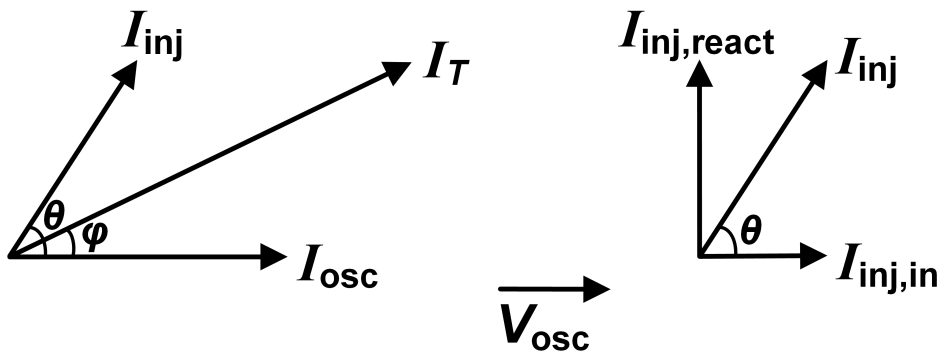

Figure 3.2: Phasor diagram depicting the injection current, the oscillator current, the tank current, the injection current's orthogonal decomposition, and the phase of the oscillation voltage.

parts of the entire RLC tank's impedance) at the injection frequency ω_{inj}:

$$\chi_{\text{tank}} \coloneqq \frac{R_P}{\omega_{\text{inj}} L}\left(1 - \frac{{\omega_{\text{inj}}}^2}{{\omega_0}^2}\right). \tag{3.6}$$

If the injection and free-running frequencies are close to one another as most papers assume, or more precisely $|\Delta\omega| \ll \omega_0$ where $\Delta\omega \coloneqq \omega_{\text{inj}} - \omega_0$ is the frequency difference, we can approximate

$$\chi_{\text{tank}} \approx -2Q\left(\frac{\Delta\omega}{\omega_0}\right) \tag{3.7}$$

where $Q = R_P/\omega_0 L$ is the tank's quality factor. The importance and convenience of this parameter χ_{tank} will become apparent later on. For now, observe that 1) $|\chi_{\text{tank}}|$ is equal to the ratio of the oscillator's reactive current to its in-phase current at the injection frequency which serves as a measure of how "far away" the tank is from resonance at ω_{inj}, and 2) the lock range (defined as the range of injection frequencies for which the oscillator remains locked) should be expressed in terms of $|\chi_{\text{tank}}|$ instead of $\Delta\omega$ in case the approximation of Eq. (3.7) does not hold.

Finally, let us discuss the various angles in Fig. 3.2. We see that $\phi \coloneqq \angle\overrightarrow{V}_{\text{osc}} - \angle\overrightarrow{I}_T$ is the phase difference between the oscillation voltage and the tank current, which is equal to the phase of the tank's impedance. It is bounded between $\pm 90°$ since the tank has a positive conductance. So,

$$\phi = \tan^{-1}\left[\frac{R_P}{\omega_{\text{inj}} L}\left(1 - \frac{{\omega_{\text{inj}}}^2}{{\omega_0}^2}\right)\right] = \tan^{-1}(\chi_{\text{tank}}). \tag{3.8}$$

Next, $\theta \coloneqq \angle \overrightarrow{V}_{\text{osc}} - \angle \overrightarrow{I}_{\text{inj}}$ is the phase difference between the oscillation voltage and the injection current. We will adopt the convention that the angular domain is $\theta \in [-\pi, \pi]$. Much of the literature on injection locking and pulling focuses on the dynamics of θ, the most notable result being Adler's original equation [7]. Note that ϕ and θ are both positive (negative) if the voltage *leads* (*lags*) the currents, which occurs if $\Delta\omega < 0$ ($\Delta\omega > 0$) and we inject below (above) resonance. In the analysis that follows, we will assume for the sake of simplicity that $\phi \in [0, \pi/2]$ and $\theta \in [0, \pi]$ (i.e., they merely denote angles *between* phasors regardless of which leads/lags), with the understanding that the correct sign can be supplied.

On a final note, before proceeding with the formal analysis, one should be able to intuit that a *sufficient* condition for the oscillator to lock is that the injection be large enough to supply all of the reactive current the LC tank needs to oscillate away from resonance at the injection frequency. Now that the problem setup has been explicated, our objectives for this section are to 1) examine the lock range and 2) compute the steady-state oscillation amplitude V_{osc} and phase θ of an injection locked oscillator.

3.3 A Geometric Analysis of the Lock Range

We will initially proceed along the same lines as Section II of [5]. The law of sines applied to the left diagram of Fig. 3.2 gives

$$\frac{\sin\phi}{I_{\text{inj}}} = \frac{\sin(\pi - \theta)}{I_T} = \frac{\sin\theta}{I_T}. \tag{3.9}$$

To eliminate the tank current, we use the law of cosines:

$$\begin{aligned} {I_T}^2 &= {I_{\text{inj}}}^2 + {I_{\text{osc}}}^2 - 2I_{\text{inj}}I_{\text{osc}}\cos(\pi - \theta) \\ &= {I_{\text{inj}}}^2 + {I_{\text{osc}}}^2 + 2I_{\text{inj}}I_{\text{osc}}\cos\theta. \end{aligned} \tag{3.10}$$

Combining both equations, we get

$$\sin\phi = \frac{I_{\text{inj}}\sin\theta}{\sqrt{{I_{\text{osc}}}^2 + {I_{\text{inj}}}^2 + 2I_{\text{osc}}I_{\text{inj}}\cos\theta}}, \tag{3.11}$$

Now, we would like to use this framework to find the lock range. That is, given the injection and oscillator current amplitudes, what is the maximum allowable frequency deviation $\Delta\omega$? Well, we know that $\Delta\omega$ relates to the geometry of the situation through ϕ, the angle between the tank current $\overrightarrow{I}_T$ and the tank voltage $\overrightarrow{V}_{\text{osc}}$; specifically, one can verify from Eq. (3.8) that as ω_{inj} deviates from ω_0, the

magnitude of ϕ increases monotonically. But, maximizing ϕ using Eq. (3.11) in an *unconstrained* manner would not work, since nothing mathematically prevents ϕ from exceeding $\pi/2$, which is physically impossible. Instead, we need a surrogate parameter that reaches its maximum when $|\Delta\omega| \to \infty$ and $\phi = \pi/2$. This suggests maximizing $\sin\phi$, which also increases monotonically with the frequency difference (since $\sin x$ increases monotonically with x over the domain $0 \leq x \leq \pi/2$), but reaches its maximum (unity) when $\phi = \pi/2$. The maximum value of $\sin\phi$ can then be mapped back to a maximum frequency difference, or more fundamentally, a maximum value for χ_{tank}.

Next, what should we maximize with respect to? Well, the only remaining parameter that changes when the injection frequency changes is θ, the phase difference the injection $\overrightarrow{I}_{\text{inj}}$ bears with the the oscillator current $\overrightarrow{I}_{\text{osc}}$ or the oscillation voltage $\overrightarrow{V}_{\text{osc}}$. Since $\theta \mapsto \cos\theta$ is an isomorphism over $\theta \in [0, \pi]$, a more convenient decision variable would be $\cos\theta$. So, let us define $x \coloneqq \cos\theta$ and note that $\sin\theta = \sqrt{1 - x^2}$ since $\theta \in [0, \pi]$. Then we solve

$$\frac{d}{dx} \sin\phi = 0, \tag{3.12}$$

which yields the following solutions:

$$\cos\theta_{\max} = \begin{cases} -\dfrac{I_{\text{inj}}}{I_{\text{osc}}}, & I_{\text{inj}} \leq I_{\text{osc}} \\ -\dfrac{I_{\text{osc}}}{I_{\text{inj}}}, & I_{\text{inj}} \geq I_{\text{osc}} \end{cases} \tag{3.13}$$

Substituting this maximizer back into Eq. (3.11) gives us

$$\sin\phi_{\max} = \begin{cases} \dfrac{I_{\text{inj}}}{I_{\text{osc}}}, & I_{\text{inj}} \leq I_{\text{osc}} \\ 1 \ , & I_{\text{inj}} \geq I_{\text{osc}} \end{cases} \tag{3.14}$$

and so the lock range on $|\chi_{\text{tank}}|$ is

$$\begin{aligned} |\chi_{\text{tank}}| &\leq \tan\phi_{\max} \\ &= \begin{cases} \dfrac{1}{\sqrt{\dfrac{{I_{\text{osc}}}^2}{{I_{\text{inj}}}^2} - 1}}, & I_{\text{inj}} < I_{\text{osc}} \\ +\infty \quad , & I_{\text{inj}} \geq I_{\text{osc}} \end{cases} \end{aligned} \tag{3.15}$$

This is depicted geometrically in Fig. 3.3.

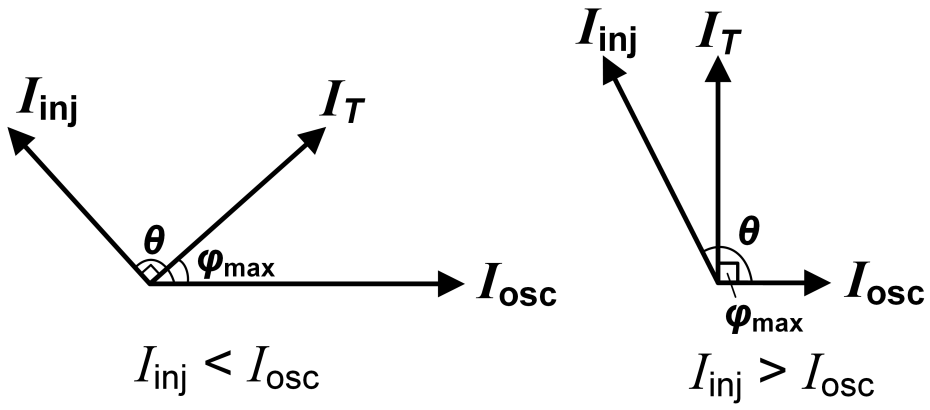

Figure 3.3: Phasor diagram depicting the edge of the lock range as dictated by Eqs. (3.13) and (3.14). Two separate cases where $I_{inj} < I_{osc}$ (left) and where $I_{inj} > I_{osc}$ (right) are shown.

The $I_{inj} < I_{osc}$ case is well-documented in [5], [8]. But, this result does bring up the interesting notion of an infinite lock range is infinite when $I_{inj} \geq I_{osc}$. What is going on here physically? We will return to this question in Section 3.5, but suffice it to say for now that the lock range is not actually infinite when the injection current exceeds the oscillator current.

3.4 A Physically Based Analysis

We start by illustrating that the parameter χ_{tank} yields a very specific relationship between the currents within the oscillator. Notice that the oscillation amplitude is given by

$$V_{osc} = \left(I_{osc} + I_{inj,in}\right) R_P \tag{3.16}$$

and also by

$$V_{osc} = I_{inj,react} \frac{R_P}{\chi_{tank}}. \tag{3.17}$$

Here, we leave open the possibility that $I_{inj,in} < 0$. That is, the non-reactive component of the injection could be 180° *out-of-phase* with the oscillation voltage and *oppose* the oscillator current (see Fig. 3.3). Note that we are also adopting the convention that $I_{inj,react}$ shares the same sign as θ and ϕ. Combining Eqs. (3.16) and (3.17) and using Eq. (3.4) yields

$$I_{osc} + I_{inj,in} = \frac{\sqrt{{I_{inj}}^2 - {I_{inj,in}}^2}}{|\chi_{tank}|}. \tag{3.18}$$

Solving for $I_{\text{inj,in}}$, we get

$$I_{\text{inj,in}} = \frac{\pm\sqrt{\left(1+{\chi_{\text{tank}}}^2\right){I_{\text{inj}}}^2 - {\chi_{\text{tank}}}^2{I_{\text{osc}}}^2} - {\chi_{\text{tank}}}^2 I_{\text{osc}}}{1+{\chi_{\text{tank}}}^2} \tag{3.19}$$

which indicates two possible solutions or modes [9], [10]. Geometrically, these solutions correspond to the ways in which the injection current phasor $\overrightarrow{I}_{\text{inj}}$ can be oriented while maintaining the direction of the tank current phasor $\overrightarrow{I}_T$, which is fixed by χ_{tank}. For the solutions to be real, we need

$$\begin{aligned} &\left(1+{\chi_{\text{tank}}}^2\right){I_{\text{inj}}}^2 - {\chi_{\text{tank}}}^2{I_{\text{osc}}}^2 \geq 0 \\ \implies &{I_{\text{inj}}}^2 + {\chi_{\text{tank}}}^2\left({I_{\text{inj}}}^2 - {I_{\text{osc}}}^2\right) \geq 0 \end{aligned} \tag{3.20}$$

Of course, if $I_{\text{inj}} \geq I_{\text{osc}}$, this inequality always holds. Assume not. Then we need

$$\begin{aligned} {\chi_{\text{tank}}}^2 &\leq -\frac{{I_{\text{inj}}}^2}{{I_{\text{inj}}}^2 - {I_{\text{osc}}}^2} \\ \implies |\chi_{\text{tank}}| &\leq \frac{1}{\sqrt{\dfrac{{I_{\text{osc}}}^2}{{I_{\text{inj}}}^2} - 1}} \end{aligned} \tag{3.21}$$

Notice that we have re-derived Eq. (3.15), albeit in a much simpler way! Therefore, we have the following interesting observation: the *lock range* derived in Section II-B is precisely the condition that needs to be satisfied in order for the oscillator to have a sinusoidal steady-state solution at the injection frequency ω_{inj}. In other words, Eq. (3.15) *is a necessary condition for injection locking to occur.*

We will now consider the two solutions of Eq. (3.19) separately. The first solution is

$$I_{\text{inj,in}} = \frac{\sqrt{\left(1+{\chi_{\text{tank}}}^2\right){I_{\text{inj}}}^2 - {\chi_{\text{tank}}}^2{I_{\text{osc}}}^2} - {\chi_{\text{tank}}}^2 I_{\text{osc}}}{1+{\chi_{\text{tank}}}^2}. \tag{3.22}$$

It can be shown that $I_{\text{inj,in}} \geq 0$ if and only if $I_{\text{inj}} \geq |\chi_{\text{tank}}|\, I_{\text{osc}}$. This result is highly intuitive. If the non-reactive portion of the injection current is in-phase with the oscillation voltage and therefore adds to the oscillator current, then the oscillation amplitude is at least $I_{\text{osc}}R_P$ (the free-running amplitude). Therefore, the injection must be able to supply at least $|\chi_{\text{tank}}/R_P|\, I_{\text{osc}}R_P$ of reactive current. In other words, we need $I_{\text{inj}} \geq |\chi_{\text{tank}}|\, I_{\text{osc}}$. From this physical insight, we can see that

$$|\chi_{\text{tank}}| \leq \frac{I_{\text{inj}}}{I_{\text{osc}}} \tag{3.23}$$

is a sufficient condition for injection locking to occur, since there will always exist a *stable* sinusoidal steady-state solution at ω_{inj} provided that Eq. (3.23) holds. We will consider the issue of stability in more detail in Section 3.5.

Next, the second solution is

$$I_{\text{inj,in}} = \frac{-\sqrt{\left(1 + \chi_{\text{tank}}{}^2\right) I_{\text{inj}}{}^2 - \chi_{\text{tank}}{}^2 I_{\text{osc}}{}^2} - \chi_{\text{tank}}{}^2 I_{\text{osc}}}{1 + \chi_{\text{tank}}{}^2}. \tag{3.24}$$

To ensure its validity, we need to check $I_{\text{osc}} + I_{\text{inj,in}} \geq 0$, as indicated by the original equation Eq. (3.18). One can therefore show that this mode comes into existence if and only if $I_{\text{inj}} \leq I_{\text{osc}}$. (Note that the two solutions coincide at the edge of the lock range.) However, this mode is problematic since it allows the oscillation amplitude to become arbitrarily small, a physically unrealistic scenario, by taking $I_{\text{inj}} \to I_{\text{osc}}$ which results in $I_{\text{inj,in}} \to -I_{\text{osc}}$. Therefore, as it turns out, even though Eq. (3.24) is a mathematically valid solution, this mode actually never sustains [9], [10]. Thus, the only physically viable mode is the one with the higher oscillation amplitude, given by Eq. (3.22). This is also verifiable through simulation (see Section III).

We end this analysis with the following caveat. For well-designed oscillators, I_{osc} should not depend on V_{osc} (e.g., sufficient loop gain $G_m := f'(0) \gg 1/R_P$); this was assumed throughout since we took I_{osc} to be a known constant. In the unlikely event that the oscillator is near the edge of the start-up condition, Eq. (3.18) must be solved alongside Eqs. (3.2) and (3.16) as additional *constraints*. This most likely significantly complicates the analysis.

3.5 Discussion of the Lock Range

Now we return to the question posed at the end of the previous subsection regarding the possibility of an infinite lock range. Consider the situation where $I_{\text{inj}} = I_{\text{osc}}$. Then Eq. (3.13) tells us that $\theta = \pi$ at the edge of the lock range. This means that all of the injection current is used to cancel the oscillator current, resulting in an oscillation amplitude of zero, which obviously requires *no* reactive current whatsoever at *any* frequency offset. This explains the infinite lock range. How about when $I_{\text{inj}} > I_{\text{osc}}$? Here, the oscillation amplitude can be made arbitrarily small if the the in-phase component of the injection $I_{\text{inj,in}}$ opposes the oscillator current I_{osc}. Then, for any injection frequency, we simply need to make the oscillation amplitude *small enough* such that the remaining reactive injection current quenches the amount of current the LC tank needs to oscillate at the injection frequency. In the extreme case, depicted in Fig. 3.3, $I_{\text{inj,in}}$ completely cancels I_{osc}, resulting in zero oscillation amplitude for

an injection frequency infinitely far away from resonance. Of course, both scenarios described here are physically nonsensical for the following two reasons.

First, note that the edge of the lock range, as depicted in Fig. 3.3, always corresponds to the scenario where $I_{\text{inj,in}} < 0$ and $I_{\text{inj}} < |\chi_{\text{tank}}|\, I_{\text{osc}}$, implying that the injection's non-reactive component is 180° out-of-phase with the oscillation voltage. Energetically, this implies that although the oscillator current is supplying power to the tank, the non-reactive component of the injection current is dissipating power. This is not a stable scenario, as any negative variation (perhaps due to noise) in the injection strength would cause the oscillation voltage to grow (since the supplied power exceeds the dissipated power), which increases the reactive component of the injection current, further decreasing its non-reactive component and increasing the oscillation amplitude, thereby creating a runaway process. A symmetric argument holds for positive variations in the injection strength.[2] Therefore, even though a sinusoidal steady-state solution at ω_{inj} *always* exists whenever Eq. (3.15) is satisfied, as we continue to increase $|\chi_{\text{tank}}|$ beyond $I_{\text{inj}}/I_{\text{osc}}$, at some point it will become energetically favorable for the oscillator to lose lock altogether and become *injection pulled*.

Second, notice that decreasing the oscillation amplitude V_{osc} will eventually impede the transconductor's generation of oscillator current I_{osc}, ultimately preventing the oscillator from oscillating! Indeed, in a realistic transconductor, if $V_{\text{osc}} \to 0$, then obviously $I_{\text{osc}} \to 0$ as well.[3]

3.6 Summary

Let us summarize our analysis results. The non-reactive component of the injection current is given by

$$I_{\text{inj,in}} = \frac{\sqrt{\left(1 + {\chi_{\text{tank}}}^2\right) {I_{\text{inj}}}^2 - {\chi_{\text{tank}}}^2 {I_{\text{osc}}}^2} - {\chi_{\text{tank}}}^2 I_{\text{osc}}}{1 + {\chi_{\text{tank}}}^2}. \tag{3.25}$$

The oscillation amplitude is given by

$$V_{\text{osc}} = \left(I_{\text{osc}} + I_{\text{inj,in}}\right) R_P. \tag{3.26}$$

[2] This physical argument is used by Mirzaei in [9], [10] to show that the mode associated with the solution of Eq. (3.24) cannot sustain, which is true. Here, we see that the argument holds not just for that mode, but whenever $I_{\text{inj,in}} < 0$.

[3] Interestingly, this discussion does allude to the fact that an RLC tank *without* a transconductor does indeed have an infinite "lock range" since it is an LTI system.

The oscillator's phase, relative to the injection and accounting for the correct sign, is given by

$$\theta = -\operatorname{sign}(\Delta\omega) \cdot \cos^{-1}\left(\frac{I_{\text{inj,in}}}{I_{\text{inj}}}\right). \tag{3.27}$$

Note that the oscillator's phase $|\theta|$ increases monotonically from 0 as $|\chi_{\text{tank}}|$ increases from 0, and it reaches 90° when $I_{\text{inj}} = |\chi_{\text{tank}}|\, I_{\text{osc}}$.

Now for the lock range: a *sufficient* condition for injection locking is

$$\boxed{|\chi_{\text{tank}}| \leq \frac{I_{\text{inj}}}{I_{\text{osc}}}}_{\text{Sufficient}}, \tag{3.28}$$

whereas a *necessary* condition for injection locking is

$$\boxed{|\chi_{\text{tank}}| \leq \begin{cases} \dfrac{1}{\sqrt{\dfrac{{I_{\text{osc}}}^2}{{I_{\text{inj}}}^2} - 1}}, & I_{\text{inj}} < I_{\text{osc}} \\ +\infty \quad , & I_{\text{inj}} \geq I_{\text{osc}} \end{cases}}_{\text{Necessary}}. \tag{3.29}$$

Notice that if the sufficient condition is satisfied, then so is the necessary one. Unfortunately, given the current framework, we do not believe that a necessary *and* sufficient condition for injection locking exists.

Next, we would like to demonstrate how this framework reduces when the transconductor turns off ($I_{\text{osc}} = 0$) and the system is not an oscillator—just a damped LC tank. Notice that based on Eq. (3.28), the "lock range" is now infinite. Then

$$I_{\text{inj,in}} = \frac{I_{\text{inj}}}{\sqrt{1 + {\chi_{\text{tank}}}^2}}. \tag{3.30}$$

This yields an oscillation amplitude of

$$V_{\text{osc}} = \frac{R_P}{\sqrt{1 + {\chi_{\text{tank}}}^2}} I_{\text{inj}} = \left|Z_{\text{tank}}(j\omega_{\text{inj}})\right| I_{\text{inj}}, \tag{3.31}$$

where Z_{tank} is the tank's impedance, and an oscillation phase of

$$\begin{aligned} \theta &= -\operatorname{sign}(\Delta\omega) \cdot \cos^{-1}\left(\frac{1}{\sqrt{1 + {\chi_{\text{tank}}}^2}}\right) \\ &= \tan^{-1}(\chi_{\text{tank}}) \\ &= \phi \\ &= \angle Z_{\text{tank}}(j\omega_{\text{inj}}). \end{aligned} \tag{3.32}$$

These results are in accordance with LTI system theory. A sinusoidal input results in a sinusoidal output at the same frequency (infinite lock range), whose amplitude and phase are shaped by the magnitude and phase of the system's transfer function at the input frequency.

Finally, if the frequency deviation is small $|\Delta\omega| \ll \omega_0$ and the injection is weak $I_{\text{inj}} \ll I_{\text{osc}}$, then both Eqs. (3.28) and (3.29) simplify to the lock range originally given by Adler [5], [7]:

$$|\Delta\omega| \leq \omega_L = \frac{\omega_0}{2Q} \cdot \frac{I_{\text{inj}}}{I_{\text{osc}}}. \tag{3.33}$$

Simulations

To demonstrate the validity of the phase and amplitude expressions we derived above, we used Spectre to simulate the ideal injection locked oscillator of Fig. 3.1. The transconductor was implemented using a Verilog-A cell coded with the usual hard-limited current commutator functionality $f(x) = \text{sign}(x) \cdot I_{\text{bias}}$ and so $I_{\text{osc}} = (4/\pi)I_{\text{bias}}$. The tank featured a parallel resistance of $R_P = 300\,\Omega$, an inductance of $L = 5\,\mu$H, and a capacitance of $C = 5.066059182117$ nF, resulting in a resonant frequency of approximately $f_0 = 1$ MHz.

The first set of simulations, depicted in Fig. 3.4, sweeps the injection current while the bias current is held at $I_{\text{bias}} = 1$ mA. The injection frequency is $f_{\text{inj}} = 1.1$ MHz, resulting in $\chi_{\text{tank}} \approx -1.823$.

The second set of simulations, depicted in Fig. 3.5, sweeps the bias current while the injection current is held at $I_{\text{inj}} = 2.5\text{mA}$. The injection frequency is $f_{\text{inj}} = 0.98\text{MHz}$. The plots are given as a function of the oscillator current. A smooth plot for the theoretically predicted results could not be generated here, since changing the strength of the oscillator current slightly perturbs the tank's resonant frequency due to the higher-order harmonics contained in its square waveform [36], [37]. We therefore simulated the free-running oscillation frequency f_0 and computed χ_{tank} at each simulation point.

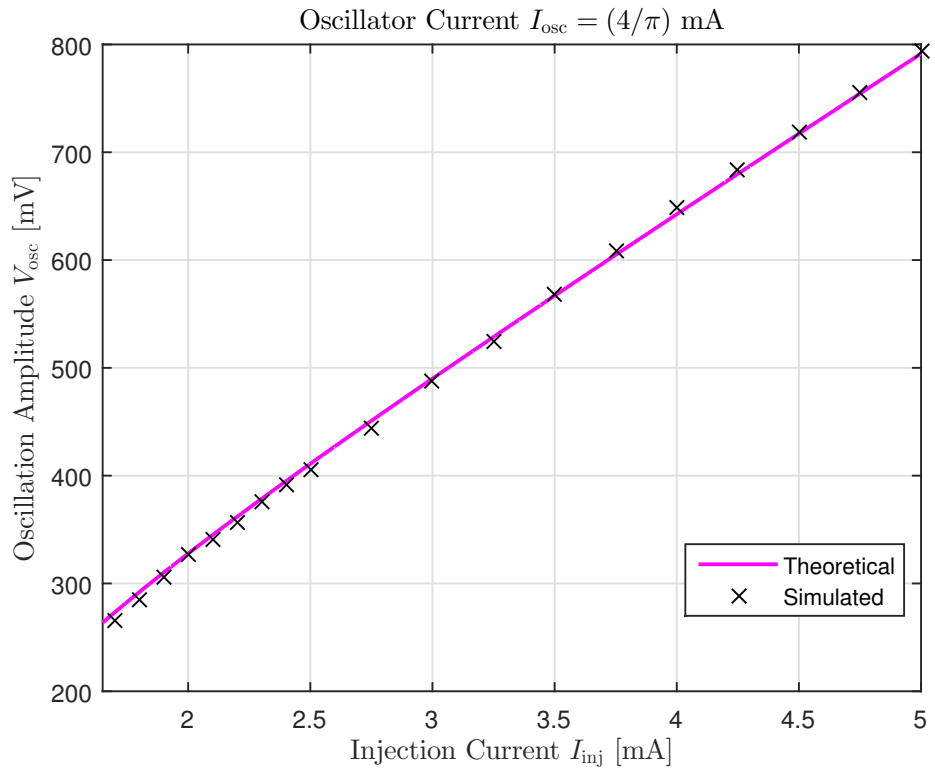

(a)

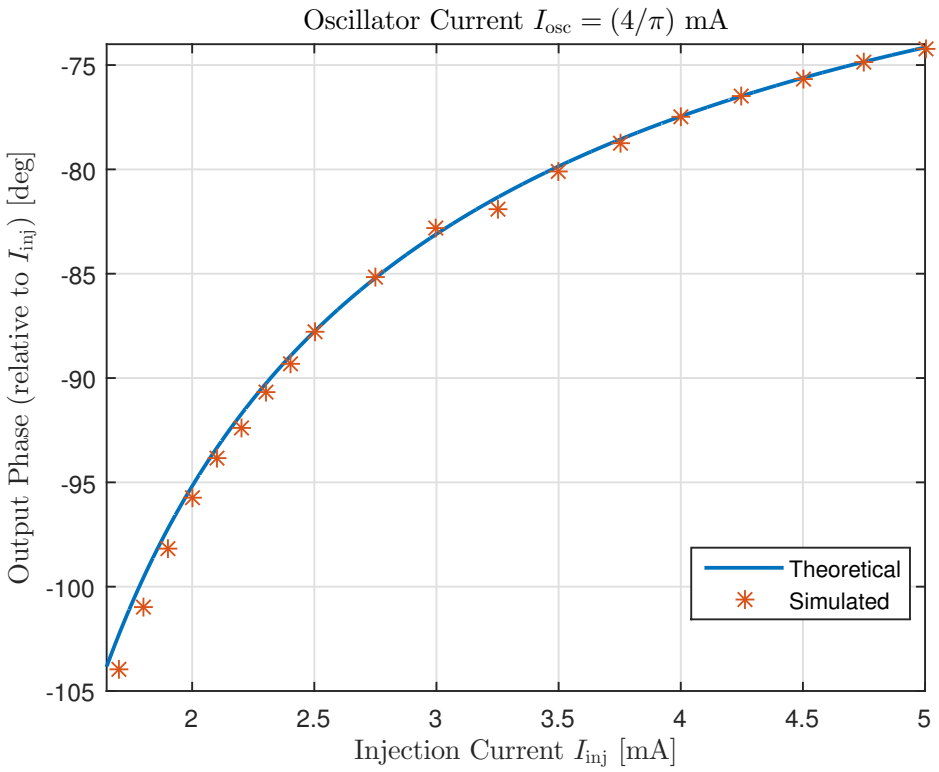

(b)

Figure 3.4: Theoretical and simulated (a) oscillation amplitude V_{osc} and (b) oscillation phase θ plotted against the injection current I_{inj}.

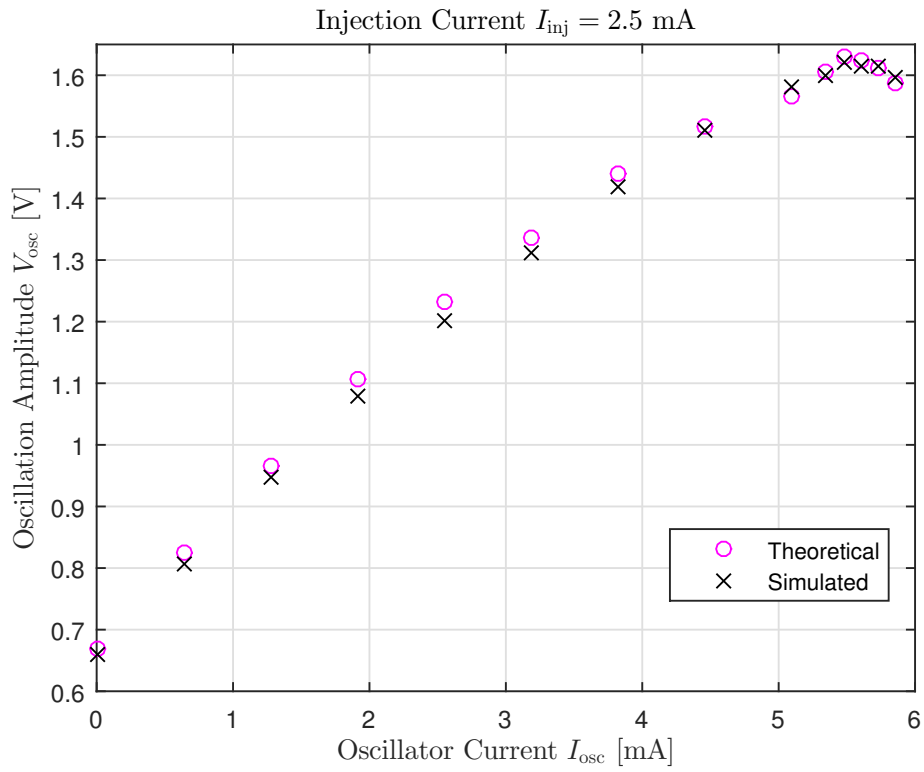

(a)

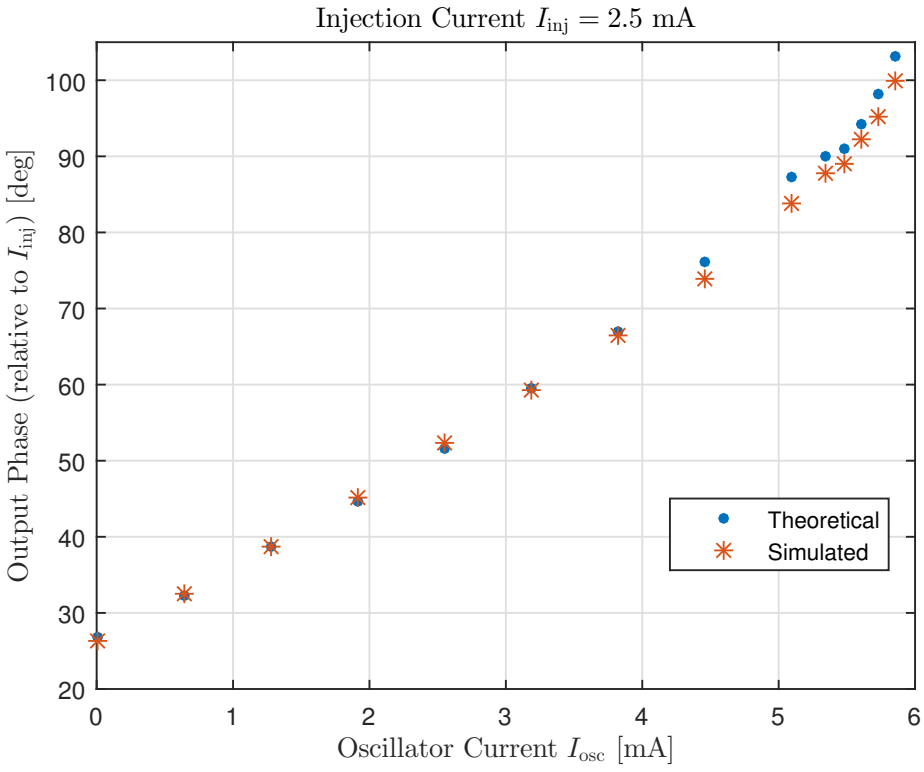

(b)

Figure 3.5: Theoretical and simulated (a) oscillation amplitude V_{osc} and (b) oscillation phase θ plotted against the oscillator current I_{osc}.

There is excellent agreement between the presented model and the example simulations. Note that since we are not presenting a new theory of injection locking—merely a new *perspective* into how injection locking works—the simulations are only meant to be briefly illustrative, not representative of all possible edge cases. The error seems to increase near the edge of the lock range, which is in accordance with our discussion in Section 3.5 that our sinusoidal steady-state framework is incapable of predicting when and how the energetics and dynamics of injection pulling become apparent.

3.7 General Considerations for LC Oscillators under Sinusoidal Injection

In this section, we will shed some light on the underlying conceptual and analytical connections between our analysis in Section 3.4 and the existing literature. To do so, we will use the same circuit model of Fig. 3.1, but without the assumption of sinusoidal steady state.

The Transconductor's Effect on Phase Modulation

An important but often overlooked issue is how the transconductor reacts to phase modulation (PM) in the oscillation voltage. We showed in Section 3.2 that if $v_{\text{osc}}(t)$ is *purely* sinusoidal at a single tone (constant phase), then the fundamental component of the transconductor current $i_{G_m}(t) = f[v_{\text{osc}}(t)]$ has the same phase as $v_{\text{osc}}(t)$. But, what if the oscillation voltage has a time-varying phase $\theta(t)$? Although intuitively we would expect a memoryless, time-invariant system to be incapable of changing the time- or phase- dynamics of its input, the situation is complicated by the higher order harmonics that are introduced by the nonlinearity.

It is typical in injection locking and pulling applications to assume that the carrier frequency is the injection frequency $\omega_{\text{osc}} = \omega_{\text{inj}}$ and any phase modulation $\theta(t)$ in the oscillation voltage would therefore be referred to $\omega_{\text{inj}}t$. In other words, we will assume that for the usual setting of an oscillator under injection, the spectrum of the oscillation voltage is spread around ω_{inj}. Therefore, let us assume that the oscillation voltage is $v_{\text{osc}}(t) = V_{\text{osc}} \cos\left[\omega_{\text{inj}}t + \theta(t)\right]$, where $\theta(t)$ is an arbitrary signal. Define the PM free $v_0(t) \coloneqq V_{\text{osc}} \cos\left(\omega_{\text{inj}}t\right)$ and its corresponding output $i_0(t) \coloneqq f[v_0(t)]$. It is not difficult to see that because $f(\cdot)$ is memoryless and time-invariant, its response

to the oscillation voltage is

$$\begin{aligned} i_{G_m}(t) &= f[v_{\text{osc}}(t)] \\ &= f\left(V_{\text{osc}} \cos\left[\omega_{\text{inj}} t + \theta(t)\right]\right) \\ &= f\left[v_0\left(t + \frac{\theta(t)}{\omega_{\text{inj}}}\right)\right] \\ &= i_0\left(t + \frac{\theta(t)}{\omega_{\text{inj}}}\right) \end{aligned} \tag{3.34}$$

The last step follows from the fact that for any $t_0 \in \mathbb{R}$, $f\left[x(t_0)\right]$ depends only on the *value* that $x(t)$ takes on at $t = t_0$ and not explicitly on t_0 itself (time-invariant) or on what $x(t)$ is when $t \neq t_0$ (memoryless).

Next, recall that $i_0(\cdot)$ is an even, periodic function with period ω_{inj} and therefore has the Fourier series representation shown in Eq. (3.1) (with $\omega_{\text{osc}} = \omega_{\text{inj}}$). Therefore, we can similarly expand the transconductor current as

$$i_{G_m}(t) = \sum_{n=0}^{\infty} G_n \cos\left(n\left[\omega_{\text{inj}} t + \theta(t)\right]\right). \tag{3.35}$$

This analysis elicits the core issue. The question of interest now is clear: what happens when $i_{G_m}(t)$ passes through a bandpass filter with center frequency ω_0? Under what conditions would we recover the "fundamental" carrier along with its phase modulation: $G_1 \cos\left[\omega_{\text{inj}} t + \theta(t)\right]$? Of course, the complete answer depends on the nature of $f(\cdot)$, the filter, and obviously the phase modulation $\theta(t)$ itself. Furthermore, the analysis is not trivial because the spectrum of $\cos\left(n\left[\omega_{\text{inj}} t + \theta(t)\right]\right)$ is not easily described for arbitrary $\theta(t)$. (For example, a single-tone PM $\theta(t) \propto \sin(\omega_m t)$ results in a spectrum with infinitely many side-tones about ω_{inj}, separated by ω_m, whose strengths are modulated by Bessel functions of the first kind.)

To solve this problem in a tractable fashion, we can use Carson's bandwidth rule to approximate the bandwidths (up to a 2% error in the energy) of the individual components of $i_{G_m}(t)$. Specifically, the (one-sided) bandwidth of the n^{th} harmonic (centered about $n\omega_{\text{inj}}$ is given by

$$\sigma_n \approx n\|\theta'(t)\|_\infty + \sigma_\theta, \tag{3.36}$$

where $\|\theta'(t)\|_\infty = \sup_{t\in\mathbb{R}} |\theta'(t)|$ is the maximum absolute slope of $\theta(t)$ (the notation $\|\cdot\|_\infty$ represents the *uniform norm*), and σ_θ is the one-sided bandwidth of or maximum frequency present within $\theta(t)$. For PM of the fundamental to be preserved, two criteria must be satisfied: (1) PM of higher order harmonics ($n > 1$)

cannot interfere with that of the fundamental, and (2) all of the fundamental PM actually passes through the passband of the filter. To ensure criterion (1), we require $\sigma_n \leq (n-1)\omega_{\text{inj}} - \sigma_1$ for every integer $n > 1$:

$$n\|\theta'(t)\|_\infty + \sigma_\theta \leq (n-1)\omega_{\text{inj}} - (\|\theta'(t)\|_\infty + \sigma_\theta)\,. \tag{3.37}$$

Rearranging, we obtain

$$\left(\frac{n+1}{n-1}\right)\|\theta'(t)\|_\infty + \frac{2\sigma_\theta}{n-1} \leq \omega_{\text{osc}}, \tag{3.38}$$

whose left-hand-side is maximized when $n = 2$; thus, interference from the 2^{nd} harmonic yields the tightest constraint. Therefore, criterion (1) simplifies to

$$3\|\theta'(t)\|_\infty + 2\sigma_\theta \leq \omega_{\text{osc}}. \tag{3.39}$$

For criterion (2) to be satisfied, assuming the filter's one-sided bandwidth is that of the RLC tank $\omega_0/(2Q)$, we also need

$$\begin{gathered}\omega_{\text{inj}} + \|\theta'(t)\|_\infty + \sigma_\theta \leq \omega_0 + \frac{\omega_0}{2Q} \\ \text{and} \\ \omega_{\text{inj}} - \|\theta'(t)\|_\infty - \sigma_\theta \geq \omega_0 - \frac{\omega_0}{2Q}\end{gathered} \tag{3.40}$$

which simplifies to

$$\|\theta'(t)\|_\infty + \sigma_\theta \leq \frac{\omega_0}{2Q} - |\Delta\omega|\,. \tag{3.41}$$

Note that we are assuming our filter is only capable of passing and suppressing harmonic content; the phase-shift induced by the RLC tank (at ω_{inj}) is abstracted away into the full analysis. For reasonable quality factors, Eq. (3.41) is typically more stringent than Eq. (3.39). Of course, for both constraints to be satisfied, we require

$$\boxed{\|\theta'(t)\|_\infty \leq \min\left\{\frac{\omega_{\text{osc}} - 2\sigma_\theta}{3},\ \frac{\omega_0}{2Q} - |\Delta\omega| - \sigma_\theta\right\}}. \tag{3.42}$$

It is noteworthy that by comparing the spectra of $v_{\text{osc}}(t)$ and $i_{G_m}(t)$, Samori et. al. [38], [39] prove that PM is preserved for "small-angles" $|\theta(t)| \ll 1$, with an implicit assumption that the bandwidth σ_θ is sufficiently small compared to that of the filter. "Small-angle" phase modulations $|\theta(t)| \ll 1$ of course falls under our more general condition since Bernstein's inequality [40] allows us to bound the derivative of a bounded, band-limited signal as $\|\theta'(t)\|_\infty \leq \sigma_\theta\|\theta(t)\|_\infty \ll \omega_{\text{osc}}$.

Although Eq. (3.42) is difficult to check *a priori* to determining $\theta(t)$, these conditions serve as a useful benchmark in evaluating the validity of the analysis *a posteriori*. More importantly, however, they demonstrate that the usual assumption adopted in injection locking literature that the oscillator current and oscillation voltage are always in phase is not always true. This is particularly paramount since the spectrum of an oscillator under injection depends critically on the behavior of its nonlinear transconductor. This is because the injection only supplies current into the tank at the injection frequency ω_{inj}, and so it is up to the transconductor to balance out the current created by the RLC tank at all the other frequencies present within the oscillation voltage. Indeed, without the $-G_m$-cell, the system is linear and the only frequency that would appear in the oscillation voltage is the excitation frequency ω_{inj}. In passing, we remark that it is interesting that a memoryless, time-invariant nonlinearity can give rise to infinitely many tones.

Oscillation Amplitude and Phase—A Time-Domain Model

Referring to the circuit of Fig. 3.1, KCL yields

$$\frac{v_{\text{osc}}(t)}{L} + C\frac{d^2 v_{\text{osc}}(t)}{dt^2} + \frac{1}{R_P}\frac{dv_{\text{osc}}(t)}{dt} = \frac{d}{dt}\left[i_{G_m}(t) + i_{\text{inj}}(t)\right]. \tag{3.43}$$

We assume the injection current is $i_{\text{inj}}(t) = I_{\text{inj}}e^{j\omega_{\text{inj}}t}$, and we utilize the following ansatz for the oscillation voltage $v_{\text{osc}}(t) = V_{\text{osc}}(t)e^{j\cdot\theta_{\text{osc}}(t)}$ (which allows for amplitude modulation in the envelope $V_{\text{osc}}(t)$). Denote $\theta(t) \coloneqq \theta_{\text{osc}}(t) - \omega_{\text{inj}}t$ as the phase difference between the oscillator and the injection. Assuming the conditions of Section 3.7 are met and accounting for the filtering action of the tank, we approximate the oscillator current as $i_{G_m}(t) \approx I_{\text{osc}}(t)e^{j\cdot\theta_{\text{osc}}(t)}$, which has the same phase as the oscillation voltage. We also typically assume that the amplitude of $V_{\text{osc}}(t)$ is large enough such that it fully saturates or commutates the transconductor, and so $i_{G_m}(t)$ does not exhibit appreciable amplitude modulation which means that I_{osc} is constant in time.

Substituting these expressions into Eq. (3.43) and separating out the real and imaginary parts (i.e., sine and cosine components), and noting that the tank's quality factor is related to the original parameters via $Q = R_P C\omega_0$, we get the two coupled differential equations Eqs. (3.44) and (3.45). Below, we will use these equations to

illustrate various connections to analyses in the existing literature.

$$\begin{aligned}\frac{Q}{\omega_0\omega_{\text{inj}}}\frac{d^2V_{\text{osc}}}{dt^2}+\frac{1}{\omega_{\text{inj}}}\frac{dV_{\text{osc}}}{dt}+\left[\chi_{\text{tank}}-2\frac{Q}{\omega_0}\frac{d\theta}{dt}-\frac{Q}{\omega_0\omega_{\text{inj}}}\left(\frac{d\theta}{dt}\right)^2\right]V_{\text{osc}}\\ =\left(\frac{1}{\omega_{\text{inj}}}\frac{dI_{\text{osc}}}{dt}+I_{\text{inj}}\sin\theta\right)R_P\end{aligned} \tag{3.44}$$

$$\frac{Q}{\omega_0\omega_{\text{inj}}}V_{\text{osc}}\frac{d^2\theta}{dt^2}+\left(2\frac{Q}{\omega_0}\frac{dV_{\text{osc}}}{dt}+V_{\text{osc}}-I_{\text{osc}}R_P\right)\left(1+\frac{1}{\omega_{\text{inj}}}\frac{d\theta}{dt}\right)=I_{\text{inj}}R_P\cos\theta. \tag{3.45}$$

Reduction to the Locked Model of Section 3.4

In an injection locked oscillator in steady state, all quantities V_{osc}, I_{osc}, and θ are constant in time. Therefore, taking $d/dt \to 0$, Eqs. (3.44) and (3.45) reduce to

$$\chi_{\text{tank}}V_{\text{osc}} = I_{\text{inj}}R_P\sin\theta \tag{3.46}$$

and

$$V_{\text{osc}} = \left(I_{\text{osc}} + I_{\text{inj}}\cos\theta\right)R_P \tag{3.47}$$

respectively. Recalling that (see Fig. 3.2) $I_{\text{inj,in}} = I_{\text{inj}}\cos\theta$ and $I_{\text{inj,react}} = I_{\text{inj}}\sin\theta$, we can simplify these to

$$V_{\text{osc}} = \left(I_{\text{osc}} + I_{\text{inj,in}}\right)R_P \tag{3.48}$$

and

$$V_{\text{osc}} = I_{\text{inj,react}}\frac{R_P}{\chi_{\text{tank}}}, \tag{3.49}$$

which respectively match Eqs. (3.16) and (3.17), the entire analytical basis for the exact model of an injection locked LC oscillator derived in Section 3.4.

Reduction to Mirzaei's "Generalized Adler's Equation" [9], [10]

Here, we show how Eqs. (3.44) and (3.45) can be reduced to Mirzaei's Generalized Adler's equation [9], [10]. Assuming that 1) the envelopes of the oscillation voltage V_{osc} and oscillator current I_{osc} are roughly constant in time, 2) the injection frequency is close to resonance $|\Delta\omega| \ll \omega_0$ and so $\chi_{\text{tank}} \approx -2Q\,(\Delta\omega/\omega_0)$, and 3) the PM is sufficiently narrow-band such that $|\theta'(t)| \ll \omega_0$ and $|\theta''(t)| \ll {\omega_0}^2/Q$ (we will check this assumption a posteriori), Eqs. (3.44) and (3.45) can be simplified as

$$\begin{aligned}\frac{d\theta}{dt} &\approx \omega_0 - \omega_{\text{inj}} - \frac{\omega_0}{2Q}\frac{I_{\text{inj}}R_P\sin\theta}{V_{\text{osc}}}\\ V_{\text{osc}} &\approx \left(I_{\text{osc}} + I_{\text{inj}}\cos\theta\right)R_P.\end{aligned} \tag{3.50}$$

Next, Mirzaei assumes hard-limited current commutator which results in an oscillator current of $I_{\text{osc}} = 4I_{\text{bias}}/\pi$. Therefore, eliminating V_{osc} in Eq. (3.50), we get

$$\frac{d\theta}{dt} = \omega_0 - \omega_{\text{inj}} - \frac{\omega_0}{2Q}\frac{I_{\text{inj}}\sin\theta}{\frac{4I_{\text{bias}}}{\pi} + I_{\text{inj}}\cos\theta}, \tag{3.51}$$

which matches Eq. (8) from [10], setting aside notational differences for the phase (replace $\theta_{\text{inj}} - \theta$ in [10] with $-\theta$).

Using Eq. (3.45), we can also derive a differential equation which captures the dynamics of V_{osc}, namely Eq. (7) in [10]. Again assuming the phase is sufficiently slowly varying, that is, $|\theta'(t)| \ll \omega_0$ and $|\theta''(t)| \ll {\omega_0}^2/Q$, we get

$$2R_P C\frac{dV_{\text{osc}}}{dt} + V_{\text{osc}} = \left(I_{\text{osc}} + I_{\text{inj}}\cos\theta\right) R_P \tag{3.52}$$

which matches Eq. (7) in [10] (up to a typo).

We can see that Mirzaei's Generalized Adler's equation is more general than our sinusoidal steady-state model in the sense of being able to model the *dynamics* of the phase θ. On the other hand, our analysis fully elucidates the various currents flowing inside the tank, resulting in exact expressions for the amplitude and phase of an injection locked oscillator. We also do not assume that the frequency deviation is small (i.e., $|\Delta\omega| \ll \omega_0$).

It is easy to see that further assuming $I_{\text{inj}} \ll I_{\text{osc}}$ in Eq. (3.51) yields Adler's original equation [7]

$$\frac{d\theta}{dt} = \omega_0 - \omega_{\text{inj}} - \frac{\omega_0}{2Q}\frac{I_{\text{inj}}}{I_{\text{osc}}}\sin\theta. \tag{3.53}$$

Finally, let us briefly check the validity of our narrow-band PM assumption using Adler's equation. Assuming a reasonable quality factor (e.g., $Q \sim 10$) and noting that $I_{\text{inj}} \ll I_{\text{osc}}$, we can see that $\theta'(t) \sim -\Delta\omega$. Thus, $|\theta'(t)| \sim |\Delta\omega| \ll \omega_0$, and so the condition on $|\theta'(t)|$ is satisfied. Differentiating Adler's equation with respect to time, we get

$$\frac{d^2\theta}{dt^2} = -\frac{\omega_0}{2Q}\frac{I_{\text{inj}}}{I_{\text{osc}}}\cos\theta\frac{d\theta}{dt}, \tag{3.54}$$

from which we can deduce that

$$|\theta''(t)| < (\omega_0/Q)\,|\theta'(t)| \ll {\omega_0}^2/Q, \tag{3.55}$$

which shows that the condition on $|\theta''(t)|$ is also satisfied. Checking these conditions on Mirzaei's Generalized Adler's equation is more tedious and will not be shown here. However, the point here is that it is always important to go back and check the validity of any assumptions made in the course of deriving a particular result.

The Spectrum of an Injection Pulled LC Oscillator—Qualitative Commentary

It is well known [5], [6] that the steady-state spectrum of a pulled LC oscillator consists of a countably infinite number of tones at $\omega_{\text{inj}} - \text{sign}(\Delta\omega) \cdot n\omega_b$ ($n = 0, 1, 2, \ldots$), where the beat frequency is $\omega_b = \sqrt{\Delta\omega^2 - {\omega_L}^2}$. Referring to Fig. 3.1, we know that instantaneously, the currents through each component must all sum to zero. However, in the frequency domain, in order for the total current flowing through all the components to be identically zero, harmonic balance (i.e., KCL) must be satisfied at *each* beat frequency. The injection current only supplies current at the injection frequency ω_{inj}. Therefore, it is up to the transconductor to balance out the current at all the other beats created by the RLC tank in response to the tones in V_{osc}. Hence, we argue that the spectrum (both the locations of the tones and their amplitudes) of a pulled oscillator depends critically on the behavior of the nonlinear transconductor. Indeed, without the $-G_m$-cell, the system is linear and the only frequency that would appear in the oscillation voltage is the excitation frequency ω_{inj}. In conclusion, we would like to remark that it is interesting that a memoryless, time-invariant nonlinearity gives rise to infinitely many tones.

Correction to Razavi [5]—Pulled Oscillator Sideband Locations

We would like to take this opportunity to rectify a small mistake we noticed in [5]. In Subsection C of Section III of [5], the equation on the 4$^{\text{th}}$ line from the bottom of the 2$^{\text{nd}}$ column on page 1419 should actually be

$$\frac{\left(\omega_0 - \omega_{\text{inj}}\right)^2}{{\omega_L}^2} = \frac{1}{1 - \dfrac{1}{n^2}}. \tag{3.56}$$

Therefore, contrary to the claim made in [5], it *is* possible for a sideband to appear at ω_0 when ω_{inj} is outside of the lock range, provided an integer solution to Eq. (3.56) exists for n.

There does not appear to be a *physical* reason why a sideband at ω_0 cannot exist. The reason we say the oscillator is "pulled" from its natural frequency is not because the oscillator output $V_{\text{osc},p}$ contains no components at ω_0 as [5] states, but rather because the *largest* component of $V_{\text{osc},p}$ does not appear at ω_0 [6].

To see this, let us elucidate where exactly the largest component of the oscillator output $V_{\text{osc},p}$ falls, which we will denote as ω_p. That is, ω_p is the "oscillation frequency" of an injection pulled oscillator. Note from Eq. (3.56) that $|n| > 1$, and so only a sideband at least twice the beat frequency away from ω_{inj} can coincide with

ω_0. This should also be obvious from the fact that the distance between adjacent tones, known as the beat frequency [5], is $\omega_b = \sqrt{\Delta\omega^2 - {\omega_L}^2} < |\Delta\omega|$. Thus, the beat frequency is less than the distance between ω_{inj} and ω_0, and so ω_0 always lies more than a sideband away from ω_{inj}. Next, it is convenient here to define a parameter known as the "pulling strength" [6]:

$$\zeta := \frac{\omega_L}{|\omega_0 - \omega_{\text{inj}}|}. \tag{3.57}$$

If $\zeta \geq 1$, then the oscillator is injection locked; unity ζ corresponds to the edge of the lock range. We consider the case where $\zeta < 1$ and the oscillator is injection pulled. It is easily shown [6] that if $\zeta > \sqrt{4/5}$ (≈ 0.9), then the pulled oscillator "oscillates" at the injection frequency $\left(\omega_p = \omega_{\text{inj}}\right)$ and we can say that the oscillator is "quasi-locked" as per the vocabulary in [5]; whereas if $\zeta < \sqrt{4/5}$, then $\omega_p = \omega_{\text{inj}} \pm \omega_b$. (Again, the sign in front of ω_b here is the same as the sign of $\left(\omega_0 - \omega_{\text{inj}}\right)$, since ω_p is pulled away from ω_0 towards ω_{inj}.)[4] Therefore, the claim is verified: the oscillation frequency ω_p of a pulled oscillator is no longer at its free-running value ω_0 but instead is at either the injection frequency ω_{inj} or is one sideband toward ω_0 away from the injection frequency at $\omega_{\text{inj}} \pm \omega_b$.

3.8 Conclusion

In this chapter, a novel viewpoint into the sinusoidal injection locking of electrical harmonic oscillators was presented. By decomposing a sinusoidal injection into in-phase and quadrature-phase components, we derived exact expressions for the amplitude and phase of an injection locked LC oscillator which hold for any injection strength or frequency that locks the oscillator. By exploring the physical and mathematical conditions under which a circuit solution exists, an in-depth analysis of both the necessary and the sufficient conditions for an oscillator to be injection locked was carried out, leading to a more precise notion of the lock range. Simulation results on an ideal LC oscillator that confirm the derived expressions were provided. We also illuminated an often overlooked issue: the conditions under which the transconductor preserves the time-varying phase of the oscillation voltage. Finally, conceptual and analytical connections to the existing literature were discussed.

Notice that this chapter exposes the physical insight that the "job" of the injection is to change the oscillator's phase by the right amount every cycle such that the desired

[4] If $\zeta = \sqrt{4/5}$, then the components at ω_{inj} and at $\omega_{\text{inj}} \pm \omega_b$ contain equal amounts of power. It is easily computed that the remaining sidebands carry the remaining $\sqrt{5} - 2$ (roughly $1/4$) of the total output power.

frequency difference is achieved. (When the injection is not strong enough to do so, the oscillator fails to lock and is instead injection pulled.) In certain scenarios, a portion of the injection even needs to "weaken" the oscillator such that the rest of the injection is capable of locking it. In closing, we would like to note that the foregoing analysis leads to ideas that are both highly intuitive and physically accurate, as well as technical details which are amenable to analysis.

In the next chapter, we will again see how the powerful insight obtainable from an in-depth, exact, and rigorous analysis can be used to reveal additional information from data that previously was not known to be available. Specifically, we know that the 3-dB bandwidth of an LTI circuit can be estimated using the circuit's zero-value (or infinite-value for a high-pass circuit) time constants. But, is it possible to do better and make a more precise statement than merely *estimating* the bandwidth?

Chapter 4

UPPER AND LOWER BOUNDS ON A SYSTEM'S BANDWIDTH BASED ON ITS ZERO-VALUE TIME CONSTANTS

4.1 Introduction

The estimate of a low-pass circuit's 3-dB bandwidth via the method of zero-value time constants is well-known [41]–[43]. This procedure entails computing the time constant of each reactive element in a circuit based on the resistance it sees when all other reactive elements are zero-valued (capacitors opened, inductors shorted). The inverse of the sum of these zero-value time constants, or ZVTs, is then taken to be an estimate of the circuit's 3-dB high-cutoff frequency. For a linear time-invariant n^{th}-order system with m zeros and n poles ($m < n$) whose transfer function can be written as[1]

$$H(s) = \frac{a_0 + a_1 s + a_2 s^2 + \cdots + a_m s^m}{1 + b_1 s + b_2 s^2 + \cdots + b_n s^n}, \tag{4.1}$$

it can be shown [41]–[43] that the sum of the ZVTs is equal to b_1. For now, we will consider systems with no zeros ($a_1 = a_2 = \cdots = a_m = 0$), which serve as a good model for circuits where the zeros occur at very high frequencies beyond the passband and are hence unimportant. We thus rewrite the transfer function as

$$H(s) = \frac{H_0}{1 + b_1 s + b_2 s^2 + \cdots + b_n s^n}, \tag{4.2}$$

where $|H_0| = |a_0|$ is the DC gain of the system. We then argue that as the frequency increases from DC, the first term in the denominator that becomes significant is $b_1 s$, and so near the -3-dB point the system can be approximated as

$$H(s) \approx \frac{H_0}{1 + b_1 s} \tag{4.3}$$

from which the ZVT bandwidth estimate of $\omega_c \approx 1/b_1$ follows [41], [43].

In this chapter, we prove that for a system whose poles are all real, this ZVT estimate of the bandwidth is always a lower bound on the system's actual bandwidth ω_c. We also prove a nontrivial upper bound on ω_c that depends only on the sum of the ZVTs b_1 and the system's order n.

[1] If $b_0 = 0$ as in the case of the impedance of a capacitor, one can consider the reciprocal of the transfer function instead.

4.2 Statement of the Theorem

Consider a linear time-invariant n^{th}-order low-pass system with no zeros and no complex poles whose transfer function is

$$H(s) = \frac{H_0}{1 + b_1 s + b_2 s^2 + \cdots + b_n s^n}. \tag{4.4}$$

The system's 3-dB bandwidth, or high-cutoff frequency, is defined as the (lowest) angular frequency ω_c that satisfies

$$|H(j\omega_c)| \equiv \frac{|H_0|}{\sqrt{2}}. \tag{4.5}$$

If $n = 1$, then trivially $\omega_c = 1/b_1$. For $n > 1$, the following lower and upper bounds on ω_c hold:

$$\boxed{\frac{1}{b_1} < \omega_c \leq \frac{n}{b_1}\sqrt{2^{1/n} - 1}}. \tag{4.6}$$

Furthermore, these inequalities are tight, or achievable, in the sense that there exists systems whose bandwidths are arbitrarily close to the lower bound or are given by the upper bound. ■

A couple comments are in order:

1. The lower bound also holds for systems with *complex poles* whose quality factors are no larger than $Q \leq \sqrt{2}$. (The upper bound does not.) We will prove this separately in a later section.

2. The lower bound is physically intuitive. Loosely speaking, the ZVT estimate $1/b_1$ considers the worst case scenario where the system's reactive elements "energize" one after the other, as the time constants are added together. In general, however, the system's energy-storage elements may energize in parallel, leading to a "faster" response than that dictated by b_1.

4.3 Proof of the Lower Bound

Assume $n > 1$. Since all the poles are real, by the fundamental theorem of algebra, the denominator of Eq. (4.4) can be factored as

$$H(s) = H_0 \prod_{i=1}^{n} \frac{1}{1 + \tau_i s} \tag{4.7}$$

where $\tau_i \in \mathbb{R}_{++}$ for $i = 1, \ldots, n$ are the time constants associated with the system's n poles[2]. To simplify the notation, we define the following variables for $i = 1, \ldots, n$:

$$x_i \coloneqq \omega\tau_i \tag{4.8}$$

where the frequency ω will be specified based on context. Lastly, based on the easily seen fact that $b_1 = \sum_{i=1}^{n} \tau_i$, we can also write $\omega b_1 = \sum_{i=1}^{n} x_i$.

To make the proof more analytically tractable, we reformulate the problem statement in an equivalent way. By definition of the bandwidth, the lower bound $\omega_c > 1/b_1$ is equivalent to:

$$|H(j\omega)| > \frac{|H_0|}{\sqrt{2}} \tag{4.9}$$

for all $\omega \leq 1/b_1$. That is, the system's magnitude is always above -3-dB (relative to the DC gain) for frequencies up to $1/b_1$, the ZVT estimate of the high-cutoff frequency.[3]

We can then express the problem statement as follows: for $x_i > 0 \; \forall i$, show that

$$\prod_{i=1}^{n} \left(1 + {x_i}^2\right) < 2 \tag{4.10}$$

$$\text{subject to } \sum_{i=1}^{n} x_i \leq 1. \tag{4.11}$$

Now we proceed with the proof proper. First, we establish the following claim: given constants a and b such that $0 < a, b < 1$, it holds true that

$$\begin{aligned} (1 + a^2)(1 + b^2) &= 1 + a^2 + b^2 + (ab)^2 \\ &= (1 - ab)^2 + (a + b)^2 \\ &< 1 + (a + b)^2 \end{aligned} \tag{4.12}$$

where equality is approached by taking $a \to 0$ or $b \to 0$ (or both). We need to repeat this argument for a total of $n - 1$ times, where the k^{th} step features $a = \sum_{i=1}^{k} x_i$ and $b = x_{k+1}$. For each step, it is apparent that $0 < a, b < 1$, since $x_i > 0 \; \forall i$ combined

[2]Note that the τ_i's are only equal to the system's ZVTs if the poles are *decoupled* [43] from one another. In general, each τ_i could depend on multiple energy storage elements. Indeed, there may even be fewer poles than there are reactive elements in the circuit! It is only true that the ZVTs and the τ_i's have the same *total sum*, namely b_1.

[3]We can invoke the fact that $|H(j\omega)|$ decreases monotonically with frequency ω to simplify the reformulation of the lower bound to $|H(j/b_1)| > |H_0|/\sqrt{2}$, but we choose not to do so here because monotonicity no longer holds in the presence of complex poles, which we deal with in a later section.

with the constraint Eq. (4.11) implies that $\sum_{i \in S} x_i < 1 \; \forall S \subset \{1, \ldots, n\}$. Thus, we arrive at

$$\begin{aligned} \prod_{i=1}^{n} \left(1 + {x_i}^2\right) &< \left[1 + (x_1 + x_2)^2\right] \prod_{i=3}^{n} \left(1 + {x_i}^2\right) \\ &< \quad \cdots \\ &< 1 + \left(\sum_{i=1}^{n} x_i\right)^2 \\ &\leq 2 \end{aligned} \tag{4.13}$$

where the final inequality follows from the constraint $\sum_{i=1}^{n} x_i \leq 1$. By letting one of the x_i's approach unity (which takes the remaining x_i's to zero), we can also see that this inequality is tight. This establishes the lower bound. □

Notice what is happening here *physically*. We are "merging" the system's poles together one at a time (by adding their time constants together), and with each step, the bandwidth of the system worsens until we end up with a 1^{st}-order system whose bandwidth is exactly equal to the ZVT estimate $1/b_1$. The proof also shows how this lower bound is achievable: as one of the system's poles becomes increasingly dominant (where to dominate means to have a larger time constant), the system's bandwidth will approach the lower bound dictated by Eq. (4.6).

4.4 Proof of the Upper Bound

The proof of the upper bound is somewhat similar in spirit, but we take a slightly different approach. Consider the following system:

$$H_{\max}(s) \coloneqq \frac{H_0}{(1 + \bar{\tau} s)^n}, \tag{4.14}$$

where

$$\bar{\tau} \coloneqq \frac{1}{n} \sum_{i=1}^{n} \tau_i = \frac{b_1}{n} \tag{4.15}$$

is the arithmetic mean of all the time constants. Notice that this system has the same b_1 coefficient as Eq. (4.4). We claim that of all n^{th}-order systems (with no zeros or complex poles) that share the same b_1 coefficient, $H_{\max}(s)$ has the *best*, or maximum, bandwidth. In other words, for a given sum of the ZVTs, the best bandwidth is achieved by stacking all of the poles on top of each other. Appealing to the fact that $|H_{\max}(j\omega)|$ is monotonically decreasing with ω, we can establish this claim by proving that the magnitude of $H_{\max}$ at the cutoff frequency ω_c of Eq. (4.4)

is always no less than −3-dB (relative to the DC gain):

$$|H_{\max}(j\omega_c)| \geq |H(j\omega_c)| \equiv \frac{|H_0|}{\sqrt{2}}. \tag{4.16}$$

Letting $\omega = \omega_c$ in Eq. (4.8), this is equivalent to the following: given $x_i > 0 \; \forall i$, show that

$$\left(1 + \bar{x}^2\right)^n \leq 2 \tag{4.17}$$

$$\text{subject to } \prod_{i=1}^{n} \left(1 + {x_i}^2\right) = 2, \tag{4.18}$$

where $\bar{x} \coloneqq \omega_c \bar{\tau} \equiv \sum_{i=1}^{n} x_i/n$ is the arithmetic mean of the x_i's.

The general idea of the proof is to "move" the τ_i's to $\bar{\tau}$ one by one, whilst *improving* the bandwidth of the system with each move. To that end, we will actually prove, subject to the constraint Eq. (4.18), the equivalent inequality

$$\prod_{i=1}^{n} \left(1 + {x_i}^2\right) \geq \left(1 + \bar{x}^2\right)^n. \tag{4.19}$$

We now proceed with the proof proper. If $x_i = \bar{x} \; \forall i$, the upper bound is trivially attained, so assume otherwise. Then $\exists x_p > \bar{x}, x_q < \bar{x}$. Denote $\Delta_p \coloneqq x_p - \bar{x} > 0$. We will now establish the following inequality:

$$(1 + {x_p}^2)(1 + {x_q}^2) > (1 + \bar{x}^2)\left[1 + (x_q + \Delta_p)^2\right]. \tag{4.20}$$

To see this, define the function

$$f(\zeta) \coloneqq \left[1 + (x_p - \zeta)^2\right]\left[1 + (x_q + \zeta)^2\right]. \tag{4.21}$$

We want to show that $f(0) > f(\Delta_p)$. One can compute that

$$f(0) - f(\Delta_p) = \Delta_p(\bar{x} - x_q)\left\{\Delta_p(\bar{x} - x_q) + 2\left[1 - \bar{x}(x_q + \Delta_p)\right]\right\}.$$

By construction, $x_q < \bar{x}$. Hence, to establish the strict positivity of $f(0) - f(\Delta_p)$, we can just check that $1 - \bar{x}(x_q + \Delta_p) > 0$. Since the x_i's are positive, by the constraint (4.18), we know that $x_i < 1 \; \forall i$. Then we can see that $0 < \bar{x} < x_p < 1$ and $0 < x_q + \Delta_p < \bar{x} + \Delta_p = x_p < 1$. Thus, $0 < \bar{x}(x_q + \Delta_p) < 1$, which shows that $f(0) > f(\Delta_p)$. This proves Eq. (4.20).

By renaming $x_p \leftarrow \bar{x}$ and $x_q \leftarrow x_q + \Delta_p$, we have effectively moved x_p to the mean $\bar{x}$ while moving x_q (which was on the other side of $\bar{x}$) by the same but opposite amount

in order to maintain the average $\bar{x}$. This procedure, as we just showed, decreases $\prod_{i=1}^{n}\left(1+{x_i}^2\right)$. We now repeat the above algorithm until all of the x_i's are equal to[4] $\bar{x}$, which yields the right-hand-side of Eq. (4.19), proves Eq. (4.17) and thus also Eq. (4.16), and finally establishes our claim.

Now that we have shown that $H_{\max}(s)$ is indeed the n^{th}-order system (with no zeros or complex poles) with the best bandwidth for the given b_1 coefficient, all that is left for us to do is to compute this optimal bandwidth. It is a simple exercise to show that the bandwidth of $H_{\max}(s)$, which we shall denote by $\omega_{\max}$, is given by

$$\omega_{\max} = \frac{n}{b_1}\sqrt{2^{1/n}-1}. \tag{4.22}$$

This proves the upper bound and also establishes its tightness. □

There is a simple mathematical intuition that we can glean from the upper bound. Since the lower bound is approached when one of the poles is dominant—in the extreme case all non-dominant poles are infinitely far away and we are left with the 1^{st}-order system $H_0/(1+b_1 s)$ whose bandwidth is exactly $1/b_1$—it makes sense that the upper bound is attained when *none* of the poles dominates, in which case all the poles are identical.

4.5 Impact of Complex Poles

Here, we show that the lower bound $\omega_c > 1/b_1$ of Eq. (4.6) still holds when the system has complex poles whose quality factors do not exceed $Q \leq \sqrt{2}$. Consider the canonical form of the denominator polynomial that describes a pair of complex conjugate poles:

$$D(s) = 1 + \frac{s}{Q\omega_0} + \left(\frac{s}{\omega_0}\right)^2 \tag{4.23}$$

where $Q > 1/2$. The time constant associated with this complex pole is the coefficient of the s term $\tau = 1/(Q\omega_0)$, and so we proceed to denote, just like before, $y \coloneqq \omega\tau = \omega/(Q\omega_0)$. Then it holds true that

$$|D(j\omega)|^2 = \left[1-(Qy)^2\right]^2 + y^2 < 1 + y^2 \tag{4.24}$$

if $0 < y < 1$ and $Q \leq \sqrt{2}$. Now, to account for m pairs of complex conjugate poles in the original system, the left-hand-side of Eq. (4.10) is multiplied by the additional term $\prod_{j=1}^{m}\left(\left[1-(Q_j y_j)^2\right]^2 + {y_j}^2\right)$ and the constraint Eq. (4.11) is modified

[4] Obviously, when there are only two x_i's left that are not equal to $\bar{x}$, they will be equidistant from but on opposite sides of $\bar{x}$, so this procedure "centers" both of them to $\bar{x}$.

to $\sum_{i=1}^{n} x_i + \sum_{j=1}^{m} y_j \leq 1$. Noting that $0 < y_j < 1 \; \forall j$ due to the modified constraint and applying the above reasoning of Eq. (4.24) to first deal with the complex poles, we can subsequently proceed with the proof of the lower bound as usual.

It is left as a tedious algebra exercise to show that the upper bound does not hold when the system has complex poles. That is, for any pair of complex conjugate poles, there exists a system with those poles whose bandwidth exceeds the upper bound of Eq. (4.6). To elaborate on this point a little bit more precisely, define $Q_0 \coloneqq (\sqrt{7}/2)(2\sqrt{2} - 1)^{-1/2} \approx 0.97832$. Then if $Q < Q_0$, the 2^{nd}-order system constructed from the complex poles themselves suffices. On the other hand, when $Q \geq Q_0$ (which implies resonant peaking since $Q_0 > 1/\sqrt{2}$), we need to add a dominant real pole to the system in such a way that $H_{\max}(s)$ decays to -3-dB at a frequency where $H(s)$ is still "riding" the resonant peak. This demands that the time constant of this added pole be large enough such that it dominates b_1 sufficiently, but small enough such that its frequency is still close to the resonance frequency of the complex poles.

4.6 Impact of Zeros

The effect that zeros have on the bandwidth is discussed in [43]. Assuming that the zeros are at sufficiently high frequencies, we can approximate the numerator of the transfer function Eq. (4.1) as $H_0(1 + as)$ where $a = a_1/a_0$. Then, since as is still quite small (compared to unity) around the frequencies of interest, we can write $(1 + as) \approx 1/(1 - as)$, which further allows us to crudely approximate Eq. (4.1) as, and therefore replace Eq. (4.4) with

$$H(s) \approx \frac{H_0}{1 + (b_1 - a)s + (b_2 - ab_1)s^2 + \cdots + (b_n - ab_{n-1})s^n - ab_n s^{n+1}}. \tag{4.25}$$

We can then replace the ZVTs with the *modified* ZVTs described in [43], whose sum is equal to $b_1 - a$. The bounds stated in Eq. (4.6) can then be "improved," in some sense, by using $b_1 - a$ in place of b_1. Of course, given the nature of the many approximations being made here, the rigor of these bounds (as established here) no longer holds.

4.7 Conclusion

In this chapter, we proved that the (strict) lower bound on the bandwidth of a low-pass system with no zeros, order exceeding unity, and whose complex poles feature quality factors satisfying $Q \leq \sqrt{2}$ is given by its well-known zero-value time

constant estimate

$$\omega_c > \frac{1}{b_1}, \tag{4.26}$$

and this bound can be approached by making one of the system's (real) poles increasingly dominant. We also proved that the upper bound on the bandwidth of an n^{th}-order low-pass system with no zeros and no complex poles is given by

$$\omega_c \leq \frac{n}{b_1}\sqrt{2^{1/n} - 1}, \tag{4.27}$$

and this bound is attained when all the poles are at the same location. Both bounds are equally important from a conceptual standpoint, as the lower bound should not be "favored" over the upper bound, except perhaps for the reason that the system performs at least as well as the lower bound—i.e., the lower bound serves as a conservative estimate. However, in a system where all the poles are around the same ballpark of frequencies, the upper bound may actually serve as a better estimate of the bandwidth.

In passing, we would also like to note that analogous bounds hold for the low-cutoff frequency of a high-pass filter based on its infinite-value time constants (IVTs). Specifically, for the low-cutoff $\omega_{c,l}$ of an n^{th}-order (where $n > 1$) high-pass system with no non-DC zeros and no complex poles, we have

$$\frac{1}{n\sqrt{2^{1/n} - 1}} \leq \frac{\omega_{c,l}}{\sum_k 1/\tau_k^\infty} < 1 \tag{4.28}$$

where the τ_k^∞'s are the system's IVTs[5], and again, the upper bound also holds in the presence of complex poles with $Q \leq \sqrt{2}$.

In the next chapter, we will return to the notion from Chapter 2 of utilizing abstraction, modularity, and approximation to capture the critical behavior of a complicated system in an intuitive, computationally feasible fashion. Specifically, we turn to analog multipliers, a class of circuits commonly used in communications transceivers as frequency mixers and in phase-locked loops (PLLs) as phase-frequency detectors (PFDs), for example.

[5] As a mathematical note, observe that

$$\sum_k \frac{1}{\tau_k^\infty} = \sum_{i=1}^{n} -p_i = \sum_{i=1}^{n} \frac{1}{\tau_i} = \frac{b_{n-1}}{b_n}$$

where $p_i, i = 1, \ldots, n$ are the system's poles.

Chapter 5

ANALYSIS OF A BALANCED ANALOG MULTIPLIER FOR AN ARBITRARY NUMBER OF SIGNED INPUTS

5.1 Introduction

The double-balanced four-quadrant analog multiplier, invented in the 1960s by Howard Jones [44] and then improved upon by Barrie Gilbert [45], [46], is ubiquitous in numerous modern electronic systems. Shown in Fig. 5.1, this topology effectively multiplies its two input voltages V_{RF} and V_{LO}. Furthermore, the double-balanced nature of the circuit prevents non-product terms (i.e., terms involving V_{RF} or V_{LO} alone) from appearing at or 'feeding through' to the output V_{out}, making it useful in various settings. As a result of its many applications (e.g., amplitude modulation, phase detection, active frequency mixing), it has also been the subject of much research and academic investigation (e.g., [47]–[54]).

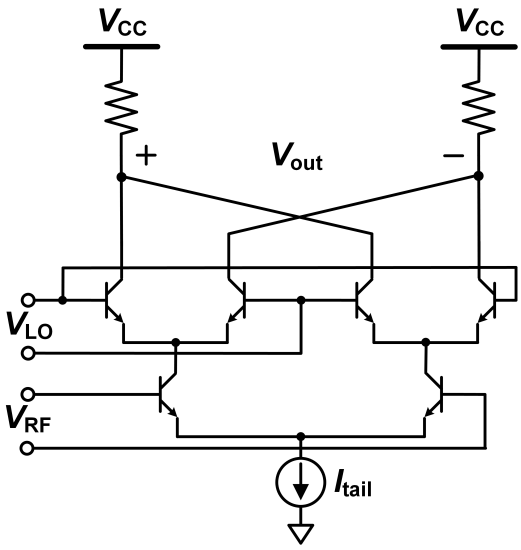

Figure 5.1: An NPN bipolar implementation of the double-balanced current-commutating analog multiplier (aka Gilbert cell).

In this chapter, we look at a natural generalization of this topology that allows for the multiplication of an arbitrary number of analog input voltages of any polarity. Through its analysis, we illustrate how the salient features of a seemingly compli-

cated circuit can be intuitively understood by properly modularizing its topology and exploiting its inherent symmetry. In doing so, we will be able to isolate the system's bare-bone operational concepts from tedious technical details that clutter up the main results.

5.2 The Topology—A General Discussion

The *stacked*, balanced, current-commutating analog multiplier is shown in Fig. 5.2. Notice that this topology features n pairs of differential pairs (known as switching stages), whose inputs are cross-coupled and outputs are connected in parallel, "stacked" on top of one another between the load and the bottom-most differential pair driven by $V_{\text{in},0}$ (known as the transconductance stage). The topology reduces to the standard (dual-input) analog multiplier of Fig. 5.1 for $n = 1$. Versions of this circuit with $n = 2$ have been reported in [55]–[60] without a detailed general analysis.

To understand how this circuit works, let us make several observations. First, notice that the circuit is balanced with respect to each input. To see this, say one of the inputs, $V_{\text{in},k}$, is zero. Then, the output current of that stage $\left(I_{\text{L},k} - I_{\text{R},k}\right)$ and therefore of any stage above it will be zero, resulting in zero output. Thus, terms that are not a product involving *every* single input cannot feedthrough to the output.

Furthermore, we argue that the output's polarity is reversed whenever the polarity of any one of the inputs is reversed. To see this, observe that switching the polarity of $V_{\text{in},k}$ interchanges the currents $I_{\text{L},k}$ and $I_{\text{R},k}$. If $k = n$, the argument is finished. If $k < n$, notice that because $I_{\text{L},k}$ and $I_{\text{R},k}$ are the tail currents of the two differential pairs of stage $(k + 1)$, we have *effectively* reversed the polarity of $V_{\text{in},k+1}$ with respect to the circuit. Recursively propagating this reasoning up the stack of switching stages, we deduce that the polarity of the output is therefore ultimately reversed.

Also note that this topology requires a voltage headroom of $(n + 1)V_{\text{act}} + I_{\text{tail}}R_L$ between the supply and the tail current, where V_{act} is the minimum voltage that must be dropped across a transistor to keep it in the proper "active" region of operation (e.g., $V_{\text{CE,sat}}$, $V_{\text{DS,sat}}$) maximized over all possible operating conditions.

In the following sections, we develop a general analytical framework for computing the output voltage V_{out} in terms of the input voltages. We assume the transistor current I is a nonlinear, monotonically increasing function $f(V)$ of the transistor's control voltage V (e.g., $|V_{\text{BE}}|$, $|V_{\text{GS}}| - |V_{\text{T}}|$). Note that second order effects (e.g., Early effect, channel length modulation, body effect) will be neglected.

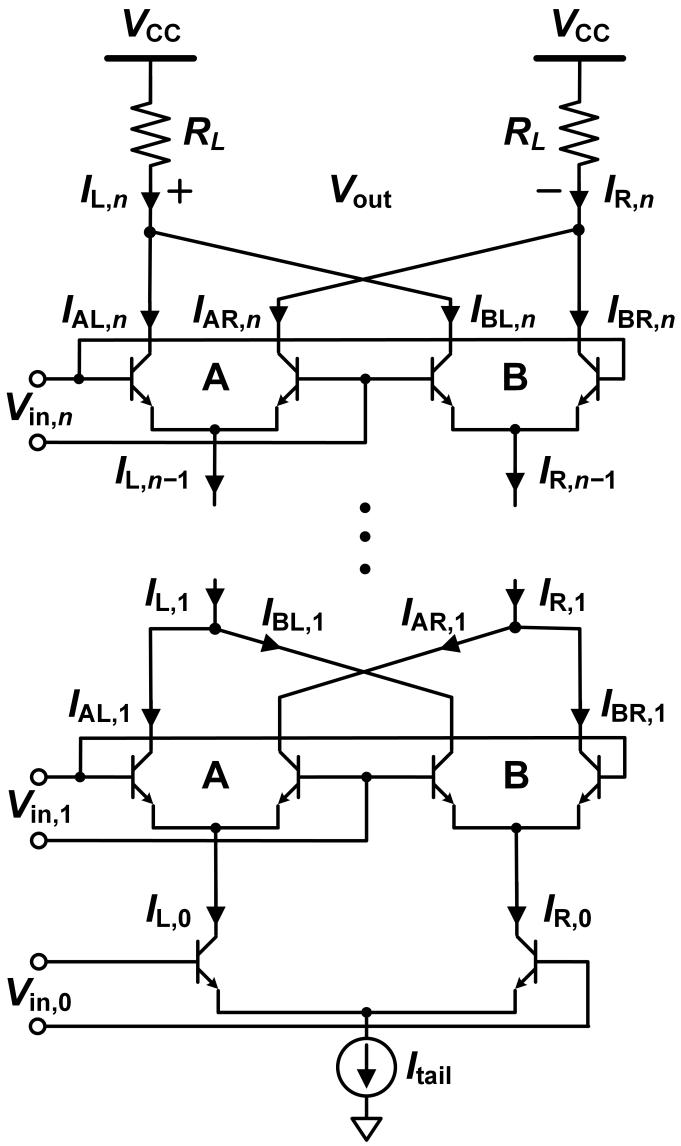

Figure 5.2: The stacked, balanced, current-commutating analog multiplier. The circuit can also be implemented using field-effect transistors.

5.3 The Differential Pair

We begin by considering the differential pair, shown in Fig. 5.3, as it is the fundamental building block of the balanced current-commutating analog multiplier. The differential input voltage V_{in} steers the tail current I_{T} between the two transistors, thereby controlling the differential output current $I_{\text{out}} \coloneqq I_{\text{L}} - I_{\text{R}}$. Throughout, we assume the transistors are matched—that is, they have identical properties.

First, write the following relationship between the transistors' currents and the tail

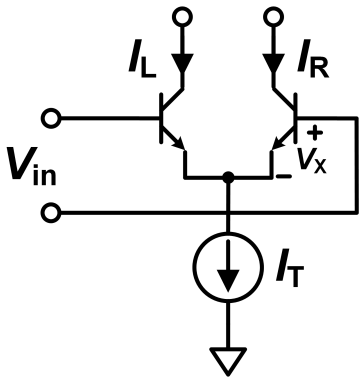

Figure 5.3: The differential pair. The circuit can also be implemented using field-effect transistors.

current:

$$I_L + I_R = f(V_X + V_{in}) + f(V_X) = I_T \tag{5.1}$$

where V_X is the control voltage of the rightmost transistor.[1] We can solve for V_X in terms of V_{in} and I_T: $V_X \equiv g\,(V_{in}, I_T)$; so, I_L and I_R can be written solely in terms of V_{in} and I_T:

$$I_L = f[g(V_{in}, I_T) + V_{in}] \tag{5.2a}$$

$$I_R = f[g(V_{in}, I_T)]\,. \tag{5.2b}$$

Then, we can write the differential output current as a function of the input voltage and the tail current:

$$I_{out} \coloneqq I_L - I_R \equiv h(V_{in}, I_T)\,. \tag{5.3}$$

Here, we point out two important facts:

1. h must be an odd function of V_{in} due to symmetry.
2. $h = 0$ if $I_T = 0$, assuming the reverse leakage current through the transistors is negligible.

The asymptotic behavior of h will be discussed in detail in Section 5.4.

We will now compute examples of h for several well-known transistors.

[1] For bipolar transistors, we can modify the right-hand-side of Eq. (5.1) to αI_T (where $\alpha \equiv I_C/I_E$) for a more accurate result.

Bipolar Differential Pair

For bipolar junction transistors, we take V to be the base-emitter voltage $|V_{\mathrm{BE}}|$. Assuming the forward active region of operation and neglecting the Early effect, the transistor current is

$$f(V) = I_{\mathrm{S}} \left(e^{V/V_{\mathrm{th}}} - 1 \right) \tag{5.4}$$

where I_{S} is the transistor's saturation current and $V_{\mathrm{th}} \coloneqq kT/q$ is the thermal voltage. Then [61]

$$h(V_{\mathrm{in}}, I_{\mathrm{T}}) = (\alpha I_{\mathrm{T}} + 2I_{\mathrm{S}}) \tanh\left(\frac{V_{\mathrm{in}}}{2V_{\mathrm{th}}} \right) \tag{5.5}$$

where $\alpha \equiv I_{\mathrm{C}}/I_{\mathrm{E}}$. Because the reverse leakage current I_{S} is typically numerous orders of magnitude smaller than the tail current, we have

$$h(V_{\mathrm{in}}, I_{\mathrm{T}}) \cong \alpha I_{\mathrm{T}} \tanh\left(\frac{V_{\mathrm{in}}}{2V_{\mathrm{th}}} \right). \tag{5.6}$$

Square-Law MOSFET Differential Pair

For metal-oxide-semiconductor field-effect transistors (MOSFETs), we take V to be the overdrive voltage $|V_{\mathrm{GS}}| - |V_{\mathrm{T}}|$. Assuming pinch-off (i.e., saturation) and neglecting channel length modulation,

$$f(V) = KV^2 \cdot \mathbb{1}\{V \geq 0\} \tag{5.7}$$

where $K \coloneqq (\mu C_{\mathrm{ox}}/2)(W/L)$, and the indicator function ensures that the transistor turns off when its overdrive voltage is negative. Then [61]

$$h(V_{\mathrm{in}}, I_{\mathrm{T}}) = \begin{cases} V_{\mathrm{in}} \sqrt{2KI_{\mathrm{T}} - (KV_{\mathrm{in}})^2}, & |V_{\mathrm{in}}| < \sqrt{\dfrac{I_{\mathrm{T}}}{K}} \\ \mathrm{sign}(V_{\mathrm{in}}) \cdot I_{\mathrm{T}}, & \text{otherwise} \end{cases}. \tag{5.8}$$

Short-Channel MOSFET Differential Pair

Accounting for velocity saturation, the drain current of Eq. (5.7) can be modified as [61]

$$f(V) = \left(\frac{KV^2}{1 + \dfrac{V}{E_{\mathrm{sat}}L}} \right) \cdot \mathbb{1}\{V \geq 0\} \tag{5.9}$$

where E_{sat} is the saturation electric field strength (i.e., the saturation velocity is μE_{sat}). Assuming the carriers in the channel are deeply velocity saturated (i.e., $E_{\mathrm{sat}}L \ll V$), Eq. (5.9) becomes

$$f(V) \cong KE_{\mathrm{sat}}LV \cdot \mathbb{1}\{V \geq 0\}. \tag{5.10}$$

Then it is straightforward to see that

$$h(V_{\text{in}}, I_{\text{T}}) = \begin{cases} KE_{\text{sat}}LV_{\text{in}}, & |V_{\text{in}}| < \dfrac{I_{\text{T}}}{KE_{\text{sat}}L} \\ \text{sign}(V_{\text{in}}) \cdot I_{\text{T}}, & \text{otherwise} \end{cases}. \tag{5.11}$$

Subthreshold Conduction

Due to the increasing popularity of the usage of metal-oxide-semiconductor (MOS) transistors under *subthreshold conduction* within low-power applications, it is prudent to quickly mention their operation at this point. If $|V_{\text{GS}}| \leq |V_{\text{T}}|$, then the MOSFET's I-V characteristic is given by [61]

$$I_{\text{D}} \propto \exp\left(\frac{|V_{\text{GS}}|}{nV_{\text{th}}}\right) \cdot \left(1 - e^{-|V_{\text{DS}}|/V_{\text{th}}}\right), \tag{5.12}$$

where $n > 1$ is an ideality factor[2]. Reasonably assuming that the drain-source voltage is at least several thermal voltages (e.g., $|V_{\text{DS}}| > 3V_{\text{th}}$), the dependence of the drain current on the drain voltage vanishes and we can take the transistor's control voltage to be the gate-source voltage $V = |V_{\text{GS}}|$. Then,

$$f(V) \propto \exp\left(\frac{V}{nV_{\text{th}}}\right). \tag{5.13}$$

In other words, a MOS transistor under weak inversion behaves similarly to a bipolar transistor, except with a worse turn-on. Because the proportionality constant in Eq. (5.13) is typically orders of magnitude smaller than the bias current, appealing to the derivation from Section 5.3, we can compute

$$h(V_{\text{in}}, I_{\text{T}}) \cong I_{\text{T}} \tanh\left(\frac{V_{\text{in}}}{2nV_{\text{th}}}\right) \tag{5.14}$$

which is identical to Eq. (5.6) except for the factor of n.

Note that subthreshold conduction becomes apparent in two different scenarios. Most importantly, if $|V_{\text{GS}}| \leq |V_{\text{T}}|$ at the differential pair's operating or bias point, then obviously, Eq. (5.14) accurately characterizes the differential pair for essentially all input voltages V_{in} of interest. On the other hand, if the transistors are biased in strong inversion (and the square-law prevails, for example), for sufficiently large inputs $|V_{\text{in}}|$ (e.g., $|V_{\text{in}}| \geq \sqrt{I_{\text{T}}/K}$ for square-law MOSFETs), due to subthreshold

[2]To elaborate slightly further,

$$n = 1 + \frac{C_S}{C_{\text{ox}}},$$

where C_S is the capacitance of the semiconductor bulk and C_{ox} is the oxide capacitance.

leakage, one of the transistors will *not* simply "turn off" abruptly and conduct no current whatsoever as implied by Eqs. (5.8) and (5.11). Instead, there will be a *smooth*, "exponential-decay like" transition that causes $h(V_{\text{in}}, I_{\text{T}})$ to asymptotically approach $\text{sign}(V_{\text{in}}) \cdot I_{\text{T}}$ in accordance with Eq. (5.14). For our purposes though, this latter scenario does not influence the overall behavior of the differential pair in a practically significant way.

Fig. 5.4 depicts normalized theoretical plots of $h(V_{\text{in}}, I_{\text{T}})$ vs. V_{in} based on Eqs. (5.6), (5.8), and (5.11).

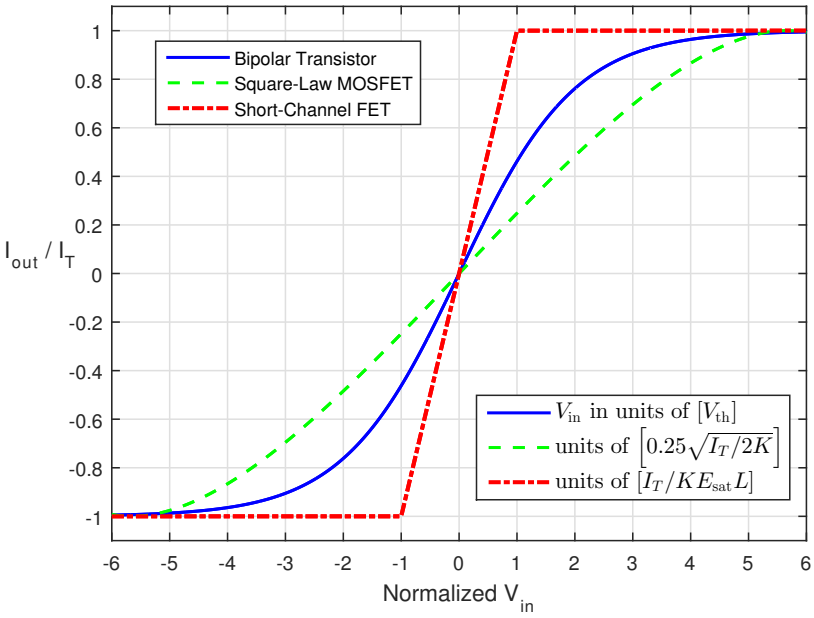

Figure 5.4: Current switching in a differential pair as a function of the input voltage. Base current and subthreshold conduction were ignored. Due to the chosen normalizations for the V_{in}-axis, the plot scales may not be *quantitatively* comparable.

5.4 The Crucial Role of Nonlinearity

Before we proceed with an analysis of the stacked analog multiplier, we briefly discuss why $f(\cdot)$ must be nonlinear in order for multiplication to occur. To see this, assume f is linear and notice that the output current can be written as

$$\begin{aligned} h(V_{\text{in}}, I_{\text{T}}) &= f(V_X + V_{\text{in}}) - f(V_X) \\ &= f(V_{\text{in}}) \end{aligned} \tag{5.15}$$

which depends solely (and linearly) upon the differential input voltage V_{in} and not on the tail current I_{T}. In this scenario, the differential behavior of each switching

stage becomes independent of and therefore isolated from the operation of the stage below it, preventing the input voltages from multiplying.[3]

Of course, this is never truly an issue, at least in large-signal: transistors, being unilateral devices, can appreciably conduct current in only one direction. Consequently, they *turn off* for control voltages that do not exceed some threshold, making f inherently nonlinear. We therefore intuit that differential input voltages above a certain magnitude (say V_{sw}, which depends on I_{T}) will turn off one of the pair's transistors, thereby completely switching the tail current to the other side (Fig. 5.4). That is,[4]

$$h(V_{\text{in}}, I_{\text{T}}) = \text{sign}(V_{\text{in}}) \cdot I_{\text{T}} \quad \text{for} \quad |V_{\text{in}}| \geq V_{\text{sw}}. \tag{5.16}$$

As a result, $|h|$ is fundamentally bounded by and therefore dependent on I_{T}.

What if $f(\cdot)$ is locally linear in some neighborhood of the transistor's operating or bias point, resulting in a range of input voltages (centered around 0) for which $h\left(V_{\text{in}}, I_{\text{T}}\right)$ is independent of the tail current I_{T} (refer to Section 5.3 for an example)? In this situation, if the input voltage to any switching stage remains poised in this range, multiplication cannot occur and the output will be zero. This claim will be proven analytically below in Section 5.5. Essentially, multiplication requires the differential pair's output current $h(V_{\text{in}}, I_{\text{T}})$ for *every* switching stage to depend on I_{T} at the point where the input voltage V_{in} is situated.

5.5 General Analysis

We now proceed with an analysis of the output voltage of the stacked analog multiplier. Throughout, we will assume that the transistors in each *stage* are identical but may differ from stage to stage. Referring to Fig. 5.2,

$$\begin{aligned} V_{\text{out}} &= -R_L \left(I_{\text{L},n} - I_{\text{R},n}\right) \\ &= -R_L \left[\left(I_{\text{AL},n} - I_{\text{AR},n}\right) + \left(I_{\text{BL},n} - I_{\text{BR},n}\right)\right] \\ &= -R_L \left[h_n\left(V_{\text{in},n}, I_{\text{L},n-1}\right) + h_n\left(-V_{\text{in},n}, I_{\text{R},n-1}\right)\right] \\ &= -R_L \left[h_n\left(V_{\text{in},n}, I_{\text{L},n-1}\right) - h_n\left(V_{\text{in},n}, I_{\text{R},n-1}\right)\right]. \end{aligned} \tag{5.17}$$

To proceed, the analysis depends on the specific form of h. However, the main idea is that for any $k \in \{1, \ldots, n\}$, we can decompose $I_{\text{L},k} = I_{\text{AL},k} + I_{\text{BL},k}$ and

[3] In fact, due to the balanced nature of the topology, one can easily deduce that the output will be identically zero if h is independent of I_{T}.

[4] In the presence of reverse bias or subthreshold leakage, V_{sw} is not well-defined. The more precise statement is

$$h(V_{\text{in}}, I_{\text{T}}) \to \text{sign}(V_{\text{in}}) \cdot I_{\text{T}} \quad \text{as} \quad |V_{\text{in}}| \to \infty,$$

assuming the leakage current is *small*. See Section 5.3.

$I_{\mathrm{R},k} = I_{\mathrm{AR},k} + I_{\mathrm{BR},k}$. Then, using $f(\cdot)$ and $g(\cdot)$ for stage k, we can write

$$\begin{aligned} I_{\mathrm{L},k} &= f\left[g\left(V_{\mathrm{in},k}, I_{\mathrm{L},k-1}\right) + V_{\mathrm{in},k}\right] + f\left[g\left(V_{\mathrm{in},k}, I_{\mathrm{R},k-1}\right)\right] \\ I_{\mathrm{R},k} &= f\left[g\left(V_{\mathrm{in},k}, I_{\mathrm{L},k-1}\right)\right] + f\left[g\left(V_{\mathrm{in},k}, I_{\mathrm{R},k-1}\right) + V_{\mathrm{in},k}\right]. \end{aligned} \tag{5.18}$$

For $k = 0$, we use Eq. (5.2) with $V_{\mathrm{in}} = V_{\mathrm{in},0}$ and $I_{\mathrm{T}} = I_{\mathrm{tail}}$.

We will now explore several important specific cases.

Output Current Proportional to Tail Current

If $h(V_{\mathrm{in}}, I_{\mathrm{T}})$ is proportional to I_{T}, the analysis proceeds via induction rather quickly. Say

$$h(V_{\mathrm{in}}, I_{\mathrm{T}}) = \zeta(V_{\mathrm{in}})\, I_{\mathrm{T}} \tag{5.19}$$

where $\zeta(\cdot)$ is a unit-less, odd function bounded by ± 1. Then, from the last step of Eq. (5.17), we have

$$V_{\mathrm{out}} = -R_L\, \zeta_n\left(V_{\mathrm{in},n}\right)\, \left(I_{\mathrm{L},n-1} - I_{\mathrm{R},n-1}\right). \tag{5.20}$$

Comparison with the first step of Eq. (5.17) allows us to use induction to obtain

$$V_{\mathrm{out}} = -R_L\, \left(I_{\mathrm{L},0} - I_{\mathrm{R},0}\right) \prod_{k=1}^{n} \zeta_k\left(V_{\mathrm{in},k}\right). \tag{5.21}$$

Therefore,

$$V_{\mathrm{out}} = -R_L I_{\mathrm{tail}} \prod_{k=0}^{n} \zeta_k\left(V_{\mathrm{in},k}\right). \tag{5.22}$$

Example with Measurements: Bipolar Multiplier

From Eq. (5.6), the large-signal output current of a bipolar differential pair is

$$h(V_{\mathrm{in}}, I_{\mathrm{T}}) \cong \alpha I_{\mathrm{T}} \tanh\left(\frac{V_{\mathrm{in}}}{2V_{\mathrm{th}}}\right), \tag{5.23}$$

which is proportional to I_{T}. Therefore, comparing Eq. (5.23) with Eq. (5.19), we can easily compute the large-signal output voltage of a bipolar implementation of the stacked analog multiplier [56]:

$$\implies V_{\mathrm{out}} = -R_L I_{\mathrm{tail}} \prod_{k=0}^{n} \alpha_k \tanh\left(\frac{V_{\mathrm{in},k}}{2V_{\mathrm{th}}}\right). \tag{5.24}$$

To verify this equation, a bipolar NPN implementation of the stacked analog multiplier with $n = 4$ was constructed using CA3083 transistor arrays. The tail current,

$I_{\text{tail}} = 1\,\text{mA}$, was implemented using an emitter degenerated 2N3904 NPN transistor. A load resistance of $R_L = 1\ \text{k}\Omega$ was used, and the supply was set to $V_{\text{CC}} = 7$ V. The DC current gain of the transistors was experimentally estimated to be around $\beta = 100$. The common-mode voltage of the k^{th} input was tuned to $(1.68 + k)$ [V].

For each of a total of 100 experiments, 5 input voltages ranging from ±25 mV to ±130 mV were randomly generated using MATLAB and fed to the circuit using a USB-3106 DAQ board by Measurement Computing.[5] The output voltage was measured and compared against $\alpha^5 \prod_{k=0}^{4} \tanh\left(V_{\text{in},k}/2V_{\text{th}}\right)$ [V] from Eq. (5.24). A histogram of the percent error is shown in Fig. 5.5, demonstrating excellent agreement between theory and experiment.

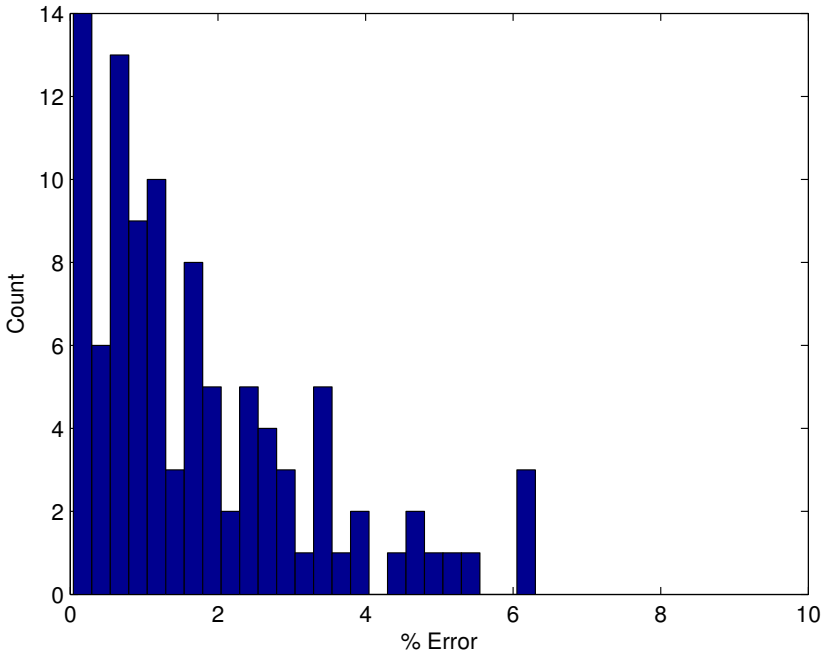

Figure 5.5: 25 bin histogram of the percent error over $N = 100$ trials. The mean of the percent error is 1.8%.

[5] "Small" input voltages were avoided because not all of the transistors in the array are matched to one another. It can easily be shown [61] that a (voltage-driven) unbalanced bipolar differential pair is equivalent to a balanced pair with a differential offset voltage equal to $V_{\text{off}} = V_{\text{th}} \ln(I_{\text{SL}}/I_{\text{SR}})$. Therefore, the impact of transistor mismatch on the error in the output current is more prominent for smaller input voltages. Experimentally, an output voltage of 3.3 mV was measured when all the inputs were nulled, which corresponds to a *mean* offset voltage of $V_{\text{off}} = 17$ mV for each pair.

Small-Signal Multiplication

Here, we assume that the input voltages are sufficiently small such that any dependence on any particular input voltage is essentially linear. The transistor's transconductance g_m is defined as the rate of change of the output current with respect to the control voltage:

$$g_m \coloneqq \frac{\partial I}{\partial V} = f'(V), \tag{5.25}$$

which can be expressed in terms of the transistor's bias current $I = I_{\text{bias}}$ by noting that $V = f^{-1}(I_{\text{bias}})$. So, we write $g_m \equiv g_m(I_{\text{bias}})$ to make this dependence explicit.

A simple small-signal analysis of the differential pair[6] reveals that its small-signal differential transconductance is

$$\left.\frac{\partial h(V_{\text{in}}, I_{\text{T}})}{\partial V_{\text{in}}}\right|_{V_{\text{in}}=0} \equiv \left.\left[\frac{\partial I_{\text{L}}}{\partial V_{\text{in}}} - \frac{\partial I_{\text{R}}}{\partial V_{\text{in}}}\right]\right|_{V_{\text{in}}=0} = g_m\left(\frac{I_{\text{T}}}{2}\right). \tag{5.26}$$

Using Eq. (5.26) to linearize the last step of Eq. (5.17) about $V_{\text{in},n} = 0$,

$$\begin{aligned} V_{\text{out}} &\approx - R_L V_{\text{in},n}\left[g_{m,n}\left(\frac{I_{\text{L},n-1}}{2}\right) - g_{m,n}\left(\frac{I_{\text{R},n-1}}{2}\right)\right] \\ &= - R_L V_{\text{in},n}\left[g_{m,n}\left(\frac{I_{\text{AL},n-1} + I_{\text{BL},n-1}}{2}\right) - g_{m,n}\left(\frac{I_{\text{AR},n-1} + I_{\text{BR},n-1}}{2}\right)\right]. \end{aligned} \tag{5.27}$$

Noting that if $V_{\text{in},k} = 0$ for any $k \in \{0, 1, \ldots, n\}$, then $I_{\text{L},k} = I_{\text{R},k} = I_{\text{tail}}/2$, we now linearize about $V_{\text{in},n-1} = 0$ to obtain

$$\begin{aligned} V_{\text{out}} &\approx -R_L V_{\text{in},n} V_{\text{in},n-1} \cdot \frac{1}{2}\left.\frac{\partial g_{m,n}}{\partial I_{\text{bias}}}\right|_{V_{\text{in},n-1}=0} \cdot \left[\frac{\partial I_{\text{AL},n-1}}{\partial V_{\text{in},n-1}} - \frac{\partial I_{\text{AR},n-1}}{\partial V_{\text{in},n-1}}\right. \\ &\qquad \left. + \frac{\partial I_{\text{BL},n-1}}{\partial V_{\text{in},n-1}} - \frac{\partial I_{\text{BR},n-1}}{\partial V_{\text{in},n-1}}\right]\Bigg|_{V_{\text{in},n-1}=0} \\ &= -R_L V_{\text{in},n} V_{\text{in},n-1} \cdot \frac{1}{2}\left.\frac{\partial g_{m,n}}{\partial I_{\text{bias}}}\right|_{I_{\text{bias}}=I_{\text{tail}}/4} \cdot \left[g_{m,n-1}\left(\frac{I_{\text{L},n-2}}{2}\right) - g_{m,n-1}\left(\frac{I_{\text{R},n-2}}{2}\right)\right]. \end{aligned} \tag{5.28}$$

By induction, we see that

$$V_{\text{out}} \approx -R_L V_{\text{in},1}\left[g_{m,1}\left(\frac{I_{\text{L},0}}{2}\right) - g_{m,1}\left(\frac{I_{\text{R},0}}{2}\right)\right] \cdot \prod_{k=2}^{n}\left(\frac{1}{2} V_{\text{in},k}\left.\frac{\partial g_{m,k}}{\partial I_{\text{bias}}}\right|_{I_{\text{bias}}=I_{\text{tail}}/4}\right). \tag{5.29}$$

[6] Rigorously, one can use Eqs. (5.1) and (5.2) to linearize Eq. (5.3) about $V_{\text{in}} = 0$.

Finally, we linearize about $V_{\text{in},0} = 0$ to obtain[7]

$$v_{\text{out}} = -R_L\, g_{m,0}\left(\frac{I_{\text{tail}}}{2}\right) v_{\text{in},0} \cdot \prod_{k=1}^{n}\left(\frac{1}{2} v_{\text{in},k}\, \frac{\partial g_{m,k}}{\partial I_{\text{bias}}}\bigg|_{I_{\text{bias}}=I_{\text{tail}}/4}\right) \tag{5.30}$$

where a lowercase variable indicates a small-signal quantity.

Here, we briefly revisit the concept from Section 5.4 that multiplication is a strictly nonlinear phenomenon, even within the small-signal regime. Notice from Eq. (5.30) that the key requisite for small-signal multiplication is that the transconductances of all the switching stage transistors ($g_{m,k},\ k > 0$) change with the bias current at the operating point. This dependency is clearly non-existent if $f(\cdot)$ is locally linear in the vicinity of the bias point $I_{\text{bias}} = I_{\text{tail}}/4$, as this also implies that $h(V_{\text{in}}, I_{\text{T}})$ does not change with I_{T} in some neighborhood of $V_{\text{in}} = 0$. For this reason, multiplication of *small-signals* is not possible if any of the switching stages are constructed from *deeply* velocity-saturated short-channel MOS transistors, for example.

Example: Square-Law MOS Multiplier

Let us apply this result to an MOS implementation of the stacked analog multiplier. Recalling that the transconductance of a square-law MOSFET is $g_m(I_{\text{bias}}) = 2\sqrt{K I_{\text{bias}}}$, we get

$$\implies v_{\text{out}} = -\sqrt{2} R_L I_{\text{tail}} \prod_{k=0}^{n}\left(\sqrt{\frac{K_k}{I_{\text{tail}}}} v_{\text{in},k}\right). \tag{5.31}$$

Hard-Switching Inputs

Finally, we explore the case where all the inputs are large enough such that for each differential pair, the current is essentially completely switched to one side (i.e., $|V_{\text{in}}| \geq V_{\text{sw}}$). Then, it is easily seen that in this scenario, the output current is proportional to the tail current with $\zeta\,(V_{\text{in}}) = \text{sign}(V_{\text{in}})$. Therefore,

$$V_{\text{out}} = -R_L I_{\text{tail}} \prod_{k=0}^{n} \text{sign}\big(V_{\text{in},k}\big) \tag{5.32}$$

which is positive if and only if an odd number of the inputs are negative. So, if "positive" and "negative" are interpreted in a binary fashion, we see that the stacked analog multiplier performs an "exclusive or" (XOR) of all the inputs.

[7] As a computational note, in light of Eq. (5.25),

$$\frac{\partial g_m}{\partial I_{\text{bias}}} = \frac{f''(V)}{f'(V)} = \frac{f''\big(f^{-1}(I_{\text{bias}})\big)}{g_m(I_{\text{bias}})}.$$

Notice that in the hard-switching situation, exactly one transistor from each stage is on, and therefore the entirety of the tail current will flow through a single path from the supply to ground (out of 2^{2n+1} possible paths).

Mixture of Small-Signal and Hard-Switching Inputs

Let $S \subset \{0, 1, \ldots, n\}$ be a (nonempty) index set. Suppose it is known that $V_{\text{in},k}$ is a small-signal if $k \in S$, whereas $V_{\text{in},k}$ is a large, hard-switching input if $k \notin S$. Denote $q \coloneqq \min(S)$ as corresponding to the bottom-most stage driven by a small-signal input. Then, it can be shown that

$$v_{\text{out}} = -R_L \, g_{m,q}\left(\frac{I_{\text{tail}}}{2}\right) v_{\text{in},q} \cdot \prod_{\substack{k \in S \\ k \neq q}} \left(\frac{1}{2} v_{\text{in},k} \left. \frac{\partial g_{m,k}}{\partial I_{\text{bias}}} \right|_{I_{\text{bias}} = I_{\text{tail}}/4} \right) \cdot \prod_{k \notin S} \text{sign}\big(V_{\text{in},k}\big) \,. \quad (5.33)$$

5.6 Simulation Results

Here, we used Spectre to run transient simulations on a stacked analog multiplier with $n = 3$ (4 inputs) implemented using identical NMOS transistors on a 55-nm bulk CMOS process. A load of $R_L = 1$ kΩ was used, and the tail was implemented with an ideal current source.

For a differential pair composed on this technology, the output current $h(V_{\text{in}}, I_{\text{T}})$ as a function of the input voltage V_{in} was simulated and is depicted in Fig. 5.6 for various values of the tail current I_{T}.

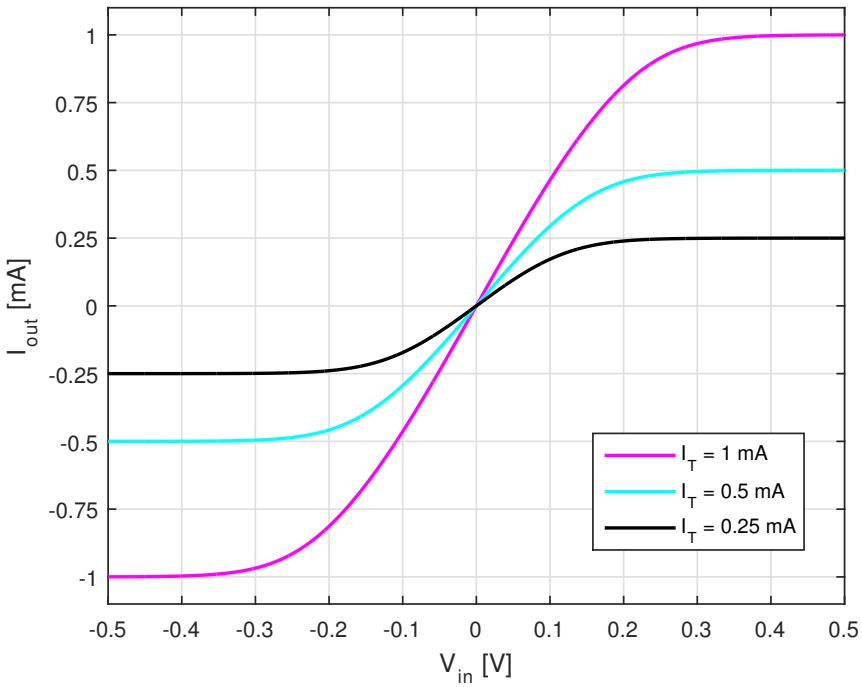

Figure 5.6: A simulated plot of the differential output current vs. the differential input voltage for various tail currents.

Sinusoidal Inputs with Different Phases

Fig. 5.7 shows the simulation result for sinusoidal input voltages, all of the same frequency, spaced at a phase of $\pi/2$ apart from one another:

$$V_{\text{in},k} = V_{\text{amp}} \sin\left(\omega_{\text{in}} t + \frac{\pi}{2} k\right) \tag{5.34}$$

where $V_{\text{amp}} = 100$ mV, $f_{\text{in}} = 250$ MHz, and $k = 0, 1, 2, 3$. Thus, in the small-signal limit, the output voltage is proportional to

$$-\prod_{k=0}^{3} \sin\left(\omega_{\text{in}} t + \frac{\pi}{2} k\right) \propto [\cos(4\omega_{\text{in}} t) - 1], \tag{5.35}$$

which is observed in the simulated output. Of course, the sine wave is not perfect, as Eq. (5.35) is a small-signal limit.

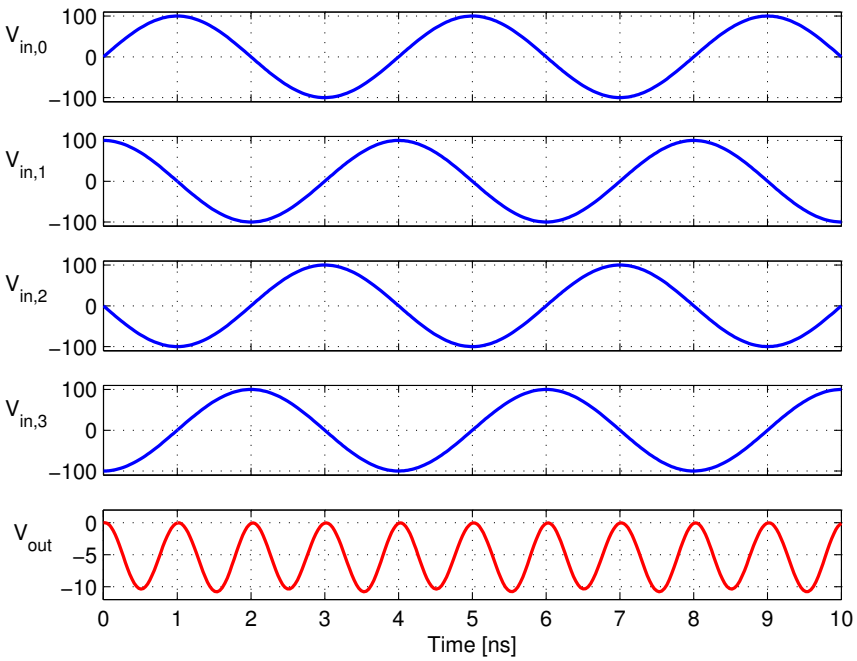

Figure 5.7: Sinusoidal inputs with different phases. Voltages are in [mV]. The tail current is 0.5 mA.

Sinusoidal Inputs at Multiple Frequencies

Fig. 5.8 shows the simulation result for sinusoidal input voltages at different frequencies:

$$V_{\text{in},k} = V_{\text{amp}} \sin[(k+1)\omega_0 t] \tag{5.36}$$

where $V_{\text{amp}} = 100\,\text{mV}$, $f_0 = 100\,\text{MHz}$, and $k = 0, 1, 2, 3$. Thus, in the small-signal limit, it can be shown that the output voltage consists of equally strong harmonics at DC, $6f_0$, $8f_0$, and $10f_0$:

$$\prod_{k=0}^{3} \sin[(k+1)\omega_0 t] \propto 1 - \cos(6\omega_0 t) - \cos(8\omega_0 t) + \cos(10\omega_0 t). \tag{5.37}$$

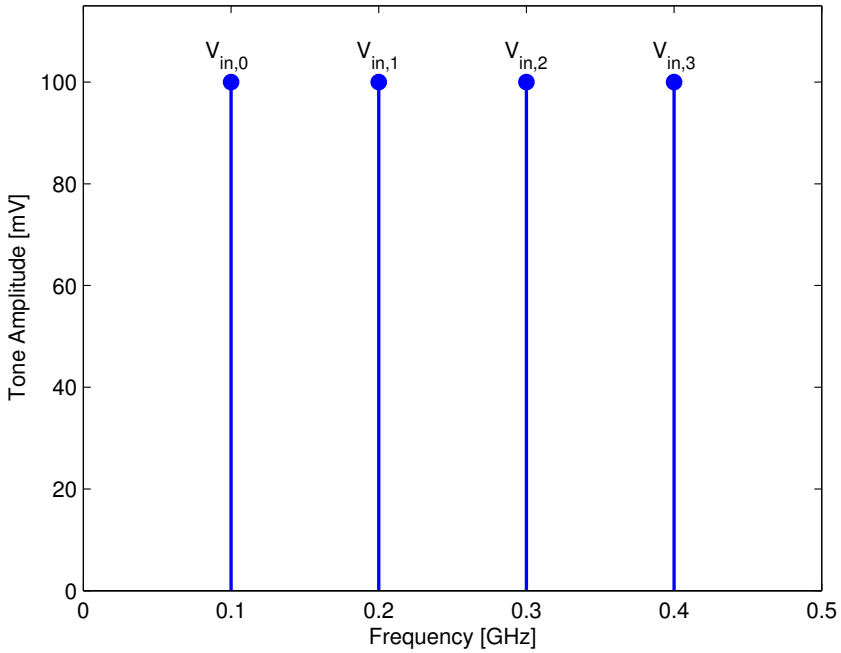

(a) Inputs

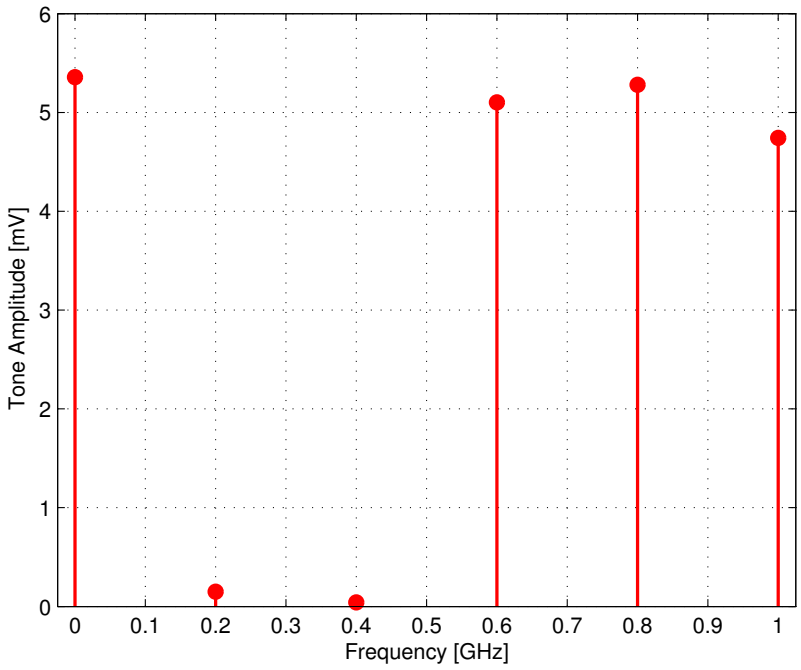

(b) Output

Figure 5.8: Magnitude spectra of (a) the multi-frequency inputs and (b) the output. The spectrum was generated by computing a 64-point fast Fourier transform (FFT) of a 1 μs transient simulation. The tail current is 0.5 mA. Roughly equally strong harmonics are seen in the output at 0 MHz (DC), 600 MHz, 800 MHz, and 1 GHz.

Accounting for gain compression (Fig. 5.6), we can use Eq. (5.30) to roughly estimate the amplitude of the outputs seen in Figs. 5.7 and 5.8. Simulations reveal $g_m(0.25\text{ mA}) = 3.45\text{ mS}$, $g_m'(0.125\text{ mA}) = 12.9\text{ V}^{-1}$, and an average per stage gain compression factor of 0.83 (defined as the factor by which the differential pair output current is reduced from $g_m V_{\text{in}}$). The constant of proportionality for Eqs. (5.35) and (5.37) is $1/8$. This results in an amplitude (Fig. 5.8b) of

$$\frac{1}{8} \times (0.83)^4 \times 1\text{ k}\Omega \times 3.45\text{ mS} \times \left(\frac{12.9\text{ V}^{-1}}{2}\right)^3 \times (0.1\text{ V})^4 = 5.49\text{ mV},$$

or a peak-to-peak amplitude (Fig. 5.7) of 11 mV, which are reasonably close to the simulated amplitudes. Note also that our analysis does not account for the current consumed by the output resistance of the transistors, which further decreases the output amplitude.

Hard-Switching Square-Wave Inputs

Fig. 5.9 shows the simulation result for ±1 V amplitude, 125 MHz frequency, square-wave inputs spaced at a delay of 1 ns apart from one another. Eq. (5.32) therefore predicts a 500 MHz square-wave output of amplitude $\pm I_{\text{tail}} R_L = \pm 1$ V, which is observed in the simulated output. Switching delays due to the transistors' capacitances are apparent.

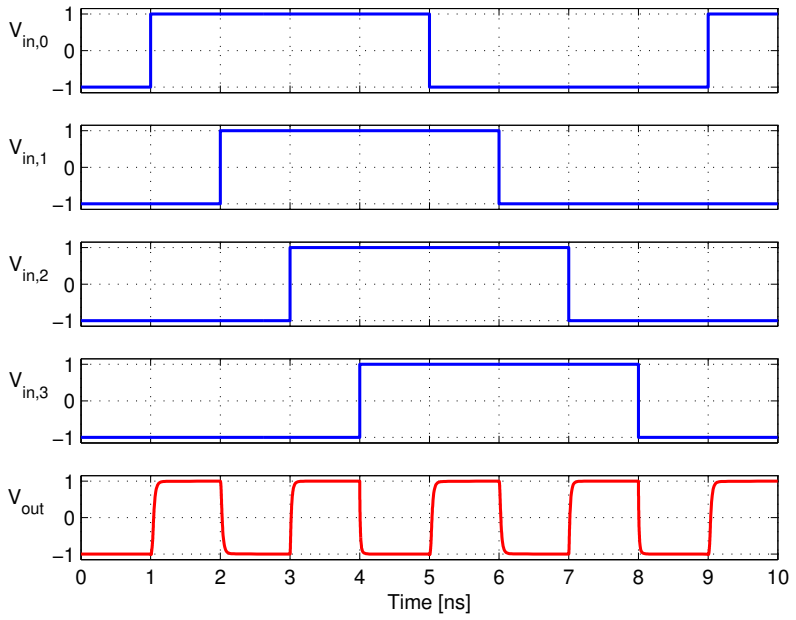

Figure 5.9: Square-wave inputs. Voltages are in [V]. The tail current is 1 mA.

5.7 Higher Order Intermodulation Products

To quantitatively characterize this circuit's nonlinearity, we can use a multi-dimensional Taylor series expansion of the output with respect to all of the input voltages:[8]

$$V_{\text{out}} = \sum_{p_0=1}^{\infty} \sum_{p_1=1}^{\infty} \cdots \sum_{p_n=1}^{\infty} G(p_0, \ldots, p_n) \prod_{k=0}^{n} {V_{\text{in},k}}^{p_k} \tag{5.38}$$

where the intermodulation product "gain" is

$$G(p_0, \ldots, p_n) = \frac{1}{p_0! \cdots p_n!} \cdot \left. \frac{\partial^{p_n + p_{n-1} + \cdots + p_0} V_{\text{out}}}{\partial {V_{\text{in},n}}^{p_n} \partial {V_{\text{in},n-1}}^{p_{n-1}} \cdots \partial {V_{\text{in},0}}^{p_0}} \right|_{V_{\text{in},k}=0 \; \forall k}.$$

It is apparent that the small-signal analysis of Section 5.5 deals with the "first" term of this expansion (where $p_k = 1 \; \forall k$). The purpose of this section is to derive the rest of the terms. The analysis is similar in spirit to that of Section 5.5, with some differences in the technical details. In order to strike a balance between accuracy and tractability, we make a crucial approximation in our analysis: Fix a stage $k \in \{1, \ldots, n\}$. Then, 1) *nonlinear* dependencies (i.e., beyond the first derivative) of the output V_{out} on the k^{th} stage's input $V_{\text{in},k}$ and 2) *any* dependence of V_{out} on the subset of input voltages $V_{\text{in},0}, \ldots, V_{\text{in},k-1}$ below the k^{th} stage are effectively encapsulated by the k^{th} stage's differential output current $\left(I_{\text{L},k} - I_{\text{R},k}\right)$. The precise meaning of this statement will become clear in the subsequent analysis. Physically, the intuition behind this statement follows from the circuit's balanced nature: the multiplier "works" by generating differences between I_{L} and I_{R} at each stage; all other signals within the circuit (such as common-mode variations) should not appear at the output. Consequently, notice that this approximation is predicated on all the differential pairs within the multiplier being perfectly balanced.

First, we introduce the notation

$$M^{(p)}(I_{\text{T}}) \equiv \left. \frac{\partial^p h(V_{\text{in}}, I_{\text{T}})}{\partial {V_{\text{in}}}^p} \right|_{V_{\text{in}}=0}, \tag{5.39}$$

where h is defined in Eq. (5.3). $M^{(p)}$ essentially represents p^{th} order nonlinearities in the differential pair.

We start by differentiating the last step of Eq. (5.17) with respect to $V_{\text{in},n}$ a total of p_n times:

$$\frac{\partial^{p_n} V_{\text{out}}}{\partial {V_{\text{in},n}}^{p_n}} = -R_L \left[\frac{\partial^{p_n} h_n\left(V_{\text{in},n}, I_{\text{L},n-1}\right)}{\partial {V_{\text{in},n}}^{p_n}} - \frac{\partial^{p_n} h_n\left(V_{\text{in},n}, I_{\text{R},n-1}\right)}{\partial {V_{\text{in},n}}^{p_n}} \right]. \tag{5.40}$$

[8] Note that the lower indices of summation are all 1 because the multiplier is balanced with respect to each input (refer to Section 5.2).

Next, we use the chain rule to differentiate with respect to $V_{\text{in},n-1}$ *once*:

$$\begin{aligned}&\frac{\partial^{1+p_n} V_{\text{out}}}{\partial {V_{\text{in},n}}^{p_n} \partial V_{\text{in},n-1}} \\ &= -R_L \left[\frac{\partial^{1+p_n} h_n\left(V_{\text{in},n}, I_{\text{L},n-1}\right)}{\partial I_{\text{L},n-1} \partial {V_{\text{in},n}}^{p_n}} \frac{\partial I_{\text{L},n-1}}{\partial V_{\text{in},n-1}} - \frac{\partial^{1+p_n} h_n\left(V_{\text{in},n}, I_{\text{R},n-1}\right)}{\partial I_{\text{R},n-1} \partial {V_{\text{in},n}}^{p_n}} \frac{\partial I_{\text{R},n-1}}{\partial V_{\text{in},n-1}} \right].\end{aligned} \tag{5.41}$$

This is where our above approximation comes into play: we assume the quantity $\left(I_{\text{L},n-1} - I_{\text{R},n-1}\right)$ dominates all *higher-order* variations of the output with respect to $V_{\text{in},n-1}$ and *all* variations with respect to the lower input voltages $V_{\text{in},n-2}, \ldots, V_{\text{in},0}$. Because the final answer is to be evaluated at the operating point where all the inputs are nulled, we decompose Eq. (5.41) using

$$\frac{\partial^{1+p_n} h_n\left(V_{\text{in},n}, I_{\text{L},n-1}\right)}{\partial I_{\text{L},n-1} \partial {V_{\text{in},n}}^{p_n}} \approx \frac{\partial^{1+p_n} h_n\left(V_{\text{in},n}, I_{\text{R},n-1}\right)}{\partial I_{\text{R},n-1} \partial {V_{\text{in},n}}^{p_n}} \approx \left.\frac{\partial M_n^{(p_n)}(I_{\text{T}})}{\partial I_{\text{T}}}\right|_{I_{\text{T}}=I_{\text{tail}}/2},$$

which leads to

$$\implies \left.\frac{\partial^{1+p_n} V_{\text{out}}}{\partial {V_{\text{in},n}}^{p_n} \partial V_{\text{in},n-1}}\right|_{V_{\text{in},n}=0} \approx -R_L \left[\left.\frac{\partial M_n^{(p_n)}(I_{\text{T}})}{\partial I_{\text{T}}}\right|_{I_{\text{T}}=I_{\text{tail}}/2} \cdot \frac{\partial\left(I_{\text{L},n-1} - I_{\text{R},n-1}\right)}{\partial V_{\text{in},n-1}} \right].$$

The first term in the brackets represents the output's dependence on the n^{th} input; the second term captures the rest of the inputs. Noting that $I_{\text{L},k} - I_{\text{R},k} = h_k\left(V_{\text{in},k}, I_{\text{L},k-1}\right) - h_k\left(V_{\text{in},k}, I_{\text{R},k-1}\right)\ \forall k = 1, \ldots, n$ and then differentiating the output voltage with respect to $V_{\text{in},n-1}$ another $p_{n-1} - 1$ times results in

$$\begin{aligned}&\left.\frac{\partial^{p_n+p_{n-1}} V_{\text{out}}}{\partial {V_{\text{in},n}}^{p_n} \partial {V_{\text{in},n-1}}^{p_{n-1}}}\right|_{V_{\text{in},n}=0} \\ &\approx -R_L \left.\frac{\partial M_n^{(p_n)}(I_{\text{T}})}{\partial I_{\text{T}}}\right|_{I_{\text{T}}=I_{\text{tail}}/2} \cdot \left[\frac{\partial^{p_{n-1}} h_{n-1}\left(V_{\text{in},n-1}, I_{\text{L},n-2}\right)}{\partial {V_{\text{in},n-1}}^{p_{n-1}}} - \frac{\partial^{p_{n-1}} h_{n-1}\left(V_{\text{in},n-1}, I_{\text{R},n-2}\right)}{\partial {V_{\text{in},n-1}}^{p_{n-1}}} \right],\end{aligned}$$

Comparison with Eq. (5.40) allows us to use induction to obtain

$$\begin{aligned}&\left.\frac{\partial^{p_n+p_{n-1}+\cdots+p_1} V_{\text{out}}}{\partial {V_{\text{in},n}}^{p_n} \partial {V_{\text{in},n-1}}^{p_{n-1}} \cdots \partial {V_{\text{in},1}}^{p_1}}\right|_{V_{\text{in},n},\ldots,V_{\text{in},2}=0} \\ &\approx -R_L \prod_{k=2}^{n} \left.\frac{\partial M_k^{(p_k)}(I_{\text{T}})}{\partial I_{\text{T}}}\right|_{I_{\text{T}}=I_{\text{tail}}/2} \cdot \left[\frac{\partial^{p_1} h_1\left(V_{\text{in},1}, I_{\text{L},0}\right)}{\partial {V_{\text{in},1}}^{p_1}} - \frac{\partial^{p_1} h_1\left(V_{\text{in},1}, I_{\text{R},0}\right)}{\partial {V_{\text{in},1}}^{p_1}} \right].\end{aligned}$$

Finally, applying the same procedure and approximation to differentiate with respect to $V_{\text{in},0}$ a total of p_0 times, noting that $I_{\text{L},0} - I_{\text{R},0} = h\left(V_{\text{in},0}, I_{\text{tail}}\right)$, and evaluating at $V_{\text{in},0} = 0$ gives us

$$\left.\frac{\partial^{p_n+p_{n-1}+\cdots+p_0} V_{\text{out}}}{\partial {V_{\text{in},n}}^{p_n} \partial {V_{\text{in},n-1}}^{p_{n-1}} \cdots \partial {V_{\text{in},0}}^{p_0}}\right|_{V_{\text{in},k}=0\ \forall k} \approx -R_L \prod_{k=1}^{n} \left.\frac{\partial M_k^{(p_k)}(I_{\text{T}})}{\partial I_{\text{T}}}\right|_{I_{\text{T}}=I_{\text{tail}}/2} \cdot M_0^{(p_0)}(I_{\text{tail}}).$$

Therefore, we have the following result:[9]

$$G(p_0, \ldots, p_n) \approx -\frac{1}{p_0! \cdots p_n!} \cdot R_L \prod_{k=1}^{n} \left. \frac{\partial M_k^{(p_k)}(I_\mathrm{T})}{\partial I_\mathrm{T}} \right|_{I_\mathrm{T}=I_\mathrm{tail}/2} \cdot M_0^{(p_0)}(I_\mathrm{tail}) \,. \tag{5.42}$$

Based on Eq. (5.42), we can infer a very important fact: *due to the balanced nature of the multiplier, only intermodulation products involving an odd power of every single input voltage will appear at the output.* This is because $h(V_\mathrm{in}, I_\mathrm{T})$ is an odd function of V_in, and the derivative of an odd function is an even function (and vice versa). As a result, only when p is odd will $M^{(p)}(\cdot)$ be nonzero.

Application: Gilbert Cell RF Input 3rd Order IMP

To demonstrate the validity of the higher order IMP analysis, we will use Eq. (5.42) to examine the third-order intermodulation product of the radio frequency (RF) input for a standard down-conversion Gilbert cell mixer (Fig. 5.1), and then compare the resulting calculation against simulation. Specifically, we will find the RF input voltage V_RF^* at which the mixing term $V_\mathrm{RF}V_\mathrm{LO}$ and the cubic nonlinearity ${V_\mathrm{RF}}^3 V_\mathrm{LO}$ have the same magnitude:

$$|G(1,1)|\, V_\mathrm{RF}^*\, V_\mathrm{LO} = |G(3,1)|\, {V_\mathrm{RF}^*}^3\, V_\mathrm{LO}. \tag{5.43}$$

Solving for V_RF^* and using Eq. (5.42) along with footnote 9 gives us the simple expression

$$V_\mathrm{RF}^* = \sqrt{\left|\frac{G(1,1)}{G(3,1)}\right|} = \sqrt{\frac{6\, g_{m,\mathrm{RF}}}{\left|M_\mathrm{RF}^{(3)}\right|}}, \tag{5.44}$$

where the bias currents and voltages can be inferred from Eqs. (5.30) and (5.42).

Next, we used SpectreRF to run transient simulations of this circuit, which was implemented using identical NMOS transistors on a 55-nm bulk CMOS process. A load resistance of $R_L = 1\ \mathrm{k\Omega}$ was used, and the tail current $I_\mathrm{tail} = 1$ mA was implemented with an ideal current source. To simulate V_RF^*, the input frequencies were set to $f_\mathrm{LO} = 190$ MHz and $f_\mathrm{RF} = 200$ MHz, and the local oscillator (LO) amplitude was set to $V_\mathrm{LO} = 10$ mV. Fig. 5.10 shows the appropriately scaled amplitudes of the output tones (obtained by computing a discrete Fourier transform (DFT) of the output waveform over 100 ns) at $f_\mathrm{RF} - f_\mathrm{LO} = 10$ MHz (the mixing

[9] Based on the fact that $M^{(1)}(I_\mathrm{T}) = g_m(I_\mathrm{T}/2)$, it is easy to check that Eq. (5.42) reduces to Eq. (5.30) when $p_k = 1\ \forall k = 0, \ldots, n$.

term) and at $3f_{\mathrm{RF}} - f_{\mathrm{LO}} = 410\,\mathrm{MHz}$ (the cubic nonlinearity) as a function of the RF amplitude.[10]

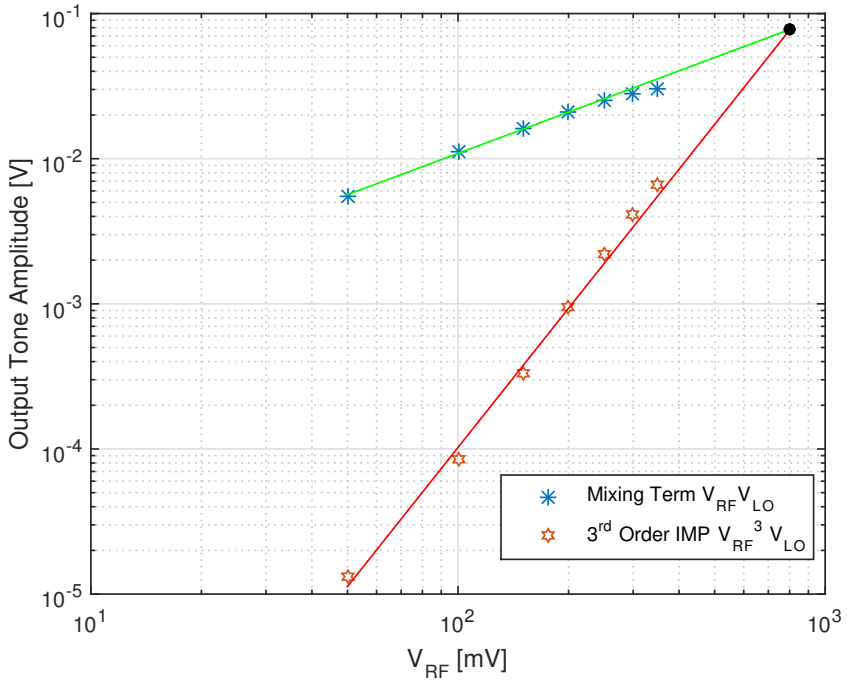

Figure 5.10: Comparison of fundamental mixing term with 3rd order IMP. Linear extrapolations on the data were used to obtain the intersection point, which occurs at $V^*_{\mathrm{RF}} = 803\,\mathrm{mV}$.

Transistor simulations reveal $g_{m,\mathrm{RF}}(0.5\,\mathrm{mA}) = 5.588\,\mathrm{mS}$ and $\left|M^{(3)}_{\mathrm{RF}}(1\,\mathrm{mA})\right| = 55.63\,\mathrm{mA/V^3}$. This leads to a theoretically computed input intercept point of $V^*_{\mathrm{RF}} = 776\,\mathrm{mV}$, which is very close to the simulated value of 803 mV.

Finally, by replacing V_{LO} with $V_{\mathrm{LO}}\cos(\omega_{\mathrm{LO}}t)$ and V^*_{RF} with $V_{\mathrm{RF}}\cos(\omega_1 t)+V_{\mathrm{RF}}\cos(\omega_2 t)$, it is easily seen that the RF amplitude for which the output tones at $\omega_{1,2} - \omega_{\mathrm{LO}}$ and $(2\omega_{1,2} - \omega_{2,1}) - \omega_{\mathrm{LO}}$ have the same amplitude, which characterizes the RF input's two-tone third-order intercept point (IIP3), is given by $V_{\mathrm{RF}}|_{\mathrm{IIP3}} = \left(2/\sqrt{3}\right) V^*_{\mathrm{RF}}$.

[10]The amplitude of the tone at $3f_{\mathrm{RF}} - f_{\mathrm{LO}}$ was scaled by a factor of 4 because

$$\cos x \cos y = \frac{1}{2}\cos(x - y) + \text{other harmonics},$$

$$\cos^3 x \cos y = \frac{1}{8}\cos(3x - y) + \text{other harmonics}.$$

5.8 Frequency Response—Bandwidth Analysis

While the previous section generalized the low-frequency, small-signal analysis of Section 5.5 by considering *higher order* intermodulation products between the inputs, in this section, we extend the discussion of Section 5.5 along a different direction by looking at high-frequency behavior. Specifically, we will develop a simple framework for computing the small-signal "bandwidth" of the stacked analog multiplier. To that end, let us assume small-signal sinusoidal inputs and look at how device parasitics influence the amplitude of the output. Although a bandwidth analysis of frequency mixers is typically somewhat complicated due to their time-varying nature [62], [63], we will introduce a reasonable approximation here that both significantly simplifies the analysis and imparts insight into some of the circuit's bandwidth limiting factors. Namely, in the presence of a sufficiently large input drive resistance R_S, the response of a differential pair to changes in its tail current (a common base/gate response) is significantly faster[11] than to changes in the differential input voltage (a common emitter/source response). What this means for our multiplier is that the k^{th} stage's dynamics can essentially be estimated by the action of the stage's (zero-value) time constant on its input frequency [43]; the time-varying tail currents $I_{\text{L},k-1}$ and $I_{\text{R},k-1}$ serve only to periodically but instantaneously switch, or modulate, the polarity of the output current $\left(I_{\text{L},k} - I_{\text{R},k}\right)$.

Under this framework, an input voltage $v_{\text{in},k}$ to stage k at frequency $\omega_{\text{in},k}$ is, to the first order, effectively altered by the following amplitude frequency response factor [43], [51]:

$$v_{\text{in},k} \longrightarrow \frac{v_{\text{in},k}}{\left|1 + j\omega_{\text{in},k}\tau_k\right|} \tag{5.45}$$

where $1/\tau_k$ is the 3-dB bandwidth of stage k when it is driven "in isolation." This is defined as the bandwidth of the k^{th} stage when it is removed from the multiplier and operated under the following conditions:

1. For $k > 0$, the tails $I_{\text{L},k-1}$ and $I_{\text{R},k-1}$ are connected to DC current sources with a small DC difference between them (otherwise the output would be zero).

2. The output port (i.e., where $I_{\text{L},k}$ and $I_{\text{R},k}$ flow into) is loaded with the equivalent "load" resistance seen by the k^{th} stage within the multiplier.

[11] Within the domain of lumped element circuits that are driven sinusoidally, speed is spoken of in a *phase-shift* (as opposed to *delay*) sense. The "faster" a system responds to an input, the less phase shift there is between that input and the output.

Alternatively, this definition is approximately equivalent to the bandwidth of the multiplier with respect to $v_{\text{in},k}$ when all other inputs are excited by small DC voltages. Theoretically, τ_k can be estimated by the stage's zero-value time constant sum [43]

$$\tau_k = 2R_{S,k}\left[C_{\text{gs},k} + \left(1 + g_{m,k}R_{L,k}\right)C_{\text{gd},k}\right] + 2R_{L,k}C_{\text{gd},k} \tag{5.46}$$

where R_S is the differential input voltage source resistance and $R_{L,k}$ is the equivalent single-ended load resistance seen by the k^{th} stage. Clearly $R_{L,n} = R_L$; for $k < n$, $R_{L,k} \approx 1/2g_{m,k+1}$. Also note that for $k = 0$, the above expression should be halved because there are half as many parasitics.

Next, any load capacitor (effective or explicit) that appears in parallel with the load resistance R_L will be encountered by the output currents $I_{\text{L},n}$ and $I_{\text{R},n}$. Therefore, assuming a single-ended load capacitance C_L, we also have the following transformation [51]:

$$R_L \longrightarrow \left|R_L \left\| \frac{1}{j\omega_{\text{out}}C_L}\right.\right| = \frac{R_L}{|1 + j\omega_{\text{out}}R_L C_L|} \tag{5.47}$$

where ω_{out} is the frequency of the output tone of interest.

Note that these expressions are not meant to provide the complete amplitude response as a function of frequency; we seek only to use them to provide a rough estimate of the multiplier's small-signal "bandwidth" with respect to each input. Also, we make no attempt to look at the phase response of the multiplier.

To test our framework, we used SpectreRF to run transient simulations on the multiplier with various input configurations, the results of which are summarized in Table 5.1. The multipliers were implemented using NMOS transistors on a 55-nm bulk CMOS process with $R_L = 1\ \text{k}\Omega$ and an ideal $I_{\text{tail}} = 0.5$ mA. All the input voltages were sinusoidal with an amplitude of 50 mV, and each input featured an internal source resistance of $R_S = 2\,\text{k}\Omega$. Each stages' input frequency $f_{\text{in},k}$ was either held constant or depended on an "input frequency" f_{in} that was varied; the bandwidth for each scenario was then defined with respect to f_{in}. The 3-dB bandwidth of the multiplier was simulated by locating the value of f_{in} for which the magnitude of the output's mixing tone at $f_{\text{out}} = \sum_{k=0}^{n} f_{\text{in},k}$ (obtained by computing a DFT of the output waveform over 20 ns) decreases by 3 dB from what it is when f_{in} is low (50 MHz). The bandwidth was theoretically estimated by assuming the amplitude of the small-signal output voltage varies with frequency according to Eqs. (5.45)

Table 5.1: Bandwidth Simulation Results

Scenario	Theoretical BW	Simulated BW	% Deviation
2 inputs, $f_{\text{in},0} = 5$ GHz, $f_{\text{in},1} = f_{\text{in}}$ varied.	5.55 GHz	5.05 GHz	9.4%
2 inputs, $f_{\text{in},0} = 100$ MHz, $f_{\text{in},1} = f_{\text{in}}$ varied.	6.53 GHz	6.55 GHz	0.3%
2 inputs, $f_{\text{in},1} = 5$ GHz, $f_{\text{in},0} = f_{\text{in}}$ varied.	5.55 GHz	5.55 GHz	0%
2 inputs, $f_{\text{in},1} = 100$ MHz, $f_{\text{in},0} = f_{\text{in}}$ varied.	6.53 GHz	7.40 GHz	12%
2 inputs, $f_{\text{in},k} = (k+1)f_{\text{in}}\ \forall k$.	2.59 GHz	2.55 GHz	1.6%
3 inputs, $f_{\text{in},k} = (k+1)f_{\text{in}}\ \forall k$.	1.43 GHz	1.25 GHz	13%
4 inputs, $f_{\text{in},k} = f_{\text{in}}\ \forall k$.	2.43 GHz	2.05 GHz	17%

and (5.47) as

$$v_{\text{out}} \propto \frac{1}{\sqrt{1 + (\omega_{\text{out}} R_L C_L)^2}} \prod_{k=0}^{n} \frac{1}{\sqrt{1 + \left(\omega_{\text{in},k}\tau_k\right)^2}}, \tag{5.48}$$

where each stage's time constant was obtained via AC simulation of the multiplier with the stage of interest being driven in isolation. Each stage was designed to have a 3-dB bandwidth of roughly 7.9 GHz, leading to a time constant of $\tau_k = 20$ ps $\forall k$. The load capacitance C_L was estimated via Miller's approximation:

$$C_L = C_{\text{gd},n}\left(1 + g_{m,n} R_L\right). \tag{5.49}$$

Based on transistor characterization simulations, we found $g_{m,n}(0.125\text{mA}) = 2.09\text{mS}$ and $C_{\text{gd},n} = 3.44$ fF.

Looking at the simulation results, we note several shortcomings of our relatively simple theoretical framework. Our model appears to be less accurate when there are more inputs, likely due to the fact that the "phase shift" from the tail currents of the bottommost stages to the output, which our approximation neglects by construction, starts becoming appreciable as the number of intermediate stages between them increases. Also, notice that we fail to account for the fact that when there are 2 inputs, the LO stage seems to have an inferior bandwidth compared to the RF stage even though both stages in isolation have the same bandwidth.

On a final note, it appears based upon comparison with simulation that the dynamics due to the time-varying tail currents *cannot* be simply modeled as that of an output pole acting on the intermediate output frequencies of each stage.

5.9 Conclusion

By stacking switching stages within a double-balanced current-commutating analog multiplier, a generalization of the topology that allows for the multiplication of an arbitrary number of input voltages was realized. A general framework for analyzing the circuit given any nonlinear transistor I-V characteristic was formulated. Throughout this chapter, we demonstrated that by employing a modular and intuitive, as opposed to brute-force and exact, analysis ideology which 1) views the system in terms of its appropriate building blocks for a given investigative context or 2) exploits the system's inherent physical or mathematical structure; we were able to temper rigor with insight and efficaciously extract the system's most important attributes and dominant characteristics. In particular, the multiplier's small-signal characteristics, higher-order intermodulation products, and frequency response were looked at. Specifically, we observed that under the right conditions, the time-varying nature of the mixing process could be abstracted away, allowing us to effectively decouple the dynamics of the individual stages from one another. Simulations and measurements that confirmed the analysis were also reported.

In passing, we would like to mention two potential advantages of this circuit that were not discussed in detail. First, the stacked nature of the multiplier's topology makes it feasible within high-voltage processes (such as those used for RF power amplifier design). Also, the low output impedance seen by each stage (except possibly the last) may result in superior bandwidth properties when compared against a mere cascade of multiple two-input analog multipliers (e.g., Gilbert cells).

In conjunction, Chapters 2–5 show that by striking a balance between rigor and intuition, between focusing on detail and thinking abstractly, and between exact and approximate analysis, we can yield novel insights into the functional behavior of various electronic systems, greatly aiding in their design and analysis.

Chapter 6

OTHER WORKS

This chapter focuses on the more significant contributions I made to the tapeouts I had the pleasure of participating in during my time in graduate school. Both works described below were implemented on TSMC's 55-nm bulk CMOS GP process.

6.1 On-Chip Temperature Sensor for Space Applications

The ability to monitor the ambient temperature on-chip is desirable in certain situations, such as for electronics to be used in outer space. The design of accurate on-chip temperature sensors that are robust against process and voltage variations has been a subject of persistent interest, with the current state-of-the-art featuring some impressive specifications [64]. To build an integrated circuit that achieves this functionality, recall that owing to the Boltzmann distribution of electrons, junction devices feature a current that is proportional to $\exp(qV/kT)$, a strong and very well-defined temperature dependence.

In this section[1], we briefly describe the design of an on-chip thermometer with a linear output characteristic, operable from 25°C to 150°C and featuring a linear output characteristic with a slope of 7.6 ± 0.15 mV/°C over the operation range. Furthermore, the sensor's output variation was bounded by ±1°C over process corners, ±2.5°C over anticipated worst-case supply variations, and ±6°C over device mismatch (3σ). The sensor occupies an area of $110 \times 110\ \mu\text{m}^2$ and consumes 1 mA of current from a 3.3 V supply; its schematic and layout are shown in Fig. 6.1.

[1]The author graciously thanks Dr. Florian Bohn and Behrooz Abiri for the invaluable guidance they provided to me with respect to this project.

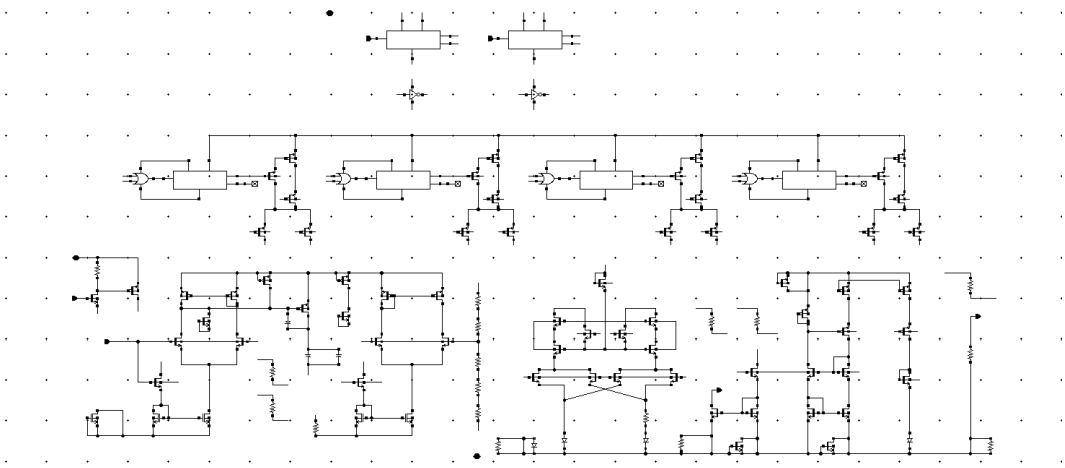

(a) Schematic (including dummy devices)

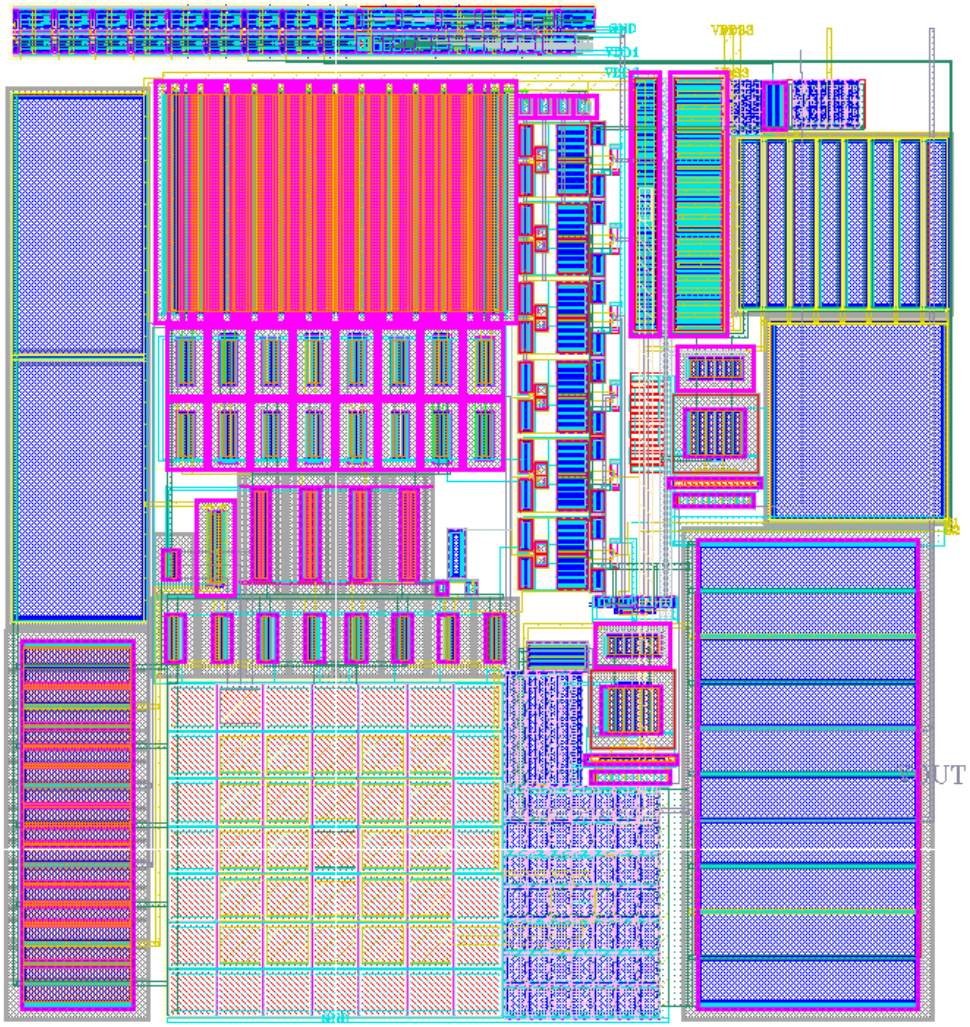

(b) Layout

Figure 6.1: (a) Schematic and (b) layout of the temperature sensor. The rectangular blocks in the schematic are 1 V-to-2.6 V digital level shifters. The top of the layout contains a shift register used for programming the switching bits.

Basic Measurement Principle: PTAT Current Generation

The underlying principle of operation for the designed sensor is the generation of a current that is proportional-to-absolute-temperature (PTAT). To that end, consider the circuit depicted in Fig. 6.2 [65]. Since the amplifier ensures that nodes X and Y are at the same potential, and since the two diodes must carry the same current, this current I must satisfy

$$\frac{kT}{q}\log\left(\frac{I}{I_S}\right) = \frac{kT}{q}\log\left(\frac{I}{nI_S}\right) + IR, \tag{6.1}$$

where I_S is the saturation current of the left diode. Rearranging, we get

$$I = \frac{1}{R}\frac{kT}{q}\log n \tag{6.2}$$

which is proportional to T, the absolute temperature. Then, if we are able to copy this PTAT current as shown and feed it to an output resistor, the voltage across the resistor will itself be PTAT and can serve as a measure of the temperature, assuming that the dependence of the resistance upon the temperature is negligible to the first order. In actuality, the amplifier shown in Fig. 6.2 was implemented using a floating cascode mirror.

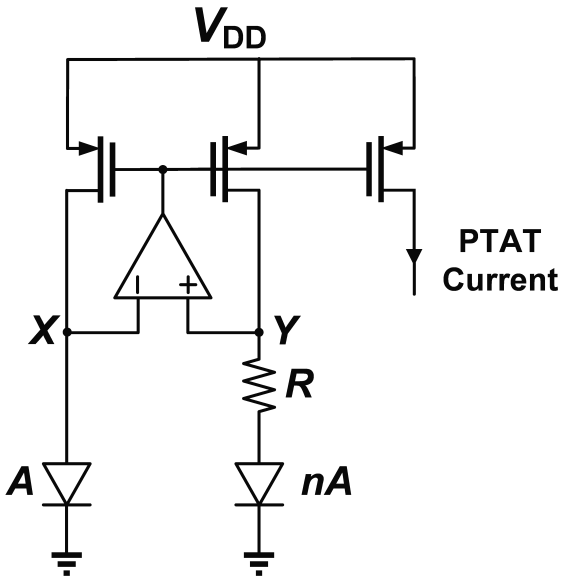

Figure 6.2: Core circuit for generating a PTAT current.

Supply Regulation

An issue unique to the chip that houses this sensor is that it contains a phased array wireless power transfer system. Therefore, the circuitry contains power amplifiers

which draw significant amounts of transient current. This can cause the on-chip supply to fluctuate (below nominal) significantly. To make the sensor robust against supply variation, we designed our circuit to work off of a lower supply (specifically 2.64 V as opposed to the nominal $V_{\mathrm{DD}} = 3.3$ V). The lower supply was generated using a PFET based supply regulator, shown in Fig. 6.3. It is easy to see that the regulated voltage for this circuit is

$$V_{\mathrm{regulated}} = \left(1 + \frac{R_2}{R_1}\right) V_{\mathrm{ref}}. \tag{6.3}$$

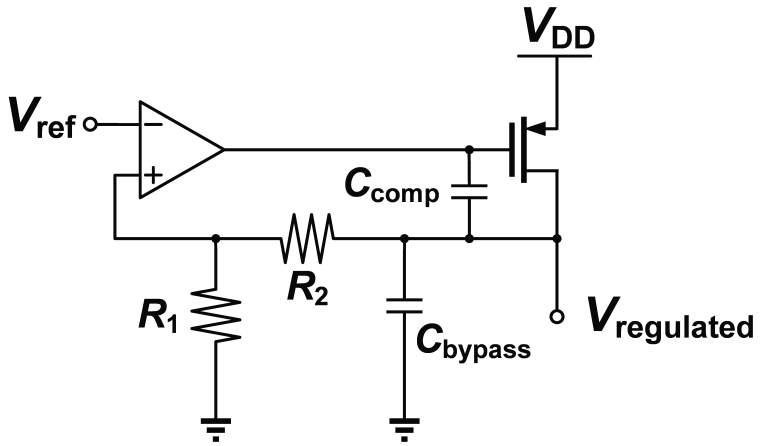

Figure 6.3: PFET based supply regulator. C_{comp} was chosen to yield a phase margin of roughly 60°. C_{bypass} was added to help filter out high frequency fluctuations in the supply.

The reference V_{ref} is a Si bandgap voltage (1.2 V which was generated elsewhere on-chip.[2] The compensation capacitor was carefully chosen to ensure stability of the feedback loop. The regulator was able to supply a voltage of $V_{\mathrm{regulated}} = 2.4$ V to the sensor while V_{DD} fluctuated over 2.7–3.4 V. A parametric simulation of the output characteristics as V_{DD} was swept is shown in Fig. 6.4.

[2]In retrospect, the bandgap could also have been generated internally, provided the startup circuitry was carefully designed.

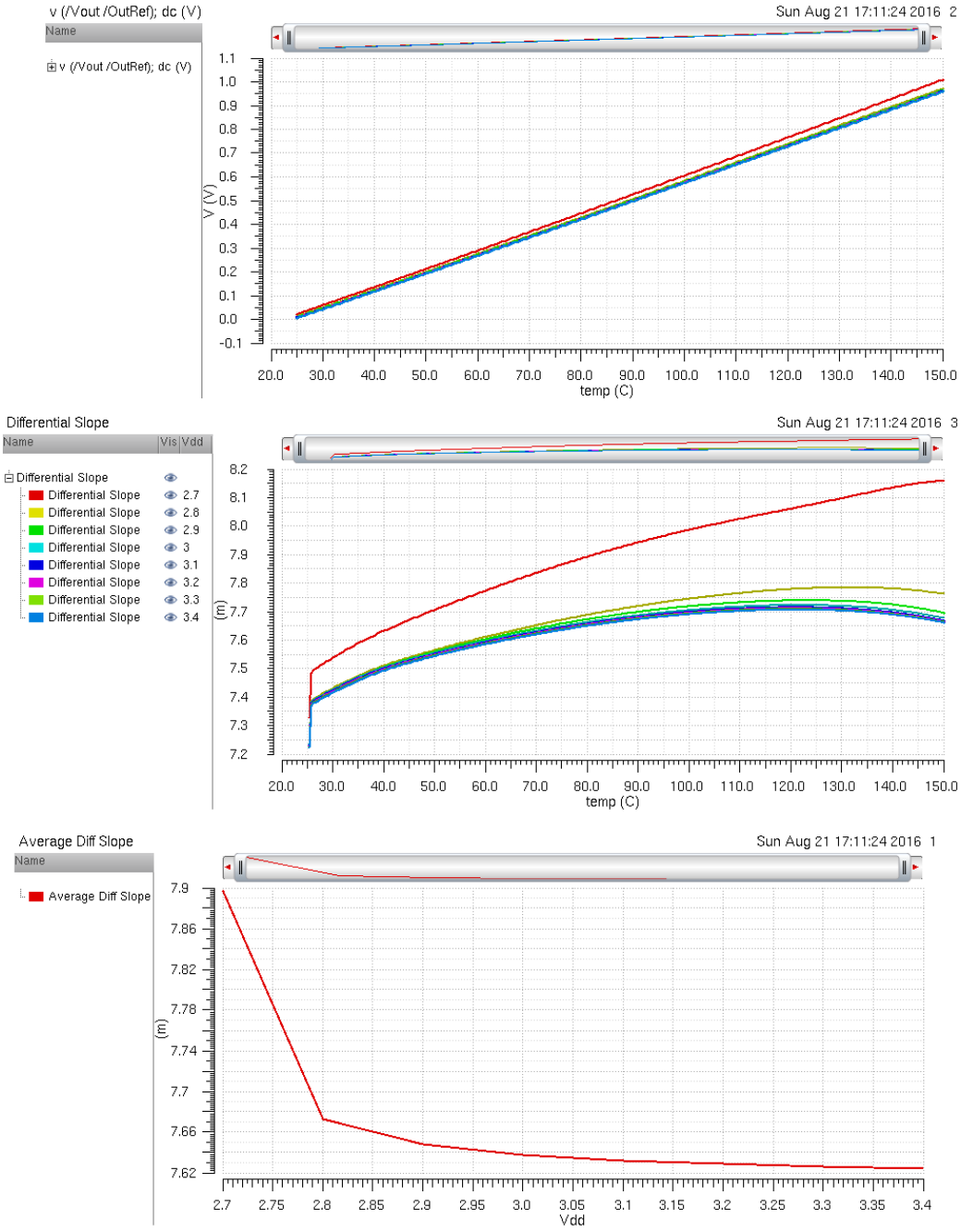

Figure 6.4: Differential output voltage (top) and slope (middle) vs. temperature as V_{DD} was swept from 2.7 V to 3.4 V in 0.1 V increments. The average slope over the entire temperature range is also plotted (bottom) for these values of V_{DD}.

Output Resolution: Current Bleeding

It was desired to have the sensor to roughly have a 1 V output range over the temperature range 25℃–150℃. This corresponds to a resolution of 8 mV/℃. A PTAT voltage with this slope would reach 8 mV/℃ × (273 + 150)℃ = 3.38 V, which is problematic since our regulated supply is at 2.6 V. Therefore, it became necessary to bleed away a fixed current from the PTAT current before feeding it to the output resistor.

It is imperative that the bled current I_{bleed} be constant with temperature. In the course of design, we discovered that the temperature dependence of the technology's threshold voltage V_T is rather significant; therefore, we needed to implement a current source that is V_T independent. To that end, we used the circuit shown in Fig. 6.5. It is easy to see that

$$I_{\text{bleed}} = \left(\frac{R_A}{R_A + R_B}\right)\frac{V_{\text{DD}}}{R_0}. \tag{6.4}$$

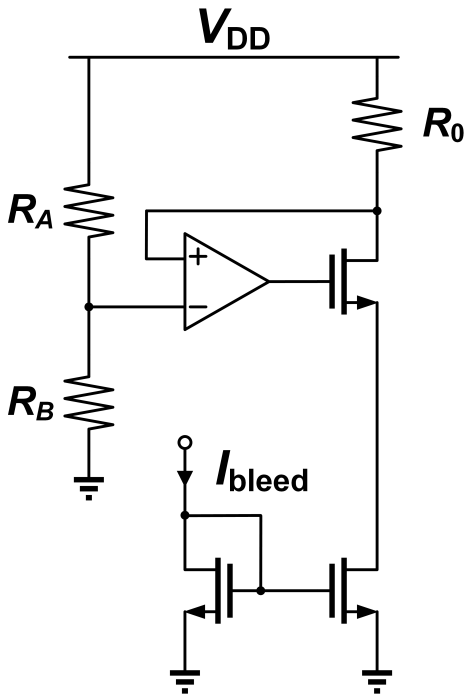

Figure 6.5: Implementation of a V_T independent current source, used as the current bleeder for the temperature sensor.

Finally, the output of this sensor went to an ADC that required a differential input between 0 V and 1 V. This was accomplished by simply connecting the positive

end to the sensor's output and the negative end to a resistive divider whose output voltage is equal to that of the sensor at 25°C.

Robustness Against Process Variation

On top of being independent to fluctuations in the supply, we also needed the sensor's output to be robust against process variations. Chip to chip variations manifest themselves as process corners, and although such variations can be compensated for by calibrating each chip's sensor separately, such a procedure is not feasible for systems that need to be produced and distributed en masse. Instead, it is better for the circuit's performance to exhibit precision from chip to chip. More specifically, we need the output characteristic to be "bias independent," so to speak. Since variations in the gain of the operational amplifiers do not affect the output much, the main bottleneck here was the bias circuitry for the floating mirror of the PTAT current generator. To that end, we generated the cascode gate biases by copying branches of the current generator circuitry, and connecting them (either directly for the NFET, or via a current mirror for the PFET) to diode-connected devices with $1/5$ the W/L ratio. This "internal" generation of the biases allows most of the voltages and currents within the circuit to change "together" as threshold voltages or channel mobilities vary, resulting in an output characteristic that is relatively independent of process corners. An extracted simulation over the worst-case corners, which we determined to be slow-slow and fast-fast, is shown in Fig. 6.6.

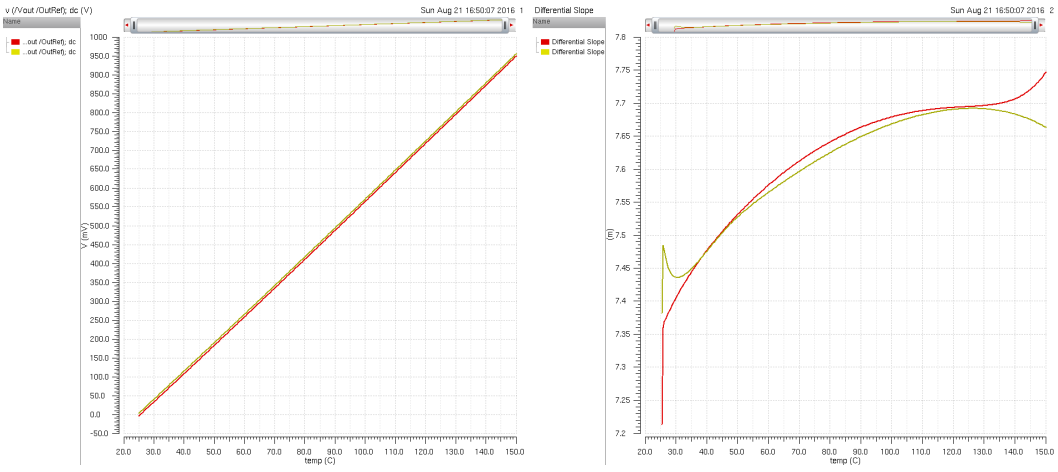

Figure 6.6: Differential output voltage (left) and slope (right) vs. temperature for the worst-case process corners, slow-slow (yellow) and fast-fast (red).

Local variations on a single chip are also problematic, since much of the design is current mirror based, a circuit which fundamentally relies on devices being identical to one another. The mismatch between branch currents is then translated into offset errors at the output. To compensate against mismatch, we first used very long-channel transistors for all of the critical devices. This serves two purposes. First, it increases the output resistance of these transistors (i.e., decreases channel-length modulation), causing them to behave more similarly to ideal current sources. Indeed, the dependence of the devices' currents upon unequal drain voltages introduces deviations between branch currents that need to be matched. Second, it increases the area of the devices, allowing local variations to average out with higher probability. Next, the floating mirrors were cascoded as mentioned above; this further decreases the output resistance of the current sources. Finally, instead of an ordinary current mirror, a four transistor Wilson current mirror was used in the bias circuitry for the gate of the PMOS cascode.

To further compensate for mismatch, we employed a "chopping and averaging" technique. Specifically, devices that needed to be matched could be interchanged with one another using switches. We determined that a total of 4 switching patterns exhausted the effective possibilities, leading to 2 input bits that could be toggled. The average of the output voltage from each of these 4 states would then be independent of device mismatch, to the first order. A Monte Carlo simulation of the output voltage is shown in Fig. 6.7, showing a 3σ variation of 15.6 mV or 6°C.

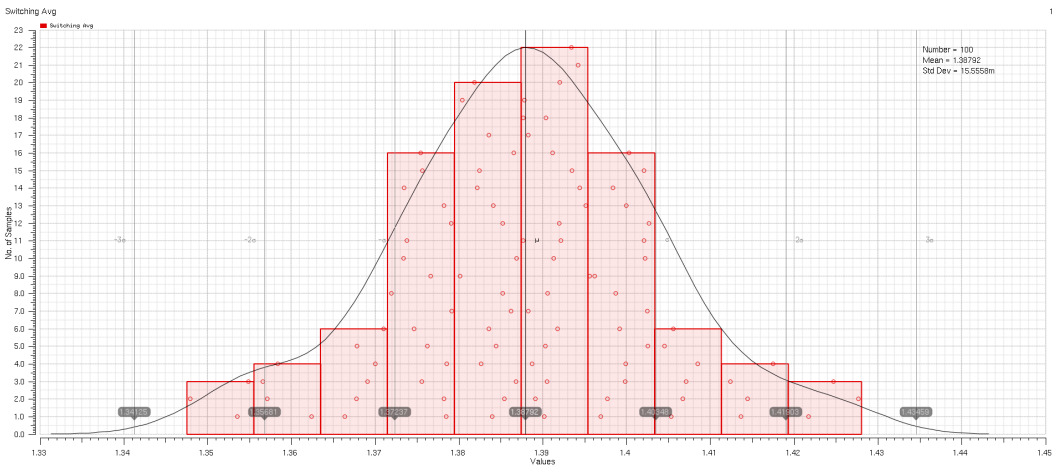

Figure 6.7: Monte Carlo simulation for device mismatch of the sensor's output voltage (single-ended) at 110°C.

6.2 DC-DC Converter

DC-DC converters see high demand in modern digital and mixed-signal systems since circuits that operate off of different supplies often need to be integrated together on-chip. Most on-chip DC-DC converters utilize switched capacitor implementations, where the primary design tradeoffs are between area consumption and power efficiency. The current state-of-the-art [66], [67] boasts 85% efficiency and 15 distinct conversion ratios through a cascade of 4 stages on a chip area of 4.645 mm^2. Through a novel switching scheme which we will briefly describe below, our design[3] achieves 89% efficiency and 42 distinct conversion ratios through coprime cascading of 3 stages on a chip area of 1.62 mm^2 in simulation. Table 6.1 summarizes this performance comparison.

Table 6.1: DC-DC Converter Performance Comparison Table

	ISSCC 2014 [66]	**Our Design**
Power Efficiency η	85%	89%
Number of Cascaded Stages	4	3
Number of Conversion Ratios	15	42
Chip Area	4.645 mm^2	1.62 mm^2

The schematic for one possible configuration of a single stage of our DC-DC converter is depicted in Fig. 6.8. This configuration yields $V_{out} = (2/3)V_{in}$ in steady state (corresponding to $V_{in}/3$ across each capacitor). It should be apparent that there are a total of 4 possible configurations, depending on whether the 2 capacitors are connected in parallel or in series for the two switching possibilities: source and ground. For example, the converse of the depicted configuration in Fig. 6.8 consists of series capacitors being connected to the source and parallel capacitors being connected to ground; this corresponds to $(2/3)V_{in}$ across each capacitor and an output voltage of $V_{out} = V_{in}/3$. The remaining two configurations are where the capacitors are connected either in series or in parallel all the time (the former is suboptimal from an efficiency standpoint), both of which obviously result in the output voltage being equal to $V_{in}/2$.

[3]This work was conducted in collaboration with Parham Khial.

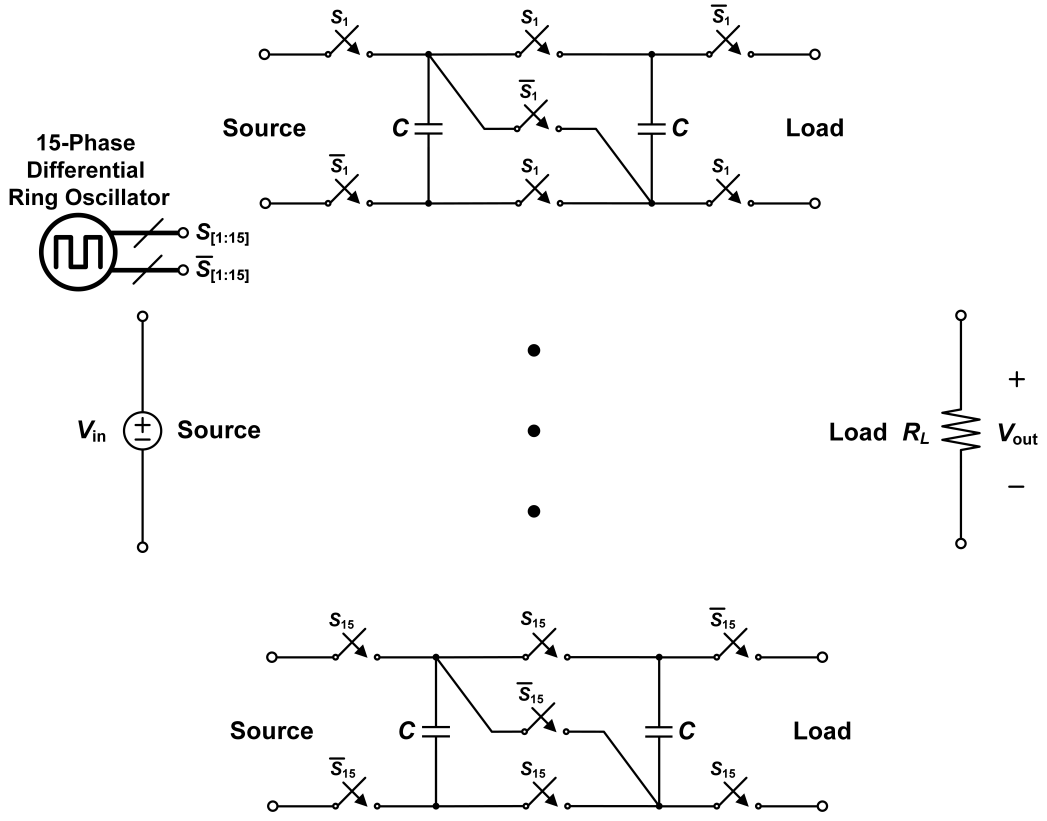

Figure 6.8: High-level schematic of one possible configuration of a single stage of the DC-DC converter, resulting in $V_{\text{out}} = (2/3)V_{\text{in}}$. For our design, we used $C = 5$ pF.

The switching signals, S_1 and $\bar{S}_1$ to S_{15} and $\bar{S}_{15}$, correspond to 15 equally distributed phases over $[0, 2\pi)$ as well as their complements. This was implemented with an on-chip 15-stage current-starved differential ring oscillator, tunable from roughly 1MHz to 500MHz. Clearly, the source ports of all 15 switching blocks are connected to the input voltage source, whereas the load ports of all 15 switching blocks are connected to the output load resistor. The layout of a single stage is shown in Fig. 6.9.

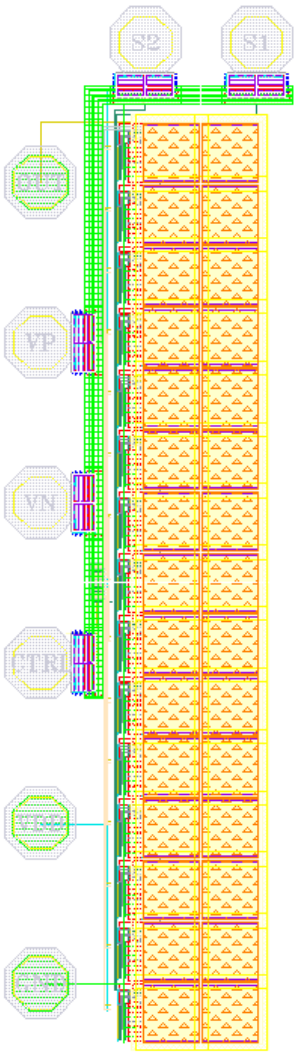

Figure 6.9: Top cell of the DC-DC converter, including pads.

A representative simulation of the extracted design is shown in Fig. 6.10, where the theoretical output voltage should be $2/3$ V. The deviation between the (average) simulated output voltage and $2/3$ V stems from the unequal capacitive loads of the switches that the ring oscillator's various phases need to drive.

Figure 6.10: Transient simulation of the output voltage (top red), S_1 (middle yellow), and $\bar{S}_7$ (bottom green) for a load of $R_L = 5\,\text{k}\Omega$. The input voltage is $V_{\text{in}} = 1$ V and the oscillation frequency is 40 MHz.

Chapter 7

CONCLUSION

In this thesis, we presented four mathematical frameworks for modeling electronic systems. The first was a coupled differential equation formulation describing the phase and amplitude of an oscillator under injection based on generalized amplitude and phase ISFs. While existing injection locking and pulling theories are restricted to particular types of oscillators or injections and typically make assumptions about the injection strength or frequency, our proposed formulation is applicable to any type of oscillator (LC, ring, relaxation, etc.) and any type of injection (large/small, periodic/aperiodic, sub-/super-harmonic, square/sinusoidal, etc.). The second was an exact, phasor based physical analysis of an ideal LC oscillator (comprised of a lossy tank replenished by a nonlinear transconductor) under sinusoidal injection. Through this analysis, we clearly exposed the commonly overlooked exact physical mechanism underlying how a sinusoidal current locks an LC oscillator. This led us to both a necessary condition and a sufficient condition for injection locking to occur, thereby generalizing the concept of the lock range. We also analyzed in detail the often made assumption that the transconductor's output current preserves phase modulation in the oscillation voltage. The third was a proof of the lower and upper bounds of an LTI system's bandwidth based on the sum of its ZVTs. Finally, the fourth was a modular analysis of a balanced analog multiplier for an arbitrary number of signed inputs—the large- and small-signal characteristics as well as the "bandwidth" were derived for an arbitrary device nonlinearity. The analysis was confirmed by some basic simulation and measurement results.

Throughout, notice that each model was motivated by physical intuition which was later justified mathematically. For example, we learned that when oscillators are subjected to periodic injections, the "objective" of the injection is to alter the phase of the oscillator sufficiently per cycle such that it can oscillate at the injection frequency. If and when this objective is accomplished, the "remaining" amount of injection simply adds energy to the oscillator and increases the oscillation amplitude in steady state. But, since the phase of a stronger oscillator responds less to injections of the same size, the dynamics of the amplitude and phase of an oscillator under injection are inherently coupled. Additionally, through this insight, we were able to discuss the "in-phase" and "reactive" portions of the injection current. Another example

lies in our analysis of the multiplier: we exploited the symmetry of the topology to extract the bare-bone operating principles of the circuit without being bogged down by computational details. As a final example, most electrical engineers would intuit that the sum of the ZVTs, which essentially constitutes a worst-case estimate of the circuit's time constant since it assumes all of the reactive elements energize in series, forms a conservative estimate (or lower bound) of the system's bandwidth. Based on the obvious reasoning that this estimate is exact for a first-order system, we can postulate that the lower bound is approached by having one of the poles dominate and that the upper bound is achieved in the opposite scenario.

We hope that not only will the specific substantive knowledge presented in this thesis be useful to circuit designers, but that the spirit of tempering mathematical rigor with physical intuition and balancing detailed analysis against abstract modularity be incorporated into the engineering thought process in general.

7.1 Future Directions

Of all the topics discussed, the one with the most room for further development as well as the highest potential for scientific impact is the modeling of oscillators under injection. Such an endeavor would produce a much-needed general theory for injection locking and pulling in electrical oscillators. Although the ideas presented in this thesis laid the groundwork, there are still numerous deficiencies that need to be addressed. While the coupled differential equation formulation for capturing amplitude and phase disturbances is reasonable, its validity as well as how its parameters can be estimated must be looked into. Specifically, although the simulation and computation of the phase ISF $\Gamma(\phi, \xi)$ for $\xi = 0$ has been studied extensively, including the derivation of closed-form expressions for well-known oscillators (LC cross-coupled pair, Colpitts, ring, relaxation), a systematic methodology for dealing with $\xi \neq 0$, calculating the amplitude ISF $\Lambda(\cdot,\cdot)$, and estimating the coefficients that govern the dynamics of amplitude restoration has not been developed. Ultimately, an analytical model for predicting how an arbitrary electrical oscillator responds to any deterministic or stochastic injection which carries mathematical rigor, bears a sufficiently accurate connection to physical reality, and exhibits the generality, insight, and ease-of-use that Hajimiri's celebrated oscillator phase noise theory[1] [1]–[4] revels in would greatly contribute to our fundamental understanding of oscillators as well as to their design.

[1] In some sense, such a model would be a generalization of Hajimiri's theory, since both are fundamentally constructed from the concept of the ISF.

BIBLIOGRAPHY

[1] A. Hajimiri and T. H. Lee, "A general theory of phase noise in electrical oscillators," *IEEE Journal of Solid-State Circuits*, vol. 33, no. 2, pp. 179–194, Feb. 1998.

[2] ——, "Design issues in CMOS differential LC oscillators," *IEEE Journal of Solid-State Circuits*, vol. 34, no. 5, pp. 717–724, May 1999.

[3] A. Hajimiri, S. Limotyrakis, and T. H. Lee, "Jitter and phase noise in ring oscillators," *IEEE Journal of Solid-State Circuits*, vol. 34, no. 6, pp. 790–804, Jun. 1999.

[4] A. Hajimiri and T. H. Lee, *The Design of Low Noise Oscillators*. Springer, 1999.

[5] B. Razavi, "A study of injection locking and pulling in oscillators," *IEEE Journal of Solid-State Circuits*, vol. 39, no. 9, pp. 1415–1424, Sep. 2004.

[6] A. Mirzaei and A. A. Abidi, "The spectrum of a noisy free-running oscillator explained by random frequency pulling," *IEEE Transactions on Circuits and Systems I: Regular Papers*, vol. 57, no. 3, pp. 642–653, Mar. 2010.

[7] R. Adler, "A study of locking phenomena in oscillators," *Proceedings of the IEEE*, vol. 61, no. 10, pp. 1380–1385, Oct. 1973.

[8] L. J. Paciorek, "Injection locking of oscillators," *Proceedings of the IEEE*, vol. 53, no. 11, pp. 1723–1727, Nov. 1965.

[9] A. Mirzaei, M. E. Heidari, and A. A. Abidi, "Analysis of oscillators locked by large injection signals: Generalized Adler's equation and geometrical interpretation," in *IEEE Custom Integrated Circuits Conference 2006*, Sep. 2006, pp. 737–740.

[10] A. Mirzaei, M. E. Heidari, R. Bagheri, S. Chehrazi, and A. A. Abidi, "The quadrature LC oscillator: A complete portrait based on injection locking," *IEEE Journal of Solid-State Circuits*, vol. 42, no. 9, pp. 1916–1932, Sep. 2007.

[11] P. Bhansali and J. Roychowdhury, "Gen-Adler: The generalized Adler's equation for injection locking analysis in oscillators," in *2009 Asia and South Pacific Design Automation Conference*, Jan. 2009, pp. 522–527.

[12] G. R. Gangasani and P. R. Kinget, "A time-domain model for predicting the injection locking bandwidth of nonharmonic oscillators," *IEEE Transactions on Circuits and Systems II: Express Briefs*, vol. 53, no. 10, pp. 1035–1038, Oct. 2006.

[13] ——, "Time-domain model for injection locking in nonharmonic oscillators," *IEEE Transactions on Circuits and Systems I: Regular Papers*, vol. 55, no. 6, pp. 1648–1658, Jul. 2008.

[14] X. Lai and J. Roychowdhury, "Capturing oscillator injection locking via nonlinear phase-domain macromodels," *IEEE Transactions on Microwave Theory and Techniques*, vol. 52, no. 9, pp. 2251–2261, Sep. 2004.

[15] ——, "Analytical equations for predicting injection locking in LC and ring oscillators," in *Proceedings of the IEEE 2005 Custom Integrated Circuits Conference*, Sep. 2005, pp. 461–464.

[16] P. Maffezzoni, "Analysis of oscillator injection locking through phase-domain impulse-response," *IEEE Transactions on Circuits and Systems I: Regular Papers*, vol. 55, no. 5, pp. 1297–1305, Jun. 2008.

[17] D. Dunwell and A. C. Carusone, "Modeling oscillator injection locking using the phase domain response," *IEEE Transactions on Circuits and Systems I: Regular Papers*, vol. 60, no. 11, pp. 2823–2833, Nov. 2013.

[18] H.-A. Tanaka, "Synchronization limit of weakly forced nonlinear oscillators," *Journal of Physics A: Mathematical and Theoretical*, vol. 47, no. 40, Sep. 2014.

[19] ——, "Optimal entrainment with smooth, pulse, and square signals in weakly forced nonlinear oscillators," *Physica D: Nonlinear Phenomena*, vol. 288, pp. 1–22, Nov. 2014.

[20] T. Nagashima, X. Wei, H.-A. Tanaka, and H. Sekiya, "Locking range derivations for injection-locked class-E oscillator applying phase reduction theory," *IEEE Transactions on Circuits and Systems I: Regular Papers*, vol. 61, no. 10, pp. 2904–2911, Oct. 2014.

[21] H. A. Tanaka, A. Hasegawa, H. Mizuno, and T. Endo, "Synchronizability of distributed clock oscillators," *IEEE Transactions on Circuits and Systems I: Fundamental Theory and Applications*, vol. 49, no. 9, pp. 1271–1278, Sep. 2002.

[22] J.-C. Chien and L.-H. Lu, "Analysis and design of wideband injection-locked ring oscillators with multiple-input injection," *IEEE Journal of Solid-State Circuits*, vol. 42, no. 9, pp. 1906–1915, Sep. 2007.

[23] M. Raj and A. Emami, "A wideband injection-locking scheme and quadrature phase generation in 65-nm CMOS," *IEEE Transactions on Microwave Theory and Techniques*, vol. 62, no. 4, pp. 763–772, Apr. 2014.

[24] A. Demir, A. Mehrotra, and J. Roychowdhury, "Phase noise in oscillators: A unifying theory and numerical methods for characterization," *IEEE Transactions on Circuits and Systems I: Fundamental Theory and Applications*, vol. 47, no. 5, pp. 655–674, May 2000.

[25] T. Djurhuus, V. Krozer, J. Vidkjær, and T. K. Johansen, "Oscillator phase noise: A geometrical approach," *IEEE Transactions on Circuits and Systems I: Regular Papers*, vol. 56, no. 7, pp. 1373–1382, Jul. 2009.

[26] F. L. Traversa and F. Bonani, "Oscillator noise: A nonlinear perturbative theory including orbital fluctuations and phase-orbital correlation," *IEEE Transactions on Circuits and Systems I: Regular Papers*, vol. 58, no. 10, pp. 2485–2497, Oct. 2011.

[27] Ö. Suvak and A. Demir, "On phase models for oscillators," *IEEE Transactions on Computer-Aided Design of Integrated Circuits and Systems*, vol. 30, no. 7, pp. 972–985, Jul. 2011.

[28] N. M. Wereley, "Analysis and control of linear periodically time varying systems," Dept. of Aeronautics and Astronautics, PhD thesis, Massachusetts Institute of Technology, Feb. 1991.

[29] P. Vanassche, G. Gielen, and W. Sansen, "On the difference between two widely publicized methods for analyzing oscillator phase behavior," in *IEEE/ACM International Conference on Computer Aided Design 2002*, Nov. 2002, pp. 229–233.

[30] S. Levantino, P. Maffezzoni, F. Pepe, A. Bonfanti, C. Samori, and A. L. Lacaita, "Efficient calculation of the impulse sensitivity function in oscillators," *IEEE Transactions on Circuits and Systems II: Express Briefs*, vol. 59, no. 10, pp. 628–632, Oct. 2012.

[31] J. G. Mesquita and A. Slavík, "Periodic averaging theorems for various types of equations," *Journal of Mathematical Analysis and Applications*, vol. 387, no. 2, pp. 862–877, Mar. 2012.

[32] H. R. Rategh and T. H. Lee, "Superharmonic injection-locked frequency dividers," *IEEE Journal of Solid-State Circuits*, vol. 34, no. 6, pp. 813–821, Jun. 1999.

[33] S. Verma, H. R. Rategh, and T. H. Lee, "A unified model for injection-locked frequency dividers," *IEEE Journal of Solid-State Circuits*, vol. 38, no. 6, pp. 1015–1027, Jun. 2003.

[34] H.-C. Chang, X. Cao, M. J. Vaughan, U. K. Mishra, and R. A. York, "Phase noise in externally injection-locked oscillator arrays," *IEEE Transactions on Microwave Theory and Techniques*, vol. 45, no. 11, pp. 2035–2042, Nov. 1997.

[35] D. Ham and A. Hajimiri, "Virtual damping and Einstein relation in oscillators," *IEEE Journal of Solid-State Circuits*, vol. 38, no. 3, pp. 407–418, Mar. 2003.

[36] J. J. Rael and A. A. Abidi, "Physical processes of phase noise in differential LC oscillators," in *Proceedings of the IEEE 2000 Custom Integrated Circuits Conference*, 2000, pp. 569–572.

[37] J. Groszkowski, "The interdependence of frequency variation and harmonic content, and the problem of constant-frequency oscillators," *Proceedings of the Institute of Radio Engineers*, vol. 21, no. 7, pp. 958–981, Jul. 1933.

[38] C. Samori, A. L. Lacaita, F. Villa, and F. Zappa, "Spectrum folding and phase noise in *LC* tuned oscillators," *IEEE Transactions on Circuits and Systems II: Analog and Digital Signal Processing*, vol. 45, no. 7, pp. 781–790, Jul. 1998.

[39] E. Hegazi, J. Rael, and A. Abidi, *The Designer's Guide to High Purity Oscillators*. Kluwer Academic, 2005.

[40] S. N. Bernstein, *Leçons sur les propriétós extrómales et la meilleure approximation des fonctions analytiques d'une variable róelle*. Paris, 1926.

[41] R. D. Thornton, C. L. Searle, D. O. Pederson, R. B. Adler, and E. J. A. Jr., *Multistage Transistor Circuits*. Wiley, 1965.

[42] B. Cochrun and A. Grabel, "A method for the determination of the transfer function of electronic circuits," *IEEE Transactions on Circuit Theory*, vol. 20, no. 1, pp. 16–20, Jan. 1973.

[43] A. Hajimiri, "Generalized time- and transfer-constant circuit analysis," *IEEE Transactions on Circuits and Systems I: Regular Papers*, vol. 57, no. 6, pp. 1105–1121, Jun. 2010.

[44] H. E. Jones, "Dual output synchronous detector utilizing transistorized differential amplifiers," U.S. Patent 3241078 A, Mar. 1966.

[45] B. Gilbert, "A new wide-band amplifier technique," *IEEE Journal of Solid-State Circuits*, vol. 3, no. 4, pp. 353–365, Dec. 1968.

[46] ——, "A precise four-quadrant multiplier with subnanosecond response," *IEEE Journal of Solid-State Circuits*, vol. 3, no. 4, pp. 365–373, Dec. 1968.

[47] J. N. Babanezhad and G. C. Temes, "A 20-V four-quadrant CMOS analog multiplier," *IEEE Journal of Solid-State Circuits*, vol. 20, no. 6, pp. 1158–1168, Dec. 1985.

[48] P. J. Sulivan, B. A. Xavier, and W. H. Ku, "Low voltage performance of a microwave CMOS Gilbert cell mixer," *IEEE Journal of Solid-State Circuits*, vol. 32, no. 7, pp. 1151–1155, Jul. 1997.

[49] L. A. NacEachern and T. Manku, "A charge-injection method for Gilbert cell biasing," in *Conference Proceedings. IEEE Canadian Conference on Electrical and Computer Engineering*, May 1998, pp. 365–368.

[50] G. Han and E. Sánchez-Sinencio, "CMOS transconductance multipliers: A tutorial," *IEEE Transactions on Circuits and Systems II: Analog and Digital Signal Processing*, vol. 45, no. 12, pp. 1550–1563, Dec. 1998.

[51] H. Kuntman and A. Toker, "Novel non-linear macromodel suitable for SPICE simulation of analogue multipliers realized with bipolar and CMOS technologies," *International Journal of Circuit Theory and Applications*, vol. 27, no. 5, pp. 485–495, Sep. 1999.

[52] M. T. Terrovitis and R. G. Meyer, "Noise in current-commutating CMOS mixers," *IEEE Journal of Solid-State Circuits*, vol. 34, no. 6, pp. 772–783, Jun. 1999.

[53] H. Darabi and A. A. Abidi, "Noise in RF-CMOS mixers: A simple physical model," *IEEE Journal of Solid-State Circuits*, vol. 35, no. 1, pp. 15–25, Jan. 2000.

[54] H. Darabi and J. Chiu, "A noise cancellation technique in active RF-CMOS mixers," *IEEE Journal of Solid-State Circuits*, vol. 40, no. 12, pp. 2628–2632, Dec. 2005.

[55] J. Choma, "A three-level broad-banded monolithic analog multiplier," *IEEE Journal of Solid-State Circuits*, vol. 16, no. 4, pp. 392–399, Aug. 1981.

[56] K. Kimura, "Some circuit design techniques using two cross-coupled, emitter-coupled pairs," *IEEE Transactions on Circuits and Systems I: Fundamental Theory and Applications*, vol. 41, no. 5, pp. 411–423, May 1994.

[57] G. Chien, "Gilbert cell and method thereof," U.S. Patent 7088982 B1, Aug. 2006.

[58] D. A. Johnson and S. Raman, "A packaged SiGe x2 sub-harmonic mixer for U-NII band applications," in *Proceedings of the 2001 Bipolar/BiCMOS Circuits and Technology Meeting*, Oct. 2001, pp. 159–162.

[59] T.-H. Wu, S.-C. Tseng, C.-C. Meng, and G.-W. Huang, "GaInP/GaAs HBT sub-harmonic gilbert mixers using stacked-LO and leveled-LO topologies," *IEEE Transactions on Microwave Theory and Techniques*, vol. 55, no. 5, pp. 880–889, May 2007.

[60] T. H. Wu, C. C. Meng, and G. W. Huang, "High-gain high-isolation CMFB stacked-LO subharmonic Gilbert mixer using SiGe BiCMOS technology," *Microwave and Optical Technology Letters*, vol. 49, no. 5, pp. 1214–1216, May 2007.

[61] P. R. Gray, P. J. Hurst, S. H. Lewis, and R. G. Meyer, *Analysis and Design of Analog Integrated Circuits*, 5th ed. Wiley, 2010.

[62] T. K. Johansen, J. Vidkjær, and V. Krozer, "Analysis and design of wide-band SiGe HBT active mixers," *IEEE Transactions on Microwave Theory and Techniques*, vol. 53, no. 7, pp. 2389–2397, Jul. 2005.

[63] M. El-Nozahi, E. Sánchez-Sinencio, and K. Entesari, "A 20–32-GHz wide-band mixer with 12-GHz IF bandwidth in 0.18-μm SiGe process," *IEEE Transactions on Microwave Theory and Techniques*, vol. 58, no. 11, pp. 2731–2740, Nov. 2010.

[64] M. A. P. Pertijs, K. A. A. Makinwa, and J. H. Huijsing, "A CMOS smart temperature sensor with a 3σ inaccuracy of ±0.1°C from –55°C to 125°C," *IEEE Journal of Solid-State Circuits*, vol. 40, no. 12, pp. 2805–2815, Dec. 2005.

[65] B. Razavi, *Design of Analog CMOS Integrated Circuits*. McGraw-Hill, 2001.

[66] L. G. Salem and P. P. Mercier, "An 85%-efficiency fully integrated 15-ratio recursive switched-capacitor DC-DC converter with 0.1-to-2.2V output voltage range," in *2014 IEEE International Solid-State Circuits Conference Digest of Technical Papers (ISSCC)*, Feb. 2014, pp. 88–89.

[67] ——, "A recursive switched-capacitor DC-DC converter achieving $2^N - 1$ ratios with high efficiency over a wide output voltage range," *IEEE Journal of Solid-State Circuits*, vol. 49, no. 12, pp. 2773–2787, Dec. 2014.